Tampere University

HEIKKI LUOMALA

Monitoring the Vertical Deformation Behaviour of Road and Railway Structures

Tampere University Dissertations 81

Tampere University Dissertations 81

HEIKKI LUOMALA

Monitoring the Vertical Deformation Behaviour of Road and Railway Structures

ACADEMIC DISSERTATION
To be presented, with the permission of
the Faculty of Built Environment
of Tampere University,
for public discussion in the auditorium RG202
of the Rakennustalo, Korkeakoulunkatu 5, Tampere,
on 25 June 2019, at 12 o'clock.

ACADEMIC DISSERTATION
Tampere University, Faculty of Built Environment
Finland

Responsible supervisor and Custos	Professor Pauli Kolisoja Tampere University Finland	
Supervisor	Professor Antti Nurmikolu (until 6.4.2017) Tampere University of Technology Finland	
Pre-examiners	Professor Elias Kassa Norwegian University of Science and Technology Norway	PhD John Tunna Federal Railroad Administration USA
Opponents	Professor Elias Kassa Norwegian University of Science and Technology Norway	Assistant Professor Pasi Lautala Michigan Tech University USA

The originality of this thesis has been checked using the Turnitin OriginalityCheck service.

Cover design: Roihu Inc.

ISBN 978-952-03-1133-9 (print)
ISBN 978-952-03-1134-6 (pdf)
ISSN 2489-9860 (print)
ISSN 2490-0028 (pdf)
http://urn.fi/URN:ISBN:978-952-03-1134-6

PunaMusta Oy – Yliopistopaino
Tampere 2019

Abstract

Vertical deformation in road and railway structures acts in many ways as an indicator of structural integrity. Traffic loading causes a vertical displacement (i.e. deflection), the magnitude of which indicates the structure's ability to withstand the effects of external loads. Deflection varies lengthwise across a road or railway structure, and the variation in deflection indicates the ability of different cross-sections to withstand traffic loading. Temporal deflection variation, in contrast, indicates a change in the structure's integrity or in the surrounding conditions. Furthermore, the structure itself can be affected by freezing, compaction or settlement and these phenomena, together with traffic loading, will result in unevenness over time.

Deformations caused by traffic loading are mainly recoverable, but a small percentage will always be permanent. These permanent deformations accumulate in proportion to the traffic volume and cause a gradual development of unevenness in the surface of the structure. The need for road and railway maintenance, and partially also the length of road and railway service life, is often determined based on the permanent deformations. Unevenness that requires maintenance first develops in those areas of structural change where the accumulation rate of permanent deformations is changing.

As part of this study, methods have been developed to measure and monitor the vertical displacements and deformations in earth structures. Sensors installed in a structure enable long-term observations (i.e. monitoring). This monitoring produces detailed data about the measured parameter from a specific location of the structure. The main benefit of monitoring comes from the assessment of a structure's load-bearing capacity. Through monitoring, the amount of permanent deformation in relation to time can be identified, and the effects of the environmental conditions and maintenance efforts can be verified. In addition, monitoring can be used to estimate future maintenance needs regarding individual cross-sections. Expanding the analyses to cover the entire road or railway network requires, however, the use of network-level measurement methods.

Therefore, a measurement device operating continuously on railways, the Stiffmaster, was developed to measure track stiffness. The device measures track deflection caused by a moving train. The measuring method helps in detecting those areas of a railway track with an abrupt deflection variation or significant changes in the deflection level. The measurement results will help in identifying the factors causing unevenness.

The measuring methods developed as part of this study will increase the understanding of how road and railway structures function and thus contribute to lengthening the service life of roads and railways. Measurement data on the structures' true behaviour will significantly ease the planning of appropriate maintenance measures.

Tiivistelmä

Tie- ja ratarakenteessa tapahtuva pystysuuntainen muodonmuutos on monin tavoin rakenteen kuntoa kuvaava indikaattori. Liikennekuormitus aiheuttaa rakenteen pintaan pystysuuntaisen siirtymän (eli jouston), jonka suuruus indikoi rakenteen kykyä kestää kuormituksia. Jousto vaihtelee rakenteen pituussuunnassa ja jouston suuruus kuvaa eri poikkileikkausten kykyä vastustaa liikennekuormituksesta aiheutuvia pysyviä muodonmuutoksia. Ajan suhteen muuttuva jousto kuvaa rakenteen kunnon tai olosuhteiden muuttumista. Rakenne itsessään voi myös routia, deformoitua tai tiivistyä ja nämä ilmiöt yhdessä liikennekuormituksen kanssa aiheuttavat ajan kuluessa epätasaisuutta.

Liikennekuormituksen aiheuttamat muodonmuutokset ovat pääasiassa palautuvia, mutta hyvin pieni osa muodonmuutoksesta jää aina pysyväksi. Pysyvät muodonmuutokset kumuloituvat liikennemäärän suhteessa ja aiheuttavat rakenteen pintaan epätasaisuutta. Tien ja radan kunnossapitotarve ja osin myös käyttöikä määräytyvät pysyvien muodonmuutosten perusteella. Kunnossapitoa vaativaa epätasaisuutta syntyy ensiksi rakenteen muutoskohtiin, joissa pysyvien muodonmuutosten kertymisen nopeus muuttuu.

Tässä työssä on kehitetty mittaus- ja monitorointimenetelmiä maarakenteiden pystysuuntaisten siirtymien ja muodonmuutosten mittaamiseen. Rakenteeseen asennettavat anturit mahdollistavat pitkäaikaisseurannan, jota kutsutaan monitoroinniksi. Monitoroinnin avulla saadaan tarkkaa tietoa mitattavasta suureesta täsmällisestä kohdasta rakennetta. Monitoroinnin suurin hyöty saavutetaan rakenteen kuormituskestävyyden arvioinnissa. Monitoroinnin avulla saadaan selville, paljonko rakenteeseen syntyy pysyvää muodonmuutosta ajan suhteen ja myös olosuhteiden ja kunnossapidon vaikutukset pystytään todentamaan. Monitoroinnin avulla pystytään ennakoimaan myös tulevaa kunnossapitotarvetta yksittäisissä poikkileikkauksissa. Analyysien laajentaminen koko tie- tai rataverkolle edellyttää kuitenkin verkkotasoisten mittausmenetelmien käyttöä.

Tähän tarpeeseen kehitettiin jatkuvatoiminen radan jäykkyyden mittauslaite Stiffmaster. Laitteella mitataan liikkuvan junan aiheuttamaa radan joustoa. Mittausmenetelmän avulla havaitaan radan kohdat, joissa jousto vaihtelee äkillisesti tai jouston taso muuttuu selkeästi. Mittaustulosten perusteella pystytään osaltaan tunnistamaan epätasaisuuden aiheuttajia.

Työssä kehitetyt mittausmenetelmät lisäävät ymmärrystä tie- ja ratarakenteiden toiminnasta ja mahdollistavat tien ja radanpidon elinkaaritehokkuuden paranemisen. Mittaustieto rakenteiden todellisesta käyttäytymisestä helpottaa merkittävästi sopivien kunnossapitotoimien suunnittelua.

Foreword

I wrote this doctoral dissertation as part of the Railway Track Structures Research Team of the Department of Civil Engineering at Tampere University of Technology. During the process, the name of the organization changed to Tampere University, Faculty of Built Environment. I compiled the research material from several research projects conducted in road and railway environments. The following people, listed in alphabetical order, are among those who helped me acquire my research material, and I owe them my sincerest thanks: Marko Happo, Ossi Peltokangas, Tommi Rantala, Riku Varis and Nuutti Vuorimies. I also received help from several others, who were very supportive. During the study, I worked as a responsible researcher in four large research projects and participated in several more. I express my gratitude to the Finnish Transport Agency (FTA) for funding these research projects. My first research project was also funded by the Finnish Funding Agency for Technology and Innovation (TEKES) and a number of Finnish construction firms.

I convey my special thanks to emeritus Senior Engineer Kauko Sahi, who, before his well-earned retirement, made a significant contribution to my measuring system's design, commented on my new ideas, and helped me turn them into something concrete. The following true story about the development process of my measuring devices describes the nature of my work. The small talk during a coffee break veered off into electrical transformers, and Kauko told me that the coils in them are bathing in oil. I asked why the oil was not causing a short circuit, and Kauko gave me a thorough explanation about the breakdown voltage of oil. I then got the idea of using oil as the fluid in the settlement pipe, which would solve the problem of protecting the sensors that I had been thinking of using. I revealed my idea to Kauko, and after thinking about it for a second, he said something along the lines of, 'Well, there it is then. It is invented. Should we start straightaway?', referring to the construction of a prototype. Similar brainstorming sessions also produced good results when developing other measuring devices. We ended up drinking several cups of coffee and tea before the first draft of the Stiffmaster was ever drawn on paper.

In addition, I sought direction for my actual dissertation from Professors Antti Nurmikolu and Pauli Kolisoja. I owe them a warm thank you for all the support and guidance they provided to keep me on the right track. Heartfelt thanks also go to my wife Suvi, who keenly listened to all my explanations about the problems that occurred during this process. Finally, I would like to mention my children Helmi and Miika, who often wondered what 'daddy's remote workdays' meant, when they were taken to day care while daddy went home to type. Those remote workdays were necessary for the peace and quiet required for my writing.

Tampere 13.5.2019

Heikki Luomala

Table of contents

Abbreviations and notations

Abbreviations

AASHO	AASHO Road Test
BOEF	beam on elastic foundation
CARS	China Academy of Railway Sciences
CHLOE	CHLOE-profilometer
FTA	Finnish Transport Agency
FWD	falling weight deflectometer
GPR	ground-penetrating radar
IRI	international roughness index
LFWD	light falling weight deflectometer
MDD	multi-depth deflectometer
PSI	present serviceability index
RSMV	Swedish rolling stiffness measurement vehicle
RTK-GPS	real-time kinematic global positioning system
SBB	Swiss railways (Schweizerische Bundesbahnen)
SKMT	Czech rolling stiffness measurement vehicle
SnapMDD	Snap multi-depth deflectometer
TDR	time domain reflectometer
TEKES	Finnish Funding Agency for Technology and Innovation
TLV	track loading vehicle
TSD	traffic speed deflectometer
TTCI	Transportation Technology Centre
TUT	Tampere University of Technology
WILD	wheel impact load detector
WIM	weight in motion

Notations

a	acceleration [m/s^2], sleeper spacing [m]
C	beginning irregularity error
D	irregularity error, to be maintained in the near future
E	elastic modulus [N/mm^2, MPa]
I	moment of inertia [mm^4]
k	elastic constant
K_0	lateral earth pressure [kN/m^2, kPa]
K_1, K_2	regression coefficients
$K_{1,2,3}$	material parameters
L	characteristic length, base length
M	bending moment [Nm]
M_r	resilient modulus [N/mm^2, MPa]

n	parameter, number
N	equivalent loading
p	linear load on rail [N/mm]
P	wheel load [kN]
P_v	design wheel load [50 kN]
q	deviator stress [kN/m^2, kPa]
Q_d	wheel load [N]
s	displacement [m]
S	total settlement
S_i	initial settlement
S_L	wheel elevation, loaded
S_p	consolidation settlement, primary settlement
S_s	secondary settlement, creep
S_τ	shear settlement
S_U	wheel elevation, unloaded
T	time
u	track modulus [N/mm/mm]
v	velocity [m/s, km/h]
x, x_i	longitudinal coordinate [mm]
y	vertical deflection [mm]
z	distance from road surface [m]
γ	volumetric weight [kN/m^3]
ε_r	recoverable strain
η	relative deflection
θ	sum of principal stresses [kPa]
θ_0	reference stress
σ_d	deviator stress [kPa]
σ_{d0}	reference stress
$\sigma_{1,2,3}$	principal stresses [kPa]
*	irregularity error, to be maintained immediately

1. Introduction

1.1. Background

A smooth road or railway track is a goal shared by passengers, transport operators, maintenance companies and owners of these infrastructures. The smoothness requirements of a road or track are primarily determined based on traffic safety and travel comfort. On the contrary, a road or a track will be made as smooth as specified in standards, and maintenance is only performed once the limit value for the smoothness is exceeded. From an owner's perspective, the load-bearing capacity of a road or railway track should be as high as possible so that any unevenness develops slowly. The amount of traffic and the available resources will also have an effect on the level of requirements. The aim is to keep the main roads and tracks in good condition, but costs need to be cut on the maintenance of low-volume roads and tracks. Large sums are spent each year on road and railway network maintenance, and therefore it is vital that maintenance is targeted in a cost-effective manner. One of the most useful tools in assessing the effects of maintenance is structural monitoring.

Several factors contribute to the development of vertical unevenness. Unevenness may develop on the surface, in the structure or in the subsoil. The types of unevenness developed on a road surface in structures paved with asphalt include surface wearing, cracks, potholes, erosion and deformation (Sivilevičius et al. 2002). On railways, these surface defects take the form of rail defects, such as wear and tear, wheel burns, corrugation, rolling contact fatigue and flattened track joints (Cannon et al. 2003). All unevenness caused by surface damage is extremely short-waved, with a longitudinal wavelength of under 1 m. The primary causes of surface damage include weak material properties, magnitude of loading, traffic volume, worn on non-compatible wheel and rail profiles, use of studded tyres and other similar factors that depend on both the vehicles and the road or railway structures (Esveld 2001, Huang 2004). However, since this study is concerned with the road and rail sub-surface, all forms of surface damage have been excluded.

Unevenness with a slightly longer wavelength is developed, for example, by hanging sleepers, which are mainly caused by the deformation and uneven degradation of the supporting layer (Nurmikolu 2005). Every other sleeper or two out of every three sleepers can be poorly supported, which will lead to a section of unevenness 1–2 m long. Augustin et al. (2003) estimated that over 50% of all sleepers on a track are poorly supported or not in contact with the supporting layer on an unloaded track. If there are several hanging sleepers in a row, the cause of an unevenness is usually some other component in the track and not the supporting layer itself. Often, in these situations, the cause is a structural transition zone, such as a bridge approach (Luomala & Nurmikolu 2012).

Unevenness with a long wavelength develops in places where the accumulation of permanent deformations varies. As a result of traffic loading, structural layers become deformed and the rate at which this happens is often relative to the stiffness of the structure and the amount of traffic

(Lekarp et al. 2000). In those structural transition zones with a considerable variation in stiffness, such as bridge approaches or when moving from soft ground to a rock cutting, permanent deformations will develop in different cross-sections at significantly different rates. This results in unevenness, because permanent deformations on a stiff bridge, for example, are smaller than on a more flexible bridge approach embankment. In addition, changes in stiffness provide vehicles with an impulse that increases the dynamic loading (Esveld 2001). The result is often a chain reaction, in which unevenness is at first small in scale but then begins to expand at an accelerating rate due to the increased dynamic loading (Banimahd et al. 2011).

A poor load-bearing capacity of a structure will initially manifest itself as unevenness at various structural transition zones, such as level crossings or bridge approaches (Banimahd et al. 2011). A similar mechanism also reveals unevenness caused by the subsoil, such as consolidation settlements of soft clay. Typically, the depth of soft ground increases relatively slowly, so that unevenness caused by the settlement of the subsoil may have an even greater wavelength than unevenness caused by a varying load-bearing capacity.

The development of unevenness may also be periodic or take place in varying ways, depending on the season. Frost heave caused by insufficient frost protection in seasonal frost areas may be either extremely small-scale or extensive, depending on the frost susceptibility of, and water infiltration to, the subsoil (Pylkkänen et al. 2014). A typical feature in unevenness caused by frost is that the unevenness is developed in early spring and mainly disappears once the frost has thawed. Especially when it comes to roads with a low traffic volume, unevenness due to frost damage that causes major disruption to traffic is only developed as the frost is thawing, when excess water released from the melting ice lenses reduces the load-bearing capacity of the road structure (Simonsen 1999). This reduced capacity results in unevenness, which will not disappear on its own and always requires maintenance.

The key objective of this study was to develop measuring methods to assess the mechanisms leading to the development of unevenness (Figure 1.1). The study discusses several measuring methods that are suitable for identifying the causes behind unevenness. The thorough understanding of these causes is need to find the appropriate remedies. A maintenance measure targeted at an incorrect structural part will not result in the desired outcome, and instead the unevenness will quickly return.

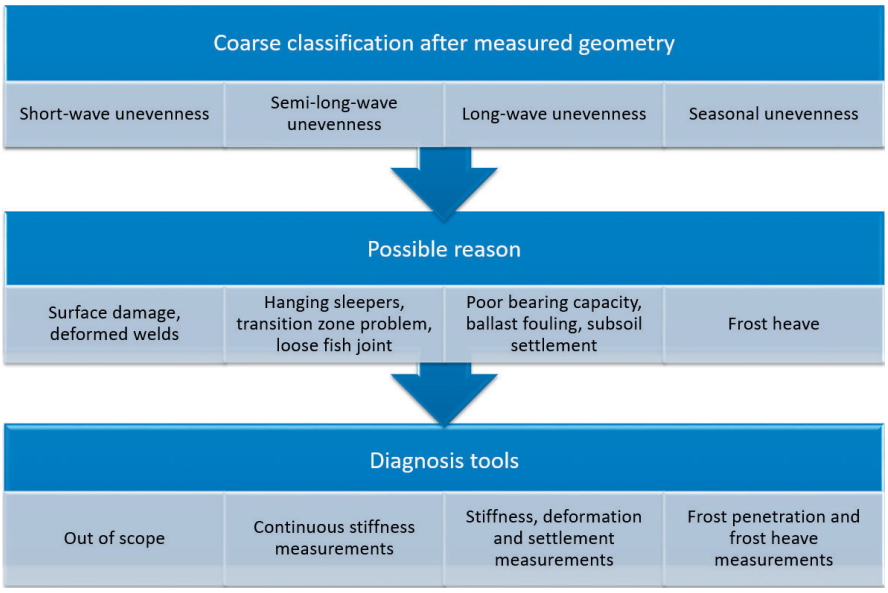

Figure 1.1. Types and possible causes of unevenness and measuring methods developed to assess them.

The diagnostic tools presented in Figure 1.1 are mainly monitoring methods. Monitoring refers to the measuring and surveying of a parameter in relation to time (SFS-EN 1997-1 2005). Except for the stiffness measurement technique, the methods that have been developed are such that, after installing the instrumentation, the monitoring will continue for months, even years. The temporal dimension brings significant benefit to the understanding of the mechanisms that developed unevenness, because the conditions will vary over the course of the monitoring period. By combining the geometric data, structural data, stiffness data and frost susceptibility data, among others, it is possible to identify the cause of unevenness and focus the required maintenance cost-effectively (Silvast et al. 2014).

1.2. Research questions

The maintenance of an existing road or track is currently based on managing its longitudinal evenness, as maintenance will first be performed in places where the unevenness exceeds a pre-determined limit. The monitoring methods could be used to predict how unevenness will develop in the future, and the monitoring will allow maintenance to be proactive.

The key research questions of this study are as follows:

- Are the currently available monitoring technologies, either commercially available ones or those developed for a specific application, able to produce meaningful data on the vertical displacements and deformation behaviour of road and railway structures that makes it possible
    - to improve the understanding about the structural behaviour of roads and railways and
    - to identify the mechanisms that are behind the development of unevenness?
- Is it possible to achieve this aim only locally or on the level of a longer road/railway section as well?
- Which of the available technologies provide this information on such a long timescale that they enable changes in the structural condition of a road or railway to be monitored?

1.3. Methodology

Exploring new information by monitoring is the key idea describing the research methods of this dissertation. This thesis combines the experiences from several individual research projects that focused on improving the lifecycle efficiency of road or railway track structures. The objective of the original projects was to discover the physical phenomena. Monitoring was the key method of obtaining the research material. Developing new monitoring methods was necessary because suitable commercial solutions did not exist. The aim of monitoring was to understand the behaviour of road and railway tracks.

The research methodology of this thesis consists of the following steps, which are presented in Figure 1.2. The first step is to identify the measurement need very accurately. In this work, all measurements are related to the vertical deformation behaviour of structures. The second step is to increase the knowledge of the studied phenomenon and suitable measurement technique by a literature search. In the third step, the potential measurement methods are evaluated in brainstorming sessions together with several specialists. In this thesis, several new measurement concepts were created on the basis of gathered information. The fourth step is to build a prototype and test it. The fifth step is to develop the method further on the basis of experiences acquired from testing. The sixth step is the calibration and verification phase where the new method is calibrated by another measurement technique, and the measurement results are verified on the basis of knowledge of the measured phenomenon. The measurement results are subjected to criticism; is the measurement data reliable and how much the results are affected by measurement errors? In the seventh step, the actual measurements are taken for the individual research projects.

Finally, the achieved new information is implemented into practice by collaboration with the designers and authorities, hoping to improve the lifecycle efficiency of road and railway structures.

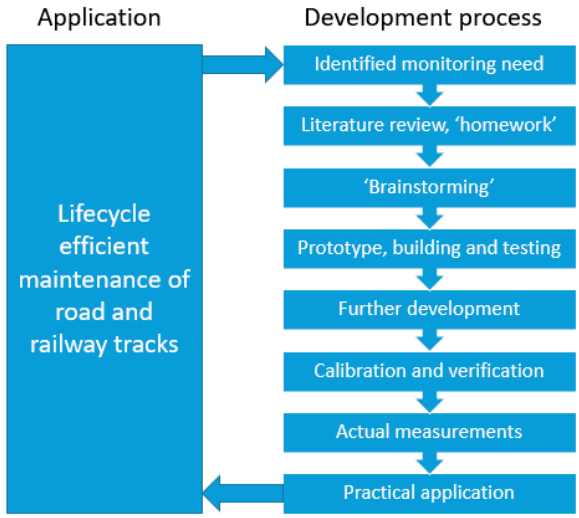

Figure 1.2. Methodology of the monitoring methods development process.

1.4. Thesis outline

This study combines the vertical deformation behaviour in both road and railway structures, as well as the related monitoring, because the phenomena taking place in the earth structures are very similar, regardless of the traffic mode. Many of the measuring methods developed during this study have been utilised in both environments, although the focus has been more on railway tracks. A number of universities and research institutes specialise in either road or railway research; however, in this study, a conscious choice was made not to separate these different modes of traffic. For this purpose, the aim was to retain the main attention of this study on the monitoring, but not to exclude the functioning of the structures either. Another main objective was to describe the phenomena that affect the functioning of the structure and require monitoring in order to detect and understand them.

The theory section of this study in Chapter 2 discusses the loads that roads and railway tracks are subjected to, load distribution in the structure, the various factors behind recoverable and permanent vertical deformation and background phenomena. The dissertation also includes a literature review on the measuring and monitoring methods used around the world. The research sections in Chapters 3 and 4 discuss the operating principle of the measuring methods that have been developed and used in practice, followed by a short description of their application, examples of the measurement results, and the main findings. Chapter 3 introduces point-based measuring methods, and Chapter 4 focuses on a continuously operating device to measure stiffness, developed for the railway environment. The measurement results are briefly discussed in Chapter

5 and summarised in Chapter 6, highlighting the main phenomena that develop permanent deformations in a road or track.

1.5. Author's contribution

The dissertation consists of several research and development projects that have been conducted between years the 2005-2015, while the author has worked as a researcher and a monitoring specialist at the Tampere University of Technology. The research work described in Chapters 3 and 4 includes only the development of measuring and monitoring techniques, in which the author has been significantly involved. In those projects, the author has been 'the brains' inventing the monitoring techniques, designing the instrumentations and the measurement devices, being in charge of instrumenting the test sites, conducting measurements, interpreting the measurement data and analysing the physical phenomena behind the results.

The author has been fully responsible for building the test arrangements in Vesilahti instrumented road (Section 3.3.1), the study on the railway bridge transition zones (Section 3.3.2), instrumented track in Viiala (Section 3.3.3), the settlement study in Paimio (Section 3.3.5) and several frost monitoring stations (Section 3.3.6). In the CTI tests carried out in Scotland (Section 3.3.4), the author had only a smaller role focusing on the instrumentation.

The author has developed several measurement devices by himself. These include:

- The use of accelerometers, originally from automotive industry, in road and railway track behaviour measurements. The author has developed the protection of the sensors and the integration process from acceleration to displacements.
- Multi-depth deflectometer (MDD). The author developed a new version of MDD, which is faster to install.
- Settlement pipe development. The author invented to sink an air pressure sensor into oil. This idea made it possible to build very accurate and cost efficient settlement measuring system.
- Frost monitoring station development. The author developed a concept of measuring temperatures and frost heave automatically. The author built the equipment and constructed several frost monitoring stations. Based on the measurement results, the author developed frost line interpretation methods. The concept of installing moisture gauges in a tube was also the author's idea and implementation.
- Stiffmaster – a rolling track stiffness measurement device. The author first sought for different possibilities to conduct such measurements in railway environment. Based on this survey, the author developed and constructed the measurement device, conducted measurements and analysed the measurement data. The process included the verification of the device and analysis of the measured deflections.

2. Unevenness of roads and railways—mechanisms and monitoring

2.1. Loadings

2.1.1. Traffic loading

Two main types of road and railway structure loadings can be distinguished: traffic loading and environmental loading. Traffic loading is created by loads due to moving vehicles. Traffic loading on a road is due to the transfer of a vehicle's static weight through its wheels to the road structure and through that to the ground. The amount of loading is influenced by the vehicle's permitted gross weight, the number of axles and their type, the number of tyres per axle and the type of tyre and tyre pressure (Figure 2.1) (Huang 2004, Ehrola 1996).

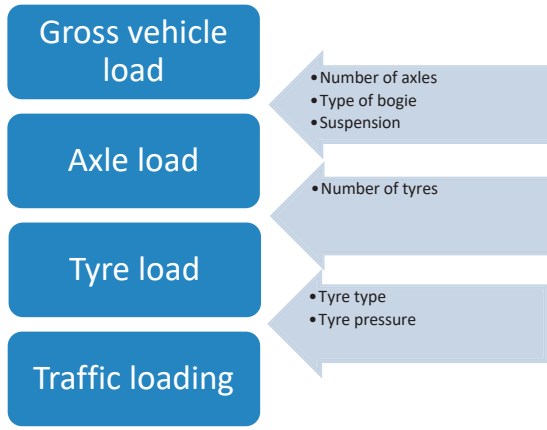

Figure 2.1. Traffic loading caused by a vehicle and factors influencing it (modified from Ehrola 1996).

In Finland, the largest permitted gross load of a vehicle is 76 t, which is significantly more than the maximum gross load of 40 or 44 t used in most other countries. With special authorisation, it is also possible to drive a so-called 'road train' that has a gross load of 90 t, and even 104 t gross loads are in test use. In certain demarcated areas of Australia and North America, road trains with a larger gross load than that in Finland are being used. In Finland, a vehicle is required to have nine axles if the maximum gross load (76 t) is in use. The greatest allowed axle load is 10 t, except in the case of driving axles, which are permitted an axle load of 11.5 t. Under certain conditions, either single wheels or dual wheels can be mounted on the axle. The maximum allowed wheel load is at most 5 t, because the driving axle must have dual wheels. The wheel load of dual wheels is always clearly smaller, at most 2.875 t (Finlex 2013).

The stresses on the road are ultimately determined in accordance with the tyre pressure used, because the tyre's contact pressure against the road surface is approximately the same as the tyre pressure. Some forestry companies allow only vehicles equipped with a central tyre inflation (CTI)

system to travel on a forest road network. It is possible to especially reduce the stresses of the upper part of the road structure by reducing tyre pressure (Vuorimies et al. 2012, Douglas 1997).

It is reasonable to assume the most significant traffic loading is almost entirely due to loads originating from heavy transport. The loading effects of passenger vehicles and vans over the lifetime of the road structure are only a fraction of the loading effects of trucks. The dependency between different wheel load is often estimated in a simplified manner by Equation (2.1) (Aasho 1962, Wu et al. 2004):

$$N = \left(\frac{P}{P_v} \right)^n \tag{2.1}$$

where

N is the stress effect of the number of loadings of magnitude P_v corresponding to a loading of magnitude P
P is the wheel load
P_v is a reference wheel load for which the value 50 kN is used in Finland
n is a parameter, for which the value $n = 4$ is usually given.

Traffic loading on a railway track is created when the train's static load is transferred to bogies, from the bogies to wheelsets, from the wheelsets to rails, through the rails to sleepers, and further to ballast, structural layers and subsoil. In Finland, the greatest permitted axle load is specific to the railway line and speed limit, but the maximum is 25 t. In Australia and North America, for example, it is possible to find higher axle loads; in Sweden, one railway line allows an axle load of 30 t. A single wheel load in Finland can be, at most, 155 kN (Rato 21), because due to uneven loading and torsion resistance of the bogies, the load is not necessarily evenly distributed among the wheels. The distribution of a train's wheel load to the earth structure significantly differs from that of a car's wheel load, because the rail as a stiff element divides the loads between several sleepers. It has often been assumed that approximately half the axle load falls directly on the sleeper underneath and one-quarter or one-fifth on the sleepers beside it (Figure 2.2) (Holm et al. 2002, Profillidis 2000). The vertical stiffness of the track affects the load distribution as follows. On a stiff track, the load is concentrated on a smaller area than on a flexible track. Owing to the rail's bending resistance, at a certain distance from the load, the sleepers are also affected by a

vertical force directed upwards. The magnitude of the upward force depends on the rail type, wheelbases and track stiffness.

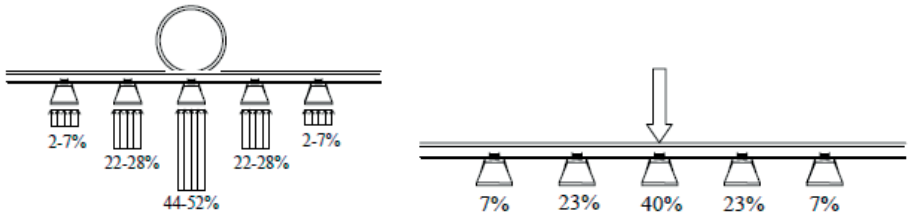

Figure 2.2. Distribution of vertical loading via rail on sleepers (Holm et al. 2002, Profillidis 2000).

The magnitude of traffic load directed on structural parts is affected not only by the wheel or axle load but also by the number of axles and their distance from each other. In road transport, the greatest permissible axle load is limited in accordance with the axle spacing so that when the wheelbase is 1.3–1.8 m, a bogie load of 18 t is allowed for two-axle bogies and 24 t for three-axle bogies. Axles farther than this are considered as separate axles (Finlex 2013). On the railway, the shortest permissible wheelbase is determined in accordance with the bogie load and the line category used (EN 15528).

From the perspective of the structure's load-bearing capacity, a short wheelbase increases the loading, especially on shallow embankments constructed on soft subgrade. The loading effect of densely positioned axles is combined deep in the structure, and the loading does not release between the axles. This increases vertical deformations, and the deformations accumulate, due to the effect of heavy trains in particular.

In addition to the static load, moving vehicles on a rough surface create dynamic forces. These are caused by different vibrations due to vehicle- and pavement-generated impulses. On the railway, the frequency of dynamic forces depends on the source of vibrations. Wheel or rail defects create very large-amplitude and high-frequency vibrations. On the contrary, longer wavelength roughness and stiffness variations create dynamic forces that are clearly of lower frequency (Samppala 2011). High-frequency vibrations are especially harmful to the rolling stock and rails, but the loading effect is quickly dampened deeper in the structure. Low-frequency vibrations penetrate the earth structure, creating additional loading, and they also spread widely to the surroundings, especially on soft ground (Esveld 2001). Dynamic mid to high frequency forces are generated especially in discontinuities and transition zones (e.g. when coming from soft ground to a bridge or tunnel). In these places, permanent deformations are often generated, which further increases dynamic loadings (Banimahd et al. 2012).

When evaluating the total impacts of loadings, static loads are increased sometimes with the help of an impact factor. Some countries' railways, including those of Finland, are undergoing a transition to a system in which wheel forces are measured and measurement results are utilised primarily in the evaluation of maintenance need of rolling stock (Lahti 2008, Numikolu 2013). The long-term goal is to remove from service any rolling stock that may be unacceptably harmful to the track.

2.1.2. Environmental loads

Environmental loads form another entity causing loads to the structure. Environmental loads are created as a consequence of variations in weather and seasons and are due to three factors: temperature, water and frost (Figure 2.3).

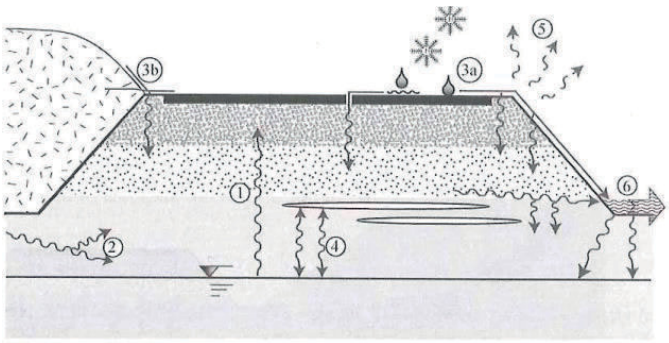

Factors contributing to water intake	1. Capillary rise
	2. Lateral moisture transfer
	3. Infiltration from precipitations
	4. Frost action
Factors contributing to moisture extraction	5. Evaporation
	6. Drainage

Figure 2.3. Environmental loads on the road structure (Doré & Zubeck 2009).

Fluctuations in temperature directly affect the properties of asphalts, because the bitumen binder material's viscosity is strongly dependent on temperature. As the temperature rises, bitumen softens and the stiffness of the asphalt layer decreases. Consequently, deformations due to traffic load will increase. In cold weather, bitumen hardens and the stiffness of the surfacing increases; at the same time, the risk of frost cracking also increases (Doré & Zubeck 2009, Huang 2004 and Roberts et al. 1996).

The water content of materials affects subgrade behaviour in particular; however, it also affects the behaviour of unbound structural layers. A high water content substantially weakens the load-bearing capacity of materials. Water ends up in the structure in various ways, via either rain or frost. Main roads are typically asphalted, which mostly prevents infiltration of water into the structure. On gravel roads and railways, a large amount of the precipitation is directly infiltrated into the structure. Water is most harmful to the structure when there is a great volume of water and the drainage has weakened. Traffic load can cause pore water overpressure in the material, strongly decreasing the strength and load-bearing capacity of the material (Dawson 2009).

In cold climates, frost is one of the largest loading factors, both directly and indirectly. When talking about frost, two basic phenomena must be distinguished: soil freezing and frost action. Soil freezing refers to freezing of the structure where the volume of soil does not increase. Frost action refers to freezing in the soil where frost heave occurs and the volume of soil increases. During the frost heaving process, ice lenses form in the freezing structure and cause frost heave, or growth in

the volume of the structure. The ice lenses form in the frost heaving structure via freezing of the water absorbed from ground or the soil layers below (Figure 2.4) (Nurmikolu 2005).

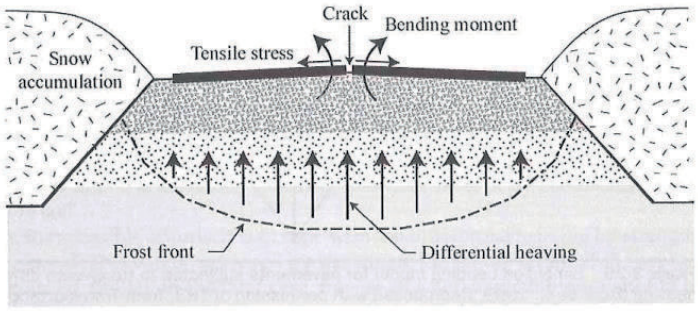

Figure 2.4. General process of frost heaving for roads (Doré & Zubeck 2009).

Frost heaving requires a freezing temperature, frost-susceptible material and water access to the material. If any of these basic requirements is not wholly realised or is lacking, frost heave will be limited or completely prevented. Frost heave usually takes place only in the subgrade or embankment, because the structural layers should be constructed of non-frost-susceptible materials. The materials in structural layers can form frost-susceptible materials due to degradation or mixing with the subgrade. The road structure in the middle of the cross-section freezes deeper than on the sides. This is due to the protecting effect of snow layers on the sides of the road. Moreover, frost heave is greater in the middle of the road. Owing to the unevenness of frost heave, tensile stresses that develop in the upper part of the structure can create a longitudinal crack on the pavement. Uneven frost heave in the longitudinal direction of the pavement causes roughness, which increases traffic loading (Doré & Zubeck 2009).

The new railway structure in Finland is dimensioned thick enough to prevent frost action in the subgrade. This is done in line with the freezing conditions (F50) occurring statistically once in every 50 years (Rato 3). However, most of Finland's railway tracks were built during a time when evaluation of the frost susceptibility of materials took place by visual inspection. Thus, some materials that are frost susceptible may have ended up in the structures (Pylkkänen et al. 2011). Along the older railway lines, there are also several sections where the thickness of the structural layers is not sufficient to prevent frost action in the subgrade or embankment material during winters that are more severe than average. If the subgrade experiences freezing, the frost heaves are often uneven, and this causes unevenness of the track, which results in dynamic loading.

Researchers who investigated stiffness and deformation properties during the freeze–thaw process include Simonsen et al. (2002) and Bilodeau et al. (2011). Soil freezing improves the load-bearing capacity of the pavement during wintertime. Problems associated with load-bearing capacity that are due to frost occur during spring when the frost starts thawing on the surface of the structure. As the lower structural layers are still frozen, the water released by thawing cannot properly drain from the road structure. The excess water causes weakening in the load-bearing capacity of the structural layers (Lekarp et al. 2000). In railway structures, ice lenses usually form rather deep in the structure; thus, unlike road structures, a similar saturation of the upper part of the structure

does not necessarily take place. Nevertheless, thawing frost and melting snow increase the water content of materials, and permanent deformations are thus most likely to be developed during spring thaw.

2.2. Structural behaviour under traffic loading

2.2.1. Resilient deformation behaviour of unbound material

Traffic loading creates displacements, the magnitude of which depends on the size of the load and the stiffness of the structure. Most of the displacements recover once the load has been removed, and most of the dimensioning and modelling methods for structures are based on this assumption (Huang 2004). Rails, sleepers and asphalt structures behave more or less elastically under traffic loading. The loading behaviour of asphalt also depends on temperature and loading speed, but that is beyond the scope of this thesis. However, the behaviour of a structure consisting of unbound soil materials is not completely elastic (Kolisoja 1997). Traffic loading on unbound material always creates both resilient and permanent deformations. The proportion between the two is dependent on the magnitude of the load and the strength of the material (Kolisoja 1997). When the load level is small, it can be assumed that the deformations will almost all be resilient. The proportion of resilient deformations increases if the same size of traffic load is repeated. The structure will become stable if the load level is sufficiently small in relation to the structure's load-bearing capacity (Lekarp 2000). After a certain amount of loading in triaxial tests, the strain–deformation cycle will settle down, and the deformation will become almost wholly recoverable (Figure 2.5) (Huang 2004).

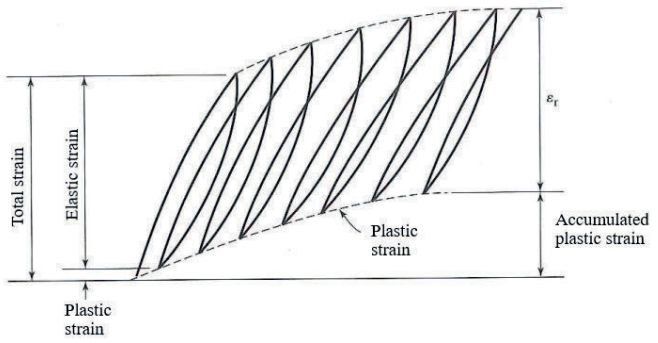

Figure 2.5. Strain–deformation behaviour of unbound materials under repeated loading (Huang 2004).

The relation between load and resilient deformation e_r presented in Figure 2.5 is used in the modelling of resilient (elastic) deformation of unbound materials in road and rail structures. The strain–deformation relation formed in this stabilised cycle is known as the resilient modulus. The resilient modulus is defined in accordance with Equation (2.2) (Seed et al. 1962, Kolisoja 1997):

$$M_r = \frac{\Delta\sigma_d}{\Delta\varepsilon_r} \tag{2.2}$$

where

M_r is the resilient modulus
$\Delta\sigma_d$ is the deviator stress range
$\Delta\varepsilon_r$ is the resilient deformation.

Soil materials are often non-linearly elastic. The resilient modulus of soil materials changes in accordance with the stress level mobilised in the material. For a description of the deformation behaviour of cohesion soils, the model resembling Equation (2.3) is often used (Baladi 1990):

$$M_r = K_1\left(\frac{\sigma_d}{\sigma_{d0}}\right)^{-K_2} \tag{2.3}$$

where

M_r is the resilient modulus [kPa]
σ_d is the deviator stress [kPa]
σ_{d0} is the comparison stress [1 kPa]
K_1 is the modulus number [kPa]
K_2 is the modulus exponent [constant].

The deviator stress σ_d can be calculated with Equation (2.4) (Huang 2004):

$$\sigma_d = \sigma_1 + \gamma z - 0.5(\sigma_2 + \sigma_3) - K_0\gamma z \tag{2.4}$$

where

σ_d is the deviator stress in a structure under load [kPa]
$\sigma_{1,2,3}$ are the principal stress components created by traffic load on the structure [kPa]
γ is the average bulk density of the structural layer materials above the level examined [kg/m^3]
z is the distance from the surface of the structural layer to the level examined [m]
K_0 is the coefficient of earth pressure at rest.

For non-cohesive soils, the strength of the material is based on the contact between interlocking grains. In that case, the stiffness of the material has been described as increasing as the stress level increases in accordance with Equation (2.5) (Brown & Pappin 1985). The difference when compared with cohesive soils is that, instead of deviator stress, the sum of the principal stresses is used in the equation.

$$M_r = K_1\left(\frac{\theta}{\theta_0}\right)^{K_2} \tag{2.5}$$

where

M_r is the resilient modulus [kPa]

θ is the sum of the principal stresses [kPa]
θ_0 is the comparison stress [1 kPa]
K_1 is the module number [kPa]
K_2 is the modulus exponent [constant].

The sum of the principal stresses can be calculated with the following equation (2.6) (Huang 2004):

$$\theta = \sigma_1 + \gamma z + \sigma_2 + \sigma_3 + 2K_0\gamma z \quad (2.6)$$

where

θ is the sum of the principal stresses in a structure under load [kPa]
$\sigma_{1,2,3}$ are the principal stress components created by traffic load on the structure [kPa]
γ is the average bulk density of the structural layer materials above the level examined [kg/m^3]
z is the distance from the surface of the earthworks to the level examined [m]
K_0 is the coefficient of earth pressure at rest.

Equation (2.6) uses the sum of the principal stresses, and it does not distinguish between the hydrostatic and deviator stresses. It has been noted that in coarse-grained soils, the deviator stress substantially affects the deformation properties of materials. For this reason, the equation for the resilient modulus has also been written in the form of Equation (2.7) (Kolisoja 1997, Uzan 1985). The sources mentioned above are excellent reference books if more in-depth information on the modelling of the deformation behaviour of unbound material is required.

$$M_r = K_1\theta_0\left(\frac{\theta}{\theta_0}\right)^{K_2}\left(\frac{q}{\theta_0}\right)^{K_3} \quad (2.7)$$

where

M_r is the resilient modulus
θ is the sum of the principal stresses
θ_0 is the comparison stress
$K_{1,2,3}$ are the material parameters
q is the deviator stress.

2.2.2. Distribution of stresses caused by traffic loading

The magnitude of deformations due to traffic loading depends on the stiffness of the material but primarily on the load level mobilised. Stresses in road structures can be calculated, for example, with the help of multilayer elastic programmes, which utilise Burmister's (1943) theory on the distribution of stresses and displacements. Vertical stresses are at their largest on the surface of the structure below the load, and stresses quickly decrease deeper in the structure. It has been observed that under Finland's conditions, the most critical stresses of the road structure are the tensile stress developing on the lower surface of the bound layer and the vertical stress created on the surface of

the upper unbound layer and the formation layer (Ehrola 1996). Two of these damage-causing mechanisms are shown in Figure 2.6 (Doré & Zubeck 2009). The stresses on top of the unbound layer are important in Finland, because rather thin asphalt layers are commonly in use.

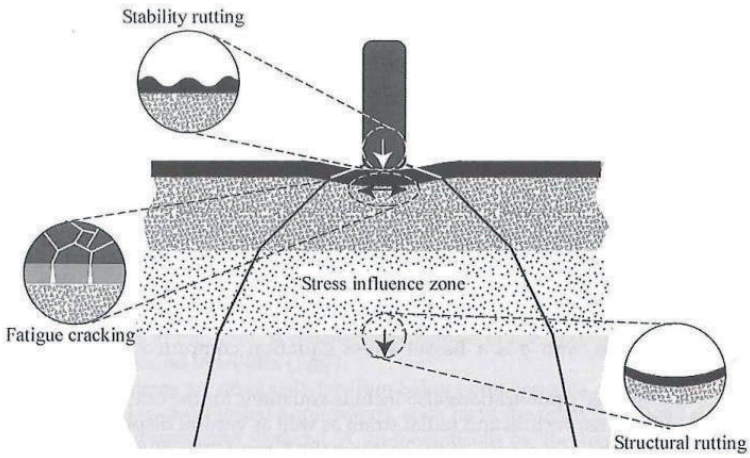

Figure 2.6. Critical stresses on the road structure, caused by traffic loading (Doré & Zubeck 2009).

Stresses on the railway structure are slightly more difficult to define than those that affect the road structure, because rails distribute traffic load on several different sleepers. A beam on an elastic foundation (BOEF), can be regarded as the classic method to resolve the rail's deflection, bending moment and shear stresses that are produced by the traffic loading (Esveld 2001). The method was first proposed by Zimmerman (1941). The method can also be used indirectly to find the force between the rail and the sleeper (*rail seat load*) and the average vertical stress between the sleeper and the supporting layer. The BOEF model is not suitable for the investigation of strains underneath the interface between the sleeper and the ballast layer.

The BOEF model is based on the modelling of both rails as a continuous Euler–Bernoulli beam on an elastic Winkler foundation, as shown in Figure 2.7. The Winkler foundation can be thought of as an indefinitely long succession of elastic springs uncoupled from one another. In Figure 2.7, Q represents a vertical wheel load, and k represents a spring constant of one spring (Hetényi 1971).

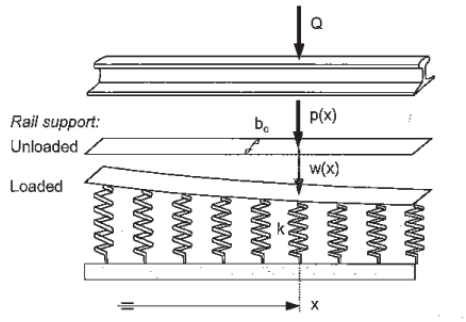

Figure 2.7. Euler–Bernoulli beam on the Winkler foundation (Esveld 2001).

The force *p(x)* that bears the rail on the Winkler foundation vertically can be defined with the equation (2.8) (Hetényi 1971)

$$p(x) = -u \cdot y(x) \tag{2.8}$$

where

$p(x)$ is the compressive force per unit length exerted on the rail at position x [N/mm]

x is the longitudinal coordinate [mm] in the direction of the rail

u is the track modulus [N/mm/mm]

$y(x)$ is the vertical deflection of the rail at position x [mm].

There is a minus sign in Equation (2.8) because *p(x)* in Figure 2.7 is in the direction contrary to the y-axis which in this case is downward positive (Hetényi 1971).

By taking the equilibrium equation between the force needed to bend the rail and the foundation resistance force according to Winkler, one arrives at differential equation (2.9) (Hetényi 1971):

$$EI\frac{d^4y}{dx^4} + uy = 0 \tag{2.9}$$

where

E is the modulus of elasticity for rail steel [MPa]

I is the moment of inertia of the rail [mm^4]

u and y are the same as in Equation (2.8).

The solution of the differential equation (2.9) can be carried out with the following boundary conditions (Hetényi 1971):

1. y approaches zero as x approaches infinity
2. y'' (the curvature) approaches zero as x approaches infinity

3. when $x = 0$, $y' = 0$
4. when $x = 0$, y''' has the value of $0.5 \cdot Q_d$

The solution of Equation (2.9) for curvature is Equation (2.10) (Hetényi 1971):

$$y(x) = \frac{Q_d}{2uL} \cdot e^{-\frac{|x|}{L}} \left(\cos\left(\frac{x}{L}\right) + \sin\left(\frac{|x|}{L}\right) \right) \tag{2.10}$$

where

$y(x)$ is the vertical deflection of the rail at position x [mm]

Q_d is the vertical wheel load [N]

u is the track modulus [N/mm/mm]

e is Neper's number ≈ 2,718 [-]

x is the longitudinal coordinate with its origin at the point where the load is applied [mm]

L is a *characteristic length* or *base length* that can be defined with Equation (2.11):

$$L = \left(\frac{4EI}{u} \right)^{\frac{1}{4}} \tag{2.11}$$

where

E and I are the same as in Equation (2.9)

L and u are the same as in Equation (2.10).

The rail bending moment M is obtained by twice differentiating x and multiplying it by the rail's negative bending stiffness EI (Equation (2.12)) (Hetényi 1971):

$$M(x) = \frac{Q_d \cdot L}{4} \cdot e^{-\frac{|x|}{L}} \cdot \left(\cos\left(\frac{x}{L}\right) - \sin\left(\frac{|x|}{L}\right) \right) \tag{2.12}$$

The symbols in Equations (2.10) and (2.11) can also be applied to Equation (2.12). Figure 2.8 shows, longitudinally, the deflection form of the rail and the form of the bending moment.

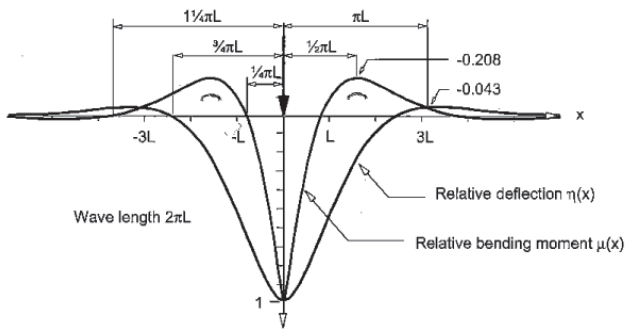

Figure 2.8. Influence lines of the rail's deflection and bending moment (Esveld 2001).

Combined effect of multiple axles

When the BOEF model is linear, it is possible to apply the superposition principle to it in the case of multiple axles or wheel load. For example, the magnitude of a deflection at $x = 0$ created by the combined effect of wheel loads at different distances can be arrived at in accordance with Equation (2.13) using the sum of the deflections calculated in Equation (2.10) (Hetényi 1971).

$$y_{sum,x=0} = y(x_1) + y(x_2) + ... + y(x_i) \tag{2.13}$$

where

$y_{sum,x=0}$ is the total deflection at x = 0 [mm]

x_i is the distance of the wheel load from the zero point of the x-axle [mm].

The combined effect of several axle or wheel loads at different distances on the deflection in Equation (2.10) can also be shown with the help of an influence line. The form of the influence line arises from Equation (2.10), from its $\eta(x)$ part that lacks a constant coefficient and is presented in Equation (2.14). The symbols are the same as in Equation (2.10) (Hetényi 1971).

$$\eta(x) = e^{-\frac{|x|}{L}}\left[\cos\left(\frac{x}{L}\right) + \sin\left(\frac{|x|}{L}\right)\right] \tag{2.14}$$

With certain combinations of wheelbases and track properties, the maximum deflection values decrease when compared with the case of a single axle. This kind of situation occurs, for example, when the wheelbase is $\pi \cdot L$ (Esveld 2001).

2.3. Appearance of permanent deformations

2.3.1. Unbound material in traffic loading

Permanent deformations keep developing in the structure, because not all deformations caused by traffic loading are resilient. Permanent deformations appear on the surface of the structure, often as a consequence of wearing of the material. However, surface defects are not included in the scope of this work. After wearing, the second most significant permanent deformations to the structure are accumulated in unbound structural layers if the thickness of the structural layers is sufficient to prevent subgrade deformations. Chai & Miura (2002) observed, in their research, that the effect of traffic loading on vertical deformations is significant to a depth of 2 m, and the effect of traffic loading, in practice, disappears at a depth of 6 m. This observation indicates that frost-dimensioned road and railway structures with rather thick unbound structural layers are prone mainly to permanent deformations of structural layers. Subgrade deformations due to traffic loading become dominant when the thickness of unbound structural layers is small.

The permanent deformation accumulation of unbound material is affected, among other things, by the following (Lekarp et al. 2000):

- loads (strain level, rotation of the principal stresses, number of loadings, load history),
- materials (granularity, maximum grain size, fines, strength, mineralogy, type and amount of binding agent) and
- state and condition of materials (compaction state/post-compaction, moisture, temperature, freezing and thawing, structural geometry).

It has been noted in numerous literature sources that the stress level is one of the greatest factors that affects permanent deformation accumulation in unbound materials. It has also been observed in several triaxial tests that the accumulation of permanent deformations is related to the growth of deviator stress, and the growth of confining pressure, in turn, reduces deformations (Lekarp et al. 2000).

A wheel creates a stress state in the structure. This can be described with the help of two principal stress directions. The principal stresses are directed vertically and horizontally below the load's centre point. Farther away from the load's centre point, the principal stress directions begin to turn so that the largest principal stress turns towards the load centre point or perpendicularly against it (Lekarp et al. 2000). As the wheel moves, the location of the load centre point changes, and the principal stress directions turn into the position described above. The movement of the load point causes rotation to the principal stress components (Figure 2.9).

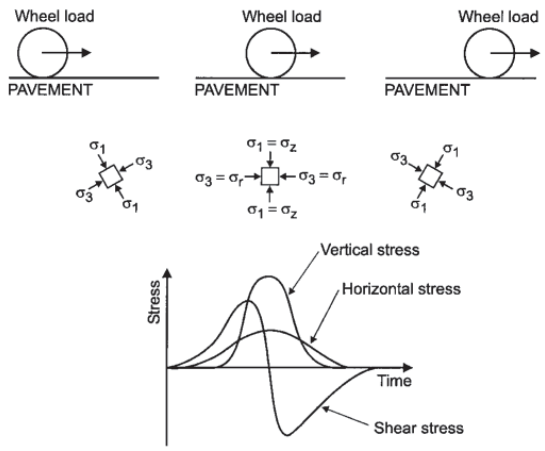

Figure 2.9. Rotation of principal stresses in a road structure under traffic loading (Lekarp et al. 2000).

As a result of rotation of the principal stresses, the stresses are not always directed perpendicularly against the surface of the grains. The grains may, in this case, slide past each other, which will cause reorganisation of the material particles. The particles always move towards a balance corresponding to the stress state. The particles can move closer to each other, in which case the structure will become more compact. Moreover, the particles can move past each other to a new position, developing a rut below the load and a crest beside the load. This phenomenon is known as plastic deformation (Kolisoja 1997).

Stress history also affects the development of the permanent deformations of unbound materials. During their triaxial experiments, Brown & Hyde (1975) found that the stepwise increase of stress level leads to a clearly larger accumulation of permanent deformations when compared with circumstances where a triaxial experiment is started with a large load level. This was thought to be a result of stiffening of material due to repeated loading and a decrease in the growth of permanent deformations. When a large load is added immediately at the start of the experiment, there will only be one of these stabilisation stages, not several as in the experiment carried out stepwise.

The water content of a material has a clear effect on the emergence of permanent deformations. Growth in the water content weakens the unbound structural layers and subgrade, and the magnitude of permanent deformations will increase. As the water content increases close to a state of saturation, permanent deformations will increase very rapidly. Figure 2.10 shows the dependency of the effects of water content and fines content on the magnitude of permanent deformations. Moisture conditions can be influenced by drainage in the structure. Proper drainage and correct material selections can help maintain the water content at a desired level.

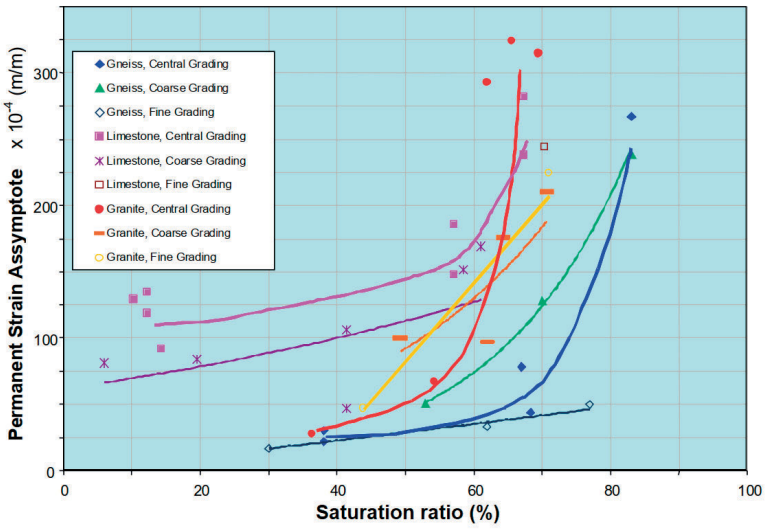

Figure 2.10. Effect of water content on permanent deformations (Dawson et al. 2004).

The degree of compaction has been found to have a clear effect on the accumulation of permanent deformations. Increasing the degree of compaction clearly decreases permanent deformations, especially in the case of crushed materials (Lekarp et al. 2000). Because the connection is clear in triaxial tests, the significance of compactness is even more important in the real structure where the load moves and uses different driving lines. A weak degree of compaction enables the movement of particles in relation to each other.

The grain size distribution, amount of fines and grain shape also influence permanent deformations. The relationships among them are specific to the material; however, according to Lekarp et al. (2000), optimal grain size distribution is the most important of these in decreasing permanent deformations. Angular, sharp-edged grains lock in better than rounded grains, increasing the friction angle and decreasing the deformation level (Kolisoja 1997). The addition of fines also often promotes the emergence of permanent deformations (Kolisoja et al. 2002).

2.3.2. Degradation of railway ballast

Most permanent deformations of the track structure under Finland's conditions are caused by deformations in the ballast. Degradation into finer particles and compacting are the most important factors. Other causes of permanent deformations in the track structure include spreading of the embankment material and subgrade deformations (Chapters 2.3.3 and 2.3.4). In Finland, the degradation of ballast is mainly due to traffic loads and maintenance (tamping) and, to a smaller extent, to chemical weathering. Elsewhere, for example, a ballast layer built of limestone is clearly more prone to chemical weathering, and significant amounts of fines can also find their way from external sources, from coal wagons, for example (Selig & Waters 1994). The mechanism of the degradation of ballast into finer particles is dealt with in Nurmikolu's (2005) thesis, where the degradation is described as a result of grain edges breaking due to high loads. As a result of this, the grains move past each other and to a new position where the material can again carry the loading. Smaller grains are created in the process, and once the degradation has advanced far

enough, the grain size distribution of the material becomes clearly finer. At the same time, the degree of compaction of the material increases, and the elevation of the track consequently is brought permanently lower. The geometry of the track is fixed by tamping: the track is lifted to its correct position, and ballast material is pushed under the sleepers. As a result of the tamping, the grain edges are again brought to face each other, and due to their small contact area, the edges again break down. Therefore, the accumulation of permanent deformations is accelerated by the provided maintenance, even though the position of the track is shortly corrected.

The degradation of ballast inevitably leads to the development of permanent deformations, which appear as a settlement in the rail's elevation (Figure 2.11). When this occurs similarly along the line, the slow subsidence appears as roughness only around fixed points, such as bridges or level crossings. Degradation can also be uneven; as a result, roughness can appear in track sections where the track structure does not have any structural discontinuity.

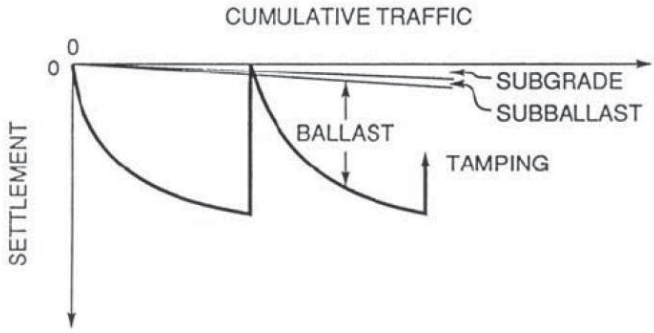

Figure 2.11. Schematic diagram of the effect of various structural layers on permanent deformations of the track (Selig & Waters 1995).

The degradation of ballast weakens it; finally, its characteristics have weakened so much that tamping results in only temporary help to the track's elevation. The limit values for cleaning, which are based on grain size distribution, have been defined for the ballast. After reaching a certain limit, it would be reasonable, in line with lifecycle economics, to clean or replace the ballast. Moreover, when the ballast weakens, its water retention capacity increases and the degradation becomes more rapid. The growth in water content accelerates the degradation process several times, which leads to the hanging sleepers. Cyclic loading together with the high water content and hanging sleepers will lead to very fast degradation of the ballast. In the worst-case scenario, the ballast turns clayish, which can make the ballast a frost-susceptible material (Nurmikolu & Kolisoja 2008).

2.3.3. Deformations of embankment and subgrade

In Finland, railway tracks have rather thick structures to provide frost protection. To save materials, embankments are made as narrow as possible and with steep slopes. It has been observed, in connection with maintenance, that the traffic loading causes settlement on the track, and the embankments widen. Kalliainen (2011) carried out a series of experiments and modelling on embankment width and slope angle. The research found that permanent deformations of the

embankment are developed by shear strain deformations due to traffic load. The magnitude of a permanent deformation is dependent on the width of the embankment and the slope angle, but above all else on the stiffness of the subgrade. The level of shear strain deformations on the embankment is determined by the stiffness of the subgrade, because large deformations affecting the embankment originate from the subgrade. As a result of the research, the practice of dimensioning the embankment width on the basis of deflection of the track due to train load was initiated. Deflection of the track was assumed to primarily indicate the characteristics of the subgrade. The development of permanent deformations to the embankment is thus managed by limiting the deformation level. If this is not possible, the secondary alternative for the management of deformations is to widen the embankment or reduce the angle of its slope.

The assumption of the dimensioning method is that the deflection of the track can be measured sufficiently reliably. The instructions (Rato 3) propose a measurement method for track deflections. The measurement method is based on accelerometer sensors, where the track's elasticity is estimated on the basis of the deflection caused by a train load. The assumption is that the effect of the structural layers on the stiffness of the track is small (Selig & Li 1994) and that the sleepers are well supported by the ballast layer. To manage the variation of the sleeper support condition, measurements are made from the middle of the sleeper, and only three of five middlemost measurement results are taken into account.

Relatively speaking, permanent subgrade deformations due to traffic loading are significant when the structural layers are made of good-quality materials; however, when the structures are thin, traffic loading is large and the subgrade is of poor quality (Dawson & Kolisoja 2004). In Finland, frost dimensioning of the track has led to rather thick structures, and subgrade deformations often present no problem. Elsewhere around the world, the situation in this respect is different, because the track structure may consist only of the ballast layer, which may or may not have only a thin formation layer beneath it. The most typical subgrade deformations due to traffic load are progressive shear failure (Figure 2.12) and excessive plastic deformation or ballast pockets (Figure 2.13) (Li & Selig 1998). These damage mechanisms mainly occur in fine-grained subgrades, and the magnitude of the deformation can be estimated with the help of deviator stress, compression strength of the subgrade and number of loadings. These damage mechanisms can be avoided by thickening the structural layers.

Other subgrade deformation mechanisms include subgrade attrition (by ballast) with mud pumping, massive subgrade shear failure (slope stability failure), and excessive consolidation settlement due to self-weight (Li & Selig 1998). The last two are not affected by traffic loading as significantly, and they cannot be prevented by building more structural layers; rather, it is the other way round (Mansikkamäki 2015).

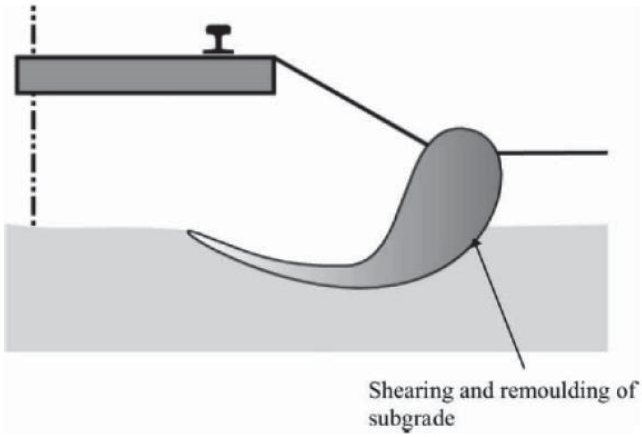

Figure 2.12. Progressive subgrade shear failure (Selig & Waters 1994).

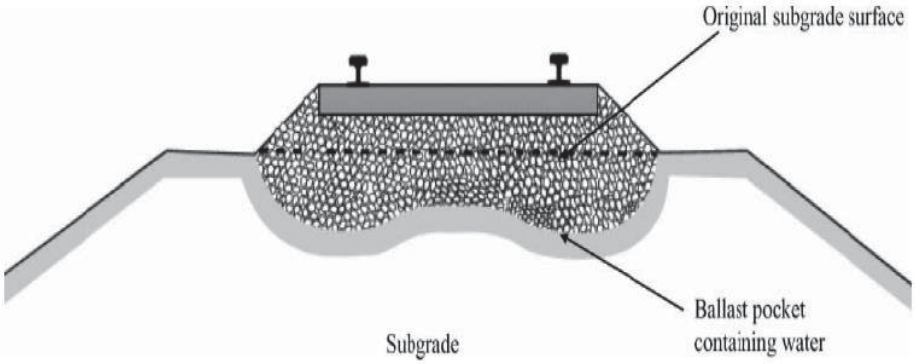

Figure 2.13. Excessive subgrade plastic deformation (Li & Selig 1998).

2.3.4. Settlement of the embankment

For numerous reasons, an embankment built on the soil generates permanent deformations after its construction. Traffic loading can develop permanent deformations in the embankment itself or in the subgrade, as noted in the earlier chapters. An embankment based on soft subgrade, however, often settles because of the subgrade deformations caused by the structure's own weight. The settlement is mainly due to the compaction of fine-grained material when water leaves it (Holtz & Kovacs 1981).

Settlement classes can be separated from each other in accordance with their nature and duration as follows (2.16):

$$S = s_i + s_p + s_\tau + s_s \tag{2.15}$$

where

S is the total settlement

s_i is the initial settlement
s_p is the consolidation or primary settlement
s_τ is the shear settlement
s_s is the secondary settlement or creep.

Initial settlement s_i takes place immediately after the load is added. In cohesive soil, the initial settlement occurs under undrained conditions and does not cause any change in volume. A settlement requires sideways movement of the soil (shear deformations). In friction soils, the settlement type is referred to as *immediate settlement* to differentiate it from the initial settlement in cohesion soils. The immediate settlement in friction soil takes place under drained conditions; as a consequence, the volume of the soil is reduced (McCarthy 1977).

In practice, consolidation settlement and immediate settlement cannot be differentiated from one another. In consolidation settlement s_p, the volume of the soil layer reduces and the layer becomes more compact (i.e. it consolidates). Water leaves the saturated soil, and the volume of soil becomes smaller as a result. As the water permeability of fine-grained soil is small, the consolidation event progresses very slowly. The settlement speed can be estimated with the help of water permeability and drainage distance (McCarthy 1977).

Settlement s_τ due to shear stresses is important only when the confidence against the failure of the subgrade is small. The settlement type does not have great importance in house building, but in the construction of road and railway structures it is important. By nature, settlement is plastic, slow movement of the soil mass. The embankment's stability can also be evaluated by measuring settlement (Skempton 1951).

Secondary settlement s_s is assumed to begin only once consolidation settlement has ended. It is very slow and continuous and has a creeping nature. This type of settlement is of importance mainly in organic peat and mud layers, because there the aggregate is strongly compacting (Craig 1997).

For all the settlement types presented above, settlement from the perspective of traffic is harmful, because the settlement generally occurs unevenly. Unevenness is developed especially in the transition zones of the subgrade, where the thickness or characteristics of the soil layer vary substantially. In Finland, several track sections were built on soft soils when the permitted axle loads were significantly lower than today. As the axle loads have continued to increase, the confidence against shear failure has decreased (Mansikkamäki 2015). In numerous cross-sections, a situation has arisen where the confidence against shear failure is not sufficient when calculated in accordance with current guidelines. However, the Finnish Transport Agency has provided guidelines to the effect that, in the existing tracks, a smaller safety factor against shear failure can be allowed if the embankment is being monitored (Rato 3). One way of carrying out the monitoring is to measure the settlement of the embankment, because a continuous settlement resulting from shear stresses indicates weak stability.

2.3.5. Deformations due to frost action

Frost is an important factor in causing structural deformations in cold climates. The freezing of pore water in soil, or soil freezing, does not necessarily cause deformations in a structure if the structure consists of non-frost-susceptible materials. This so-called massive frost in fact only increases the structure's load-bearing capacity. If the material is below groundwater level (i.e. the voids are completely saturated with water), the increase in volume due to the freezing of water causes slight frost heave because the water expands 9% when transformed into ice. For cost-related reasons, non-frost-susceptible structures are often built so thin that the frost can, at least during severe winters, also penetrate the subgrade. If the subgrade is composed of frost-susceptible materials, frost heave starts appearing under the effect of water flowing on the frost boundary. The volume of material thus increases, appearing as roughness on the surface of the structure (Andersland & Ladanyi 2004).

Frost heave in materials is a very complex phenomenon, which even the academic community finds difficult to explain satisfactorily. Frost action phenomena are possible in a suitable fine-grained material with proper water permeability, the presence of water and a sufficiently low freezing temperature (Pylkkänen et al. 2014, Nurmikolu & Kolisoja 2008). Frost heave can be prevented with massive loading, but this is only possible in rare cases and when the material is frost susceptible in a sufficiently weak manner. Often, the frost heave pressure is so great that no structure can prevent it. For example, Radd & Oertle (1973), in their laboratory experiments, observed that clay can have up to 20 N/mm^2 frost heave pressure.

Water is attached to the surface of the grains in a number of ways. Adsorption water is strongly attached to the surface of the grains and its bindings make it possible for the water to remain liquid even at temperatures below 0°C. In fine-grained materials, the grain's specific surface area is large and in relation to the volume of the material, there is a great deal of adsorption water. When the temperature falls below zero, a partially frozen layer is created on the boundary between the frozen and the non-frozen soil. The gravitational water has frozen in the partially frozen layer, which further reduces the volume of voids; however, the adsorption water still remains unfrozen. This enables the water to flow through the partially frozen layer to the frost boundary, where the water freezes causing segregation (i.e. the formation of ice lenses). The water flows to the frost boundary, because in the partially frozen layer cryo suction is increased, which moves water up from the unfrozen material. The magnitude of cryo suction is dependent on the temperature gradient and the diminished volume of voids (Ladanyi & Shen 1989).

The likelihood of the road and railway structure to experience frost heaving is usually noted during more severe than average winters when the freezing temperature penetrates to the frost-susceptible layer, causing significant frost heave. The phenomenon is noticed as surface roughness because frost heaving rarely takes place extensively and evenly. Frost heave as such does not create any significant harm to traffic, even though it may be necessary to set speed limits due to the roughness of the track. In very severe winters, the frost heaves may cause such high unevenness that it forms a serious safety risk for traffic operations. Actual frost-related problems appear usually when the frost thaws during spring. During the frost heave process, excess water finds its way into the structure as ice lenses, which begin to melt. The frost mainly thaws from the surface downwards

and significant amounts of water are released from the ice lenses to the structure. This combined with thaw waters from snow and the poor water permeability of the frozen structure underneath gives rise to significant weakening of the load-bearing capacity and is the main reason for the bad state of roads during thaw periods. This is a major problem for low-volume roads, where structures are thin and the drainage is poor. As a result of the softening due to thaw, both resilient and permanent deformations are clearly larger than during other seasons (Aho & Saarenketo 2006).

Thaw weakening and increased accumulation of permanent deformations related to springtime can also occur in materials that have not frost heaved. For example, the degradation of ballast into smaller particles continues throughout winter; however, only during spring after the frost thaws, the grains are able to be properly reorganised. This process increases the accumulation of permanent deformations during spring thaw (Metsovuori 2013, Pylkkänen & Nurmikolu 2015).

2.4. Monitoring methods related to deformations

2.4.1. Geometry inspection

The roughness requirements for tracks are very strict because of the high speeds of railway traffic. Finland's railway network is divided into maintenance levels, which have different speed limits and maximum permitted axle loads corresponding to the speeds. The track geometry is inspected several times per year depending on the maintenance level, at most 6 times a year. The track inspection variable that best describes vertical deformation behaviour is the deviation of longitudinal level that is measured continuously with the help of a track recording vehicle. In Finland, the measurement is carried out as a mid-chord offset and the measurement results are examined with the aid of a 5-m chord. In many other countries, a wider 3–25-m wavelength range is used (EN 13848-2). Table 2.1 shows the limit values for longitudinal level variation in accordance with the irregularity classification. C-class irregularity refers to an irregularity in its initial stage, D-class irregularity must be included in the maintenance plan and maintained in the near future and *-class irregularity must be immediately maintained or speed restrictions must be set (Ramo 13 2004).

Table 2.1. Limit values (mm, 5-m chord) used in track inspection for longitudinal level.

Irregularity class	Level of maintenance							
	1AA	**1A**	**1**	**2**	**3**	**4**	**5**	**6**
C	2	2	3	4	5	6	7	8
D	4	4	5	6	7	8	9	10
*	7	7	8	9	10	12	13	14

Table 2.1 shows that on the best 1AA maintenance levels, the permitted deviation of longitudinal level is very small: only 2 mm along a distance of 5 m. This kind of deviation can easily appear in the track's discontinuity points (e.g. in bridge ends). The requirements for longitudinal level does not, in practice, allow frost heave or settlement either, because these typically develop unevenly.

EN standard 13848-2 (2006) defines the measurement principles for track recording vehicles. For longitudinal level deviation measurements in track inspection, chord measurement is generally

used. It can be carried out with the help of either a measuring wheel or lasers. Another method that is being used more and more is inertia measurement, which is based on acceleration sensors or angle speed sensors that measure movement. Methods based on measuring wheels or lasers function just as well from very slow speeds up to reasonably high speeds of 80 km/h, for example. Normally, inspection speeds exceeding these are not recommended. On the contrary, inertia measurement (at least in theory) works better the faster the inspection speed. With the slowest driving speeds, the measurement accuracy of inertia measurement may suffer due to its sensor properties.

For the evaluation of roughness on roads and streets, the international roughness index (IRI) is generally used, which is a roughness indicator launched in 1986 by the World Bank. According to Sayers (1995), IRI is calculated from a measured longitudinal road profile by accumulating the output from a quarter-car model and dividing by the profile length to yield a summary roughness index with units of slope. IRI measurement was carried out at a speed of 80 km/h, where the vertical movement of suspension is measured in relation to the distance driven. Later, IRI was also calculated with the help of the measurement results by a profiler measurement car. IRI is, in principle, a unitless constant, but often units of mm/m or m/km and, in the USA, also in/mi are used. IRI does not distinguish between roughness wavelengths; thus, an IRI of the same magnitude can result from a single sharp and deep hole or from the roughness of several smaller and longer waves. For example, Kropáč & Múčka (2005) observed the underlying problems in IRI and warned about them in their article. According to this source, with respect to vibrations that the passenger experiences, IRI gives results that differ from those of accelerometer measurements taken from the human head, and the results vary between different vehicles.

Another indicator used earlier for the measurement of road roughness is the present serviceability index (PSI). In connection with the AASHO road experiments, the indicator was defined as the average of surface slope variance. The definition of the indicator was originally based on a CHLOE-type profilometer, which resembles the chord measurement used in track inspection (Sun 2001).

The ability to measure the roughness of the road or track surface correctly is important, and managing roughness requires good data about its emergence. Maintenance should be emphasised in areas where the most roughness is found.

2.4.2. Traffic loading measurement methods

The appearance of roughness on a road or railway track is greatly affected by the mobilised load level. Several different methods can be used to measure loads, and the owners of roads and railways use, for example, weight stations and wheel impact load detectors (WILD) to monitor vehicle loads. At its simplest, load accumulation can be evaluated by calculating the number of vehicles passing a cross-section and evaluating the portion of heavy trucks among that number. The deformation behaviour of the road and railway structure is not, however, explicable merely on the basis of the number of vehicles: to understand the loading mechanism, more accurate knowledge about the loadings caused by single axles and even by single wheels is needed.

Today, several countries use WILD stations, which measure loads due to trains' wheels. With the help of WILD stations, static and dynamic load due to a single wheel and a total train load can be found. WILD stations are used primarily to find faulty wheels for two different reasons: the railway infrastructure manager is interested in removing faulty wheels from traffic to prevent them from damaging the track, and the operator is interested in repairing any rolling stock unit that is on the verge of breaking down, thus minimising operating costs. WILD stations are manufactured by a number of different suppliers using techniques that vary, but most often the measurement is based on strain gauges positioned either on the rails or on load cells between the rail and the sleeper. As the fault in a rolling wheel hits the rail only at a certain frequency, WILD stations measure impacts on the track for a distance of two wheel revolutions. Thus, a possible fault creates a load peak twice during the pass. The magnitude of wheel faults is estimated either directly as force (kN) or with the help of an impact factor, which describes the relationship of dynamic load to static wheel load. The latter method also helps in identifying faulty wheels of unloaded wagons (Stratman et al. 2007).

Wheel loads can be measured from the rail, in a rather simple manner, with the help of strain gauges. The measurement is based on the measurement of the rails' shear forces with 16 strain gauges (Figure 2.14). The strain gauges are typically attached on the rail between two sleepers at an interval of 0.25 m from each other, and efforts are made to keep them on the rail's neutral axle. In the example of the figure, the gauges were attached on both sides of the rail, and the wiring was done in such a way that the measurement of the axle load could be made with one measurement channel.

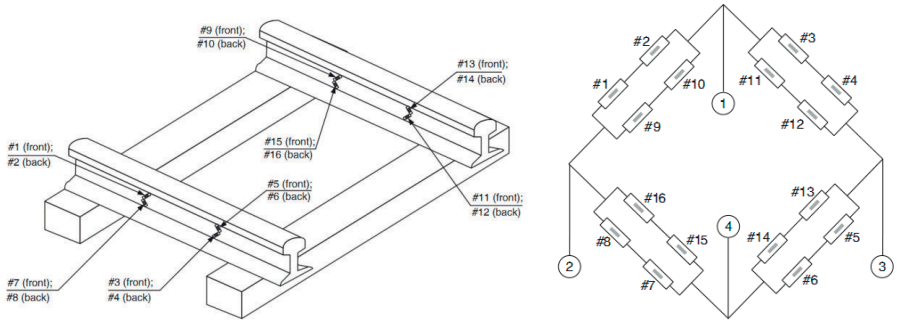

Figure 2.14. Determination of wheel loads with the help of strain gauges attached on the rails (Remennikov et al. 2008).

The weighing of axle loads can be carried out with a somewhat simpler wiring, one rail at a time, from only one side of the rail, in which case the instrumentation will consist of only two strain gauges measuring crosswise to each other. In this case, a wheel load is measured, and the axle load can be found by adding up the loads of the same axle. This type of instrumentation has been used in several monitoring sites conducted by the Tampere University of Technology (TUT). The instrumentation is calibrated with a known axle load or by loading the rail with a known load with the help of a hydraulic jack. The wiring used by TUT is shown in Figure 2.15.

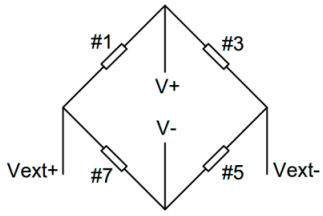

Figure 2.15. Wheatstone bridge connection for the measurement of wheel load from a rail. The numbering of strain gauges is the same as in Figure 2.14.

On roads, weight in motion (WIM) stations are used to measure traffic loading. Generally, they are meant for the identification of overloaded trucks and trailers (Jacob & O'Brien 2005). The measuring station can be located either in the road structure or in a bridge. It is not the specific purpose of WIM stations to measure road structure loadings but to measure vehicle loads. The maximum axle loads and the gross weight of vehicles are regulated by the law, and exceeding the limit values has been made illegal. The aim of the legislator in limiting the weights has been, apart from increased safety, the durability of road structures and bridges. Thus, WIM stations could be utilised more also from the viewpoint of the durability of only road structures. The operation of WIM stations is usually based on piezoelectric transducers, but fibre-optic sensors have also been used. The first sensors from the 1950s to the 1970s were plates based on strain gauges (Figure 2.16). They were accurate; however, their installation required significant effort, and the road structure could also suffer damage (Jacob & Feypell-de La Beaumelle 2010).

Figure 2.16. Two WIM stations: bending plates on the left and piezo-ceramic strip sensors on the right (Jacob & Feypell-de La Beaumelle 2010).

2.4.3. Measurement methods for stiffness

Falling weight deflectometer and similar measurement devices

The falling weight deflectometer (FWD) is a commonly used measurement method for stiffness, at least on roads. FWD has a freely falling weight, which is dropped from a chosen height. The deflection of the structure is measured with geophones or accelerometer sensors, both underneath the load and from various distances on the sides of the load point (ASTM 2009). Typically, the aim is to produce a load of 50 kN, which corresponds to the wheel load of a truck. With the help of the measured deflection basin, it is possible to 'back-calculate' the stiffness of the structure's different layers. FWD was developed in Scandinavia, and it has been found to be relatively accurate in describing wheel loads under different conditions. In North America, Dynaflect has

also been used; its action is based on the oscillation of a mass and the measurement of deflection caused by dynamic loading. Measurement methods preceding these include (i) the Benkelman beam, the operation of which is based on a dial gauge measurement of the deflection basin caused by a truck, or (ii) the plate bearing test, which is a completely static deflection measurement method. In Denmark, the travelling deflectograph has also been used: it is a slightly more automated version of the Benkelman beam and characterised as a continuous-operation measurement method (Tholen et al. 1985).

FWD is usually used directly on the surface of the structure, which is natural in the measurement of road structures and the track's formation layer. On the contrary, it is more difficult to use FWD on rails. At least in the United Kingdom, FWD has been used to measure track stiffness by modifying the device carried in a trailer so that it can move along the rails. In test measurements in Herefordshire, a load of 125 kN was used: the weight was dropped on a sleeper detached from the rails. This was done via a 1.1-m-long beam and a rubber-coated plate equipped with a load cell (Burrow et al. 2007). The beam's points of support were located near the rails distributing the load more on the end of the sleepers than on the centre area. The duration of the loading impulse in the measurements was approximately 40 ms. It is thought that this system will produce a load like that of a single axle moving with great speed on the track. Later, URS Infrastructure and Environment Ltd. (Sharpe 2014) developed a wholly new FWD for use in track environments (Figure 2.17).

Figure 2.17. FWD developed by URS Infrastructure and Environment Ltd. for track use (Sharpe 2014).

Even though the loading event of FWD has a dynamic character, several sources use the term *quasi-static sleeper stiffness* to refer to the stiffness measured (Brough et al. 2003, Burrow et al. 2007).

Moreover, lighter, portable applications (light falling weight deflectometer, LFWD) of the device have been developed: the mass of the falling weight of these is typically 10–20 kg, the height of the drop is less than a metre, and the diameter of the loading plate is 100–300 mm (ASTM 2011). LFWD does not have separate geophones; the deflection is measured only from the centre of the loading. Owing to its small load, the loading impact of the portable device does not penetrate very

deep; hence, the device is not suitable as such for the measurement of track stiffness. However, LFWD has been used in track environments: for example, for the detection of empty spaces under sleepers, for which it was found to be very useful (Kim et al. 2006).

Track loading vehicles

Track loading vehicles (TLVs) used for the measurement of stiffness take advantage of their own weight for loading the track. Typically, loading is produced with the help of hydraulic jacks and applied on top of the rails. The loading can also be applied on a sleeper detached from the rails. Simultaneously, any vertical deflection caused by the loading is measured. The magnitude of the loading and adjustment possibilities vary according to each vehicle (Berggren 2009).

In the United States, a measurement vehicle called DECAROTOR developed by Transportation Technology Centre, Inc. (TTCI) has been in use. It was originally developed for research of the stability of a rail gauge in connection with the AAR (Association of American Railroads) research project. Later, with time it was modified more suitably for various research purposes. In the beginning, DECAROTOR's vertical maximum load was relatively low, only 90 kN. In DECAROTOR measurements, the loading is applied via hydraulic jacks on the loading wheels located in the middle of the car. A more modern measuring vehicle being used by TTCI (Figure 2.18) can load the rail with a 4–267 kN static loading (Berggren 2009, Zarembski 1980).

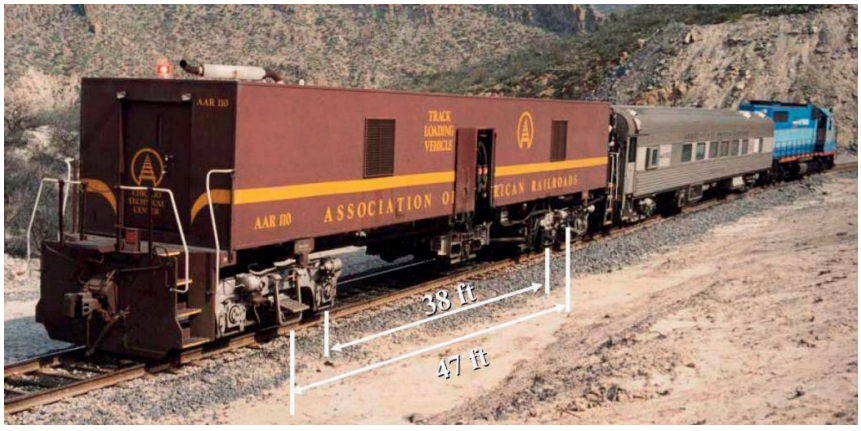

Figure 2.18. TTCI's track loading vehicle (Li et al. 2002).

A measuring vehicle developed in South Africa carries the name BSSN. It can load rails with the help of two independent hydraulic jacks. The vertical settlement of a sleeper due to loading is measured with the help of tilt sensors attached to a beam separate from the loading equipment, as shown in Figure 2.19. The source material did not give any information about the maximum loading level, but the equipment is capable of applying at least 128 kN load per rail, on both rails simultaneously (Fröhling 1997).

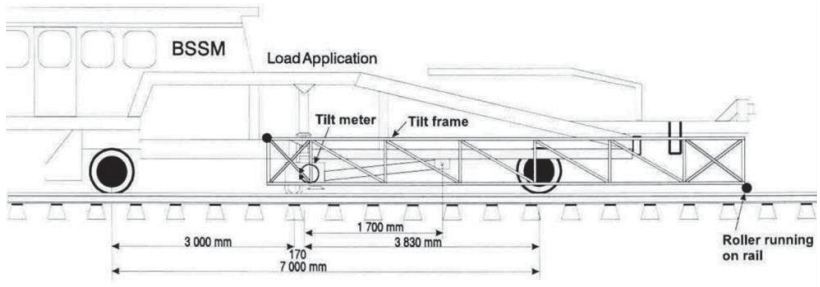

Figure 2.19. Principle of the BSSM measurement vehicle and its operation (Fröhling 1997).

Other stiffness measurement vehicles include a vehicle developed by Esveld from a tamping machine (Esveld 1980) and a TLV by Banverket from Sweden (Köhler 1999, Berggren 2009). Banverket's TLV weighs 49 t, can statically apply loads on both rails up to 150 kN and can generate dynamic loadings up to 200 Hz frequency. Furthermore, measurement of the lateral stiffness of the track is possible.

Among the most important advantages of the measurement vehicles are their great ability to regulate the loads applied and the ability of most of them to measure rail deflection instead of sleeper settlement. By virtue of the latter, the effect of the rail's bending stiffness and that of the rail rubber plate are directly included in the measurement result. Adjustable loading also makes it possible to take hanging sleepers into account. Moreover, with hydraulic jacks, it is possible to create dynamic loadings and vary their frequency.

Accelerometer sensors

In accordance with their name, accelerometer sensors can be used to measure movements based on acceleration. The acceleration measured is computationally converted into a displacement by integration of the acceleration signal twice in relation to time. The integration from acceleration into displacement is exemplified by Figure 2.20. There are certain limitations related to the use of accelerometer sensors. They are suitable only for the measurement of dynamic or rapidly occurring phenomena, and it is not possible to use the method to measure permanent deformations. Owing to the computations required, the offset of the displacement (i.e. the location of the sleeper or the rail) creeps away with time. The maximum displacement caused by one bogie or axle can nevertheless be interpreted sufficiently reliably from the measurement data: even in excess of 0.1 mm accuracy (Arraigada et al. 2009).

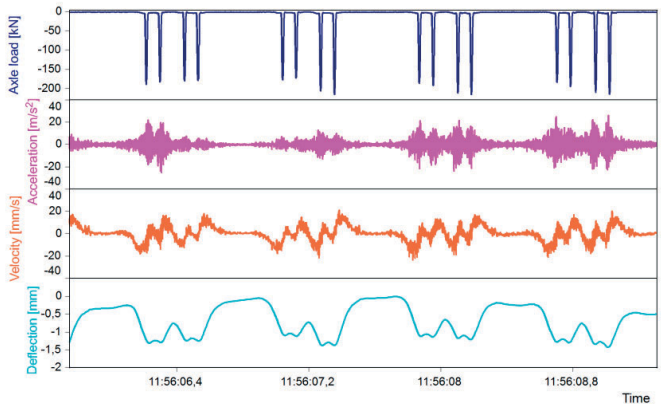

Figure 2.20. Example of integration of the accelerometer signal into displacement.

In connection with the SUPERTRACK (Supertrack 2005) project, accelerometer sensors were used to simultaneously measure both rail displacements and sleeper head displacements, with the sensor configuration as shown in Figure 2.21. The aim was to examine the usefulness of accelerometer sensors on the measurement of track stiffness.

Figure 2.21. Accelerometer sensors installed on the foot of the rail and on the sleeper head in connection with the SUPERTRACK project (Supertrack 2005).

The most important advantages of accelerometer sensors include the possibility to take measurements without immobile reference points, utilisation of actual rolling stock moving on the track as loads, and the possibility to simultaneously instrument several (even dozens of) sleepers. In addition, the equipment is relatively compact and can be easily moved and installed. To calculate track stiffness, in addition to displacement, the applied load must also be known or measured.

Geophones

The geophone is another sensor (similar to the accelerometer sensor) with which it is possible to measure displacements without a reference point. The geophone is an often-used name for electromagnetic seismometers. Its operation is based on speed measurement with the help of a coil moving in the field of a permanent magnet. An electrical signal is produced as an output of the measurement, typically in the form of a voltage proportional to the speed with the help of which it is possible to calculate the displacement. Normally, geophones' measurement data as such are not useful for observing deflections; for example, high-frequency disturbances due to noise must be filtered out.

Geophones cannot measure slowly occurring phenomena. With normal speeds in train transport, this should not create problems; however, the matter must be taken into account at the planning stage of the measurements. On the basis of their own measurement experience, Bowness et al. (2007) claimed that when the combination of the train's speed and the wheelbase produces a loading frequency of 0.5 Hz or less, the measurement results are not necessarily reliable or easy to interpret. The use of geophones for the measurement of track deflections has been going on at least in the United Kingdom (Bowness et al. 2007), where a geophone with a characteristic frequency of 1 Hz has been used and in connection with the INNOTRACK project (Innotrack 2006) using a geophone with a characteristic frequency of 2 Hz.

Displacement measurement in relation to a reference point

There are probably tens of methods for the measurement of displacement, all of which require the help of a motionless reference point. The methods include displacement sensors, lasers, cameras, optical measurement instruments, etc. The common feature of all these is that the vehicle acts as a load, and the movement of the road or track surface is measured in relation to a constructed motionless reference point. A bar embedded deep enough in the ground, a tripod or some other support structure that has been constructed far enough from the road or track can act as the reference point. The measurement frequency and resolution of displacement sensors is usually sufficient for deflection measurement; however, as far as cameras and optical measurement instruments are concerned, driving speeds and measurement accuracy can be very limited. Measurement instruments that can be installed on the side of a road or track are easier to install; for this reason, their use has often been tested (Bowness et al. 2007, Gräbe 2009). However, it has often been observed that the reference point can move, because heavy freight trains, for example, cause vibrations in their surroundings. These vibrations can spread relatively far from the track.

2.4.4. Continuous measurement methods for stiffness

Rolling stiffness measurement vehicle

The Swedish rolling stiffness measurement vehicle (RSMV) is a purpose-built device for stiffness measurement. The measuring equipment consists of a two-axle wagon, and on top of one of the axles there is a dynamic loading gear, as shown in Figure 2.22. The static axle load of the instrumented axle is 18 t, on top of which the loading can be dynamically varied by ±60 kN with the help of hydraulics. The maximum dynamic loading frequency is 50 Hz; however, in practice, measurements are useful to take with loading frequencies below 10 Hz, which correspond to the resonance frequencies of fine-grained subgrades (Berggren 2005).

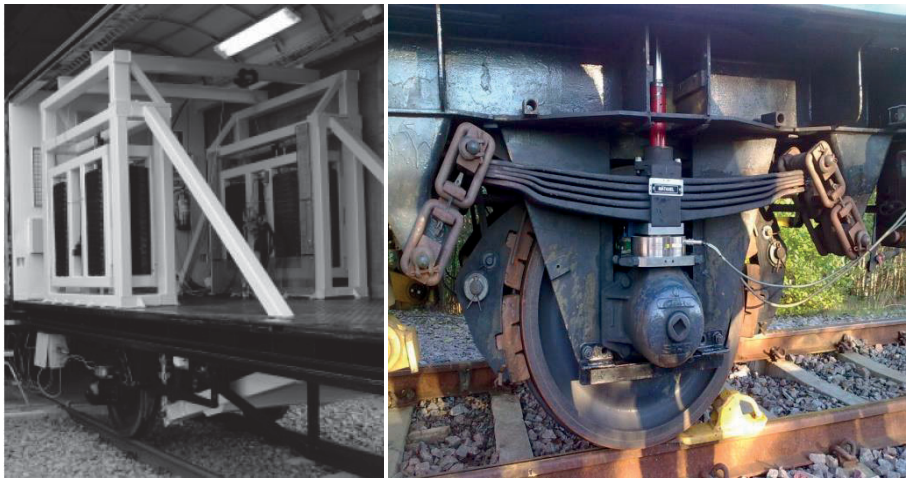

Figure 2.22. RSMV's structure. Left: counter weights installed above the loading axle; right: a close-up of the axle equipped with a hydraulic jack and instrumented with an accelerometer sensor and a force sensor (Berggren 2005).

The dynamic loading produced by RSMV has a sinusoidal form, which can be obtained using the jack to apply the load on the axle in relation to the counter weight. The counter weight is located within the vehicle and it can be moved vertically. The load event is based on the slowness of the counter weight: a fast application of load cannot move the counter weight to any great degree, but an addition to the force of the jack causes an addition to the axle load. Similarly, if the force produced by the jack is decreased rapidly, the counter weight cannot fall as fast and the axle load decreases. The magnitude of the load is measured with the force sensor, and the displacement due to the load is measured with the accelerometer sensor (Figure 2.22). The track stiffness can be calculated on the basis of the force–displacement connection. Even though the structure of the measurement vehicle is very simple in principle, there are several variables involved, especially with the load control procedure. The greatest technical challenge, according to Berggren, has in fact been in building the right kind of feedback control system with which a desired loading can be produced. The adjustment parameters cannot be constants, because the force production changes as the stiffness changes (Berggren 2005).

Track deflection and stiffness measurements from a track recording vehicle

Berggren (2014) also developed another measurement method for track stiffness measurements. The method is based on a novel way of analysing the measurement results of the track recording vehicle. A Swedish track recording vehicle, IMV100, is equipped with both the measurement system using the chord (versine) measurement based on the wheels and a measurement method based on inertia. The longitudinal level is thus measured from the same axle using two different methods. This makes it possible to differentiate between an unloaded longitudinal level and deflection due to the load. The new innovation therefore deals in particular with the calculation of track stiffness from existing measurement data. In comparison with other stiffness measurement methods, there is a clear cost saving in that the measurements are regularly carried out with the track recording vehicle. No separate stiffness measurement is needed, and thus no measurement-

related equipment and staff are required. The track stiffness can be calculated if the load is estimated or simulated.

Portancemetre

Portancemetre is the French version of the dynamic measurement device for track stiffness (Figure 2.23) (Hosseingholian et al. 2011). The measurement principle is exactly the same as in the Swedish RSMV, but there are some differences in the production of force. Portancemetre is a separate device, which is pulled by a locomotive. The part producing the loading and measurement is a separate unit of equipment; to use it, another equipment unit, which contains, among other things, the hydraulics and electronics required in loading, is needed. There is a laptop in the locomotive to collect measurement data. The equipment has sensors that measure four quantities: accelerometer sensors both in the unsprung mass and in the sprung mass, a phase/frequency sensor to synchronise the loading, and a pulse sensor to measure the distance. In addition, the equipment contains a camera, which records the surface of the track, and a GPS positioning system. The force required to convert the result into stiffness is not actually measured; however, the source presents a formula, with the help of which the force can be determined on the basis of the accelerations.

Figure 2.23. Portancemetre (Hosseingholian et al. 2011).

The dynamic load is produced with the help of an eccentric mass, as in vibrating rollers. The loading control might be slightly simpler than in RSMV, because the only variables are frequency and phase. The sprung mass of the equipment weighs 2,995 kg, and the weight of the unsprung mass can be altered. Reported test cases (Hosseingholian et al. 2011) have used unsprung masses of 1,800 and 2,940 kg; in addition to these, varying loads of the magnitude of the eccentric moment and frequency have been provided. The eccentric moments in the tests were 1.391, 0.835 and 0.556 kgm, and the frequencies were 10, 20, 25, 30 and 35 Hz. According to this information, the calculation formula for the total load cannot directly estimate the load range used, because the formula contains the accelerations of both the unsprung and sprung masses. A load applied in accordance with the example (Hosseingholian et al. 2011) would consist of approximately 50 kN static load and ±20 kN variable load. The driving speed used in the tests was 6 km/h, and the track stiffness was calculated as the average of 30 consequent load pulses.

In measurements carried out with high loading frequencies, resonance frequencies and the frequency dependencies of soil structures will be included in the equation, which makes the interpretation of the measurement results more difficult. The same problems in interpretation concern both Portancemetre and RSMV.

TLV

A further-developed version of TLV presented above in Chapter 2.4.3 is able to apply loads on the track both in situ and in a slow movement at a maximum of 16 km/h (Li et al. 2002). The loading principle somewhat resembles those in RSMV and Portancemetre. As shown in Figure 2.18, in the middle of the four-axle vehicle there is a fifth wheel set, on which loads can be applied hydraulically in both the vertical and horizontal directions. The load can vary between 4 and 267 kN. Measurements are made with a light 4.4 t axle load and a heavy 17.8 t axle load. The track deflection due to increased load can be calculated as the difference between these two measurements. The form of the track is measured with the help of laser sensors based on chord measurement. The measurement arrangements also include another vehicle, which applies only a small load to confirm the contact of the wheel with the rail. This measurement wheel set is equipped with a pressurised air cylinder producing a load of 9 kN. The measurement result produced by the very light axle represents the track's geometry errors in longitudinal level (Berggren 2009).

Figure 2.24 presents the principle of the chord measurement based on lasers. The vertical geometry of the track is defined with the help of three lasers.

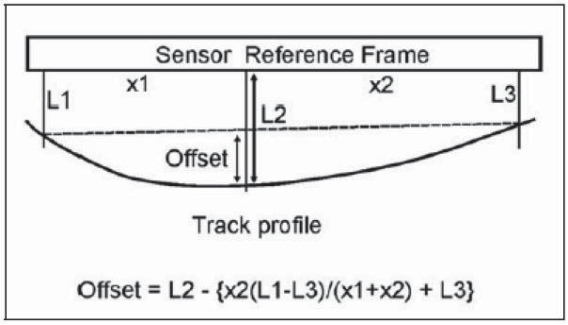

Figure 2.24. Measurement of track geometry with a chord method based on lasers (Li et al. 2002).

China Academy of Railway Sciences

The China Academy of Railway Sciences (CARS) was one of the first developers of continuous measurement equipment for track stiffness (Wangqing et al. 1997). The measurement method is based on two vehicles equipped with different axle loads. Both of them measure the track geometry using a chord measurement, as shown in Figure 2.25. The axle load of the light car is 40 kN, and it is thought to be sufficient to remove the effect of hanging sleepers from the measurement results. The axle load of the heavy car can be varied between 80 and 250 kN. As with TLV, track stiffness can be expressed through the difference in the measurement results of these two axles of different loads. By repeating the measurement with different axle loads, it is also possible to reveal the non-

linear behaviour of stiffness. The greatest allowed driving speed for the vehicle is 60 km/h (Berggren 2005, Wangqing et al. 1997).

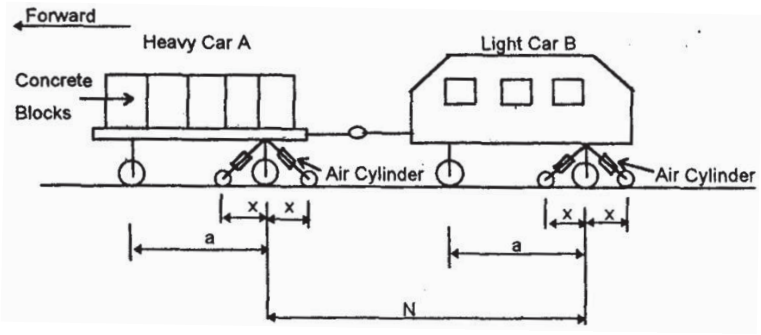

Figure 2.25. Chinese CARS stiffness measurement system (Wangqing et al. 1997).

University of Nebraska

The University of Nebraska, USA, has developed a measurement system that measures track deflection with the help of line lasers and a camera, as shown in Figure 2.26. The measurement is made in relation to the contact point between the wheel and the rail; that is, the reference point for the deflection measurement is at the bottom of the deflection bowl (Figure 2.27). The lasers and camera are installed next to the wheel and point towards the rail. When the deflection increases, the distance between the camera and the rail shortens. The distance of two lines drawn by the line lasers on the rail changes in proportion to the magnitude of the deflection, and the camera records the locations of lines photographically. The shortest distance between the lines is found in the photos by image processing techniques (Norman et al. 2004).

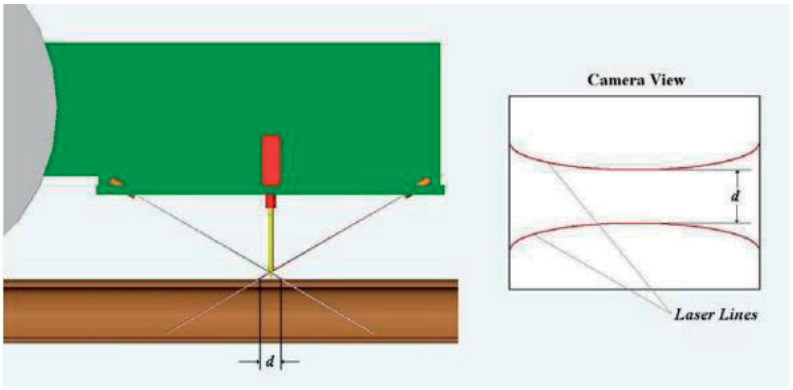

Figure 2.26. Measurement of deflection with the help of a camera and line lasers (Norman et al. 2004).

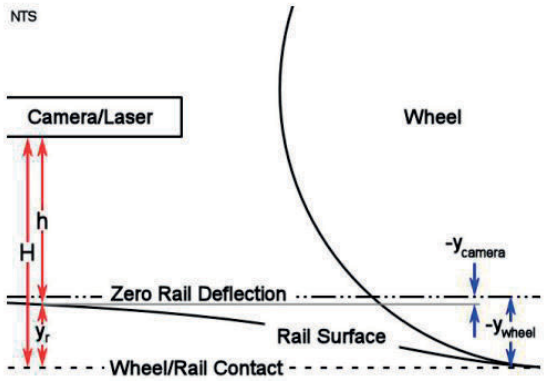

Figure 2.27. Rail deflection in relation to the measurement point (Norman et al. 2004).

A clear weakness in the measurement method is that the deflection cannot be measured in its entirety: the deflection is measured certain distance next to the wheel, where the deflection has not yet had the time to return entirely. The measurement of a partial deflection leads to modelling, in which the rail's total deflection is calculated with the help of the BOEF model. Norman et al. (2004) did not express their opinion about how the unevenness of the track affects the measurement result. The source, however, states that it is not expected that the rail profile would strongly change within a short distance, and it is assumed that the attachment of the wheel and the sensor is solid.

SKMT

The Czech Technical University in Prague and KZV (Komercni Zeleznicni Vyzkum) have developed a measurement device, SKMT, to measure continuous track stiffness. The measurement principle of the equipment is based on chord measurement, which has been realised by building two four-part frames on five axles around a tamping machine (Figure 2.28). During the measurement, the tilt angles of the frames are measured with displacement sensors, the results of which can be further converted into vertical deflection. The load, the magnitude of which per rail is 80 kN, is applied to the rails with the help of the tamping machine's modified lifting mechanism (Berggren 2005).

Figure 2.28. SKMT, the Czech measurement device (Berggren 2005).

In an SKMT measurement, two separate measurements are carried out along the track to be measured: one with the load applied and the other without. With the help of these two measurement runs, the track stiffness can be calculated based on the BOEF model (Berggren 2005).

SBB

The version of the track stiffness measurement equipment developed by the Swiss railways (Schweizerische Bundesbahnen, SBB) is based on two vehicles measuring the track geometry. The system's operational principle is very similar to those of TLV and CARS. With SBB's version, the geometry is measured with very light cars, and a freight wagon applies the load on the track. As seen in Figure 2.29, the measuring arrangements also include a third light vehicle, which seems to have the task of detecting deflections produced by the heavy axle (RIVAS 2013).

Figure 2.29. Swiss SBB's stiffness measurement system (RIVAS 2013).

In spite of being composed of several separate vehicles, the Swiss measurement system is very simple and, in principle, can be connected to any wagon. Its measurement system is based on digital displacement sensors (Heidenhain LS 220 incremental sensors) (RIVAS 2013).

Measurement based on accelerometers

Sussman (2007) researched the possibility of instrumenting a light and a heavy axle with accelerometers and measuring the track stiffness on the basis of an inertia measurement. The basic idea is to have a measurement method similar to those in TLV and CARS; thus, the stiffness is calculated as the difference between the longitudinal geometries produced by two axles of different loads. The method supposedly would require a conversion of measurement results into a certain chord measurement and a comparison between the longitudinal levels produced by the axles of different loads. In fact, the method does not really differ in any way from conducting two track inspections with track recording vehicles of different loads.

The problem with the use of accelerometers is that double integration always requires the use of a high-pass filter, and as a result the signal's offset level will be lost. In practice, this means that the method functions correctly only in situations where the stiffness continuously varies. If the stiffness (and longitudinal level) stays constant in relation to the distance, the difference between the measurement results is zero. Thus, a track with constant stiffness produces two geometries of exactly the same form; the heavier wheel just sinks deeper in the track structure. Because the zero level has been lost due to the high-pass filter, absolute stiffness cannot be obtained. In a probable case where the stiffness varies all the time in relation to the distance, the method should be able to detect stiffness changes.

Traffic speed deflectometer

The Delft University of Technology has developed a device known as the traffic speed deflectometer (TSD) for the measurement of road deflections. The measurement is based on laser Doppler sensors, which measure deflection speed instead of absolute deflection. At the time of writing, no application for railways has been built; however, Greenwood Engineering in Denmark uses the method for the measurement of deflections in road structures (Figure 2.30). (Rasmussen et al. 2002)

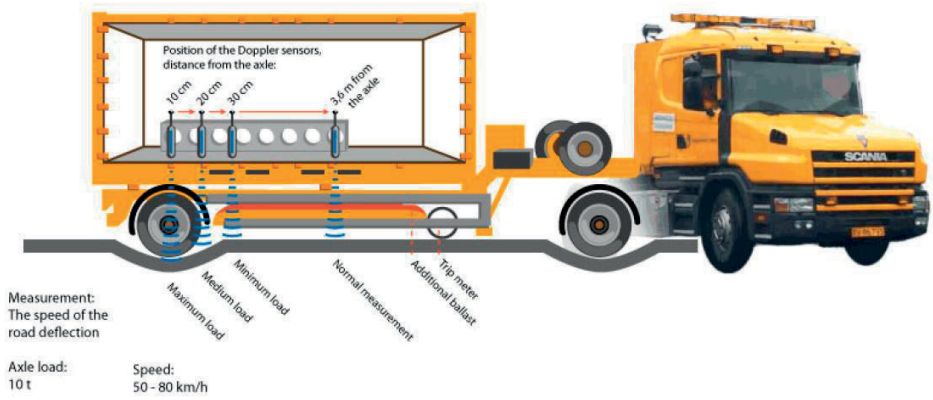

Figure 2.30. Principle of TSD (Baltzer et al. 2010).

The wheel of a truck's trailer impresses a deflection basin on the road surface in a way similar to that of a train's wheel when in contact with the track. When the vehicle moves at road speeds, the vertical component of the surface speed describes the deflection speed, which increases when the absolute deflection and driving speed increase. Rasmussen et al. (2002) presented example graphs, where the measured deflection speed in tests on a Danish road varies between approximately 0.010 and 0.015 m/s at a driving speed of 70–80 km/h. In measurements carried out with the FWD, the corresponding absolute deflection was about 0.3 mm. It has been suggested that the absolute measurement accuracy improves as the driving speed, and thus also the deflection speed, increases. In railway applications, the absolute deflection would often be many times greater; thus, the deflection speed could also be greater and the driving speed could be clearly higher. Therefore, the measurement accuracy of the deflection speed in railway applications might be even better than it is in road applications.

The measurement system requires one sensor to measure the deflection speed at a desired location in the deflection basin and another sensor to measure the roughness of the road outside the deflection basin. In addition, accelerometer sensors and gyroscopes are needed to measure the movements of the vehicle, because the measurement is carried out in relation to the trailer with suspension and the vertical movements made possible by the trailer's suspension system are also seen as a deflection speed. Rubber wheels bring their own challenges, because the wheel's response produces speed reflected in the deflection speed. The measurement must be made at a perpendicular angle to the surface being measured. Even a small inaccuracy in the perpendicularity

adds to the deflection speed a component from the driving speed. This easily increases the method's inaccuracy, because the driving speed is often a hundred-fold in comparison with the deflection speed.

If the intention of the measurement is to find the absolute deflection, more sensors are needed along the deflection basin so that, on the basis of their readings, the deflection speeds can be integrated into displacements. With TSD, it is not possible to measure the maximum deflection directly at the position of the wheel because the deflection speed at that point is zero. The measurement is at its most sensitive at the steepest point of the deflection basin slightly in front of or behind the wheel towards the driving direction.

In these measurement arrangements, there are a number of similarities with the operating principles of measurement devices for track stiffness. In a railway application, the measurement sensors could be attached to an unsprung mass. Because the response of the steel wheels is insignificant, there would be considerably fewer disturbance factors.

2.4.5. Monitoring methods for permanent deformation of the embankment

In this section, several monitoring methods studied or tested by the author are described. The list is not comprehensive because the possible methods and their variations are too many to discuss.

Levelling

Levelling is the traditional way of measuring settlements and frost heave. Levelling can be carried out either from the surface of the road or from the top of a rail at equally spaced distances along the direction of the line. By repeating the measurement sufficiently often, a single measurement turns into monitoring. Sometimes special settlement plates are used: with their help, the levelling can be easily and unambiguously repeated. Levelling can be carried out using a surveyor's level or total station and also with a slightly smaller accuracy by using the Real-Time Kinematic Global Positioning System (RTK-GPS) device. The measurements are easy to make, but as a manual measurement method require repeated measurement visits.

Settlement pipe

The settlement pipe is a method for the measurement of displacements based on the measurement of hydrostatic pressure. The method has been used (McKenna 1974) particularly for the measurement of embankment settlements. As its name indicates, the method can only be used to measure vertical movement (i.e. for settlement or frost heave). There are either water- or mercury-based settlement pipe applications (Bozozuk 1969), but their operating principle is the same. A pipe with liquid and a pressure gauge is installed under the embankment. The elevation of the gauge is determined on the basis of hydrostatic pressure. There are a host of levelling pipe applications: some of them have a top container that keeps the pressure level constant at a reference point; in others, the pipe is filled with a liquid at the beginning of the measurement. The pressure gauge can be moved around inside the pipe to measure the settlements in several places of the cross-section of the embankment.

Robotic total station

Displacement measurements can be carried out reliably with a total station (Sharma 2001). The device can measure movements within three coordinates. In several cases, manual total station measurements are the most economical solution. The markets also provide robotic total stations with which the measurement can be carried out automatically and in real time. In monitoring, the robotic total station is fixed into a motionless position that offers an unobstructed view to the measurement points (Figure 2.31). Prisms are installed into the measurement points, and the measurement device measures their position at desired intervals. The measurement software has the ability to raise an alarm if any of the measurement points move. This measurement arrangement is relatively expensive and predominantly for this reason it has not become all that widespread. The method has been tested in connection with the Perniö embankment shear failure test (Luomala et al. 2011). Although the measurement method provides the most accurate possible measurement result under good conditions, it has its shortcomings. For example, snow and ice create complications regarding the visibility of the prisms, and the prisms may frost. Moreover, vandalism can damage observation points above the ground. The robotic total station requires regular maintenance. For continuous monitoring, there should be two measurement devices in use so that measurements may continue even when one undergoes maintenance.

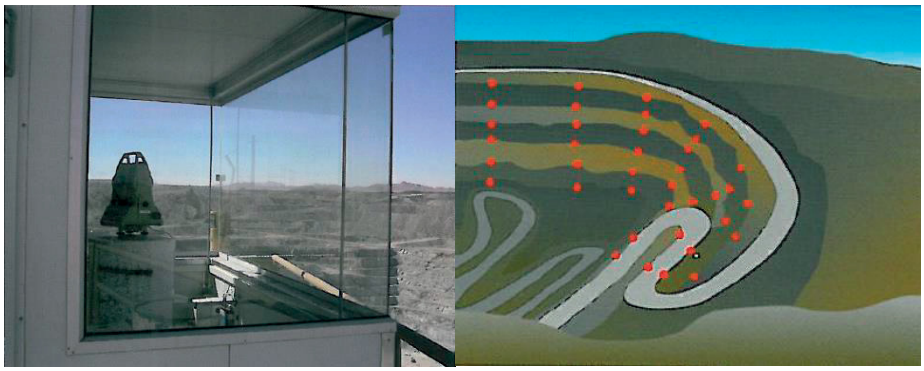

Figure 2.31. Monitoring movements of the walls of an open mine with a robotic tachymeter in South Africa (Zeiner 2007).

GPS measurement

RTK-GPS equipment enables measurements at centimetre accuracy (Nickitopoulou et al. 2006). The achieved accuracy may be sufficient for the measurement of embankment displacement. At least horizontal movements can be detected before the movements grow too large from the perspective of traffic safety. Manual measurements can be taken considerably faster than with a tachymeter because only one person is needed for the job.

GPS devices can also be automated. At the time of writing, these kinds of sites for automatic monitoring do not exist in Finland, but there are some examples abroad. For example, in Iran, movements of a massive power station dam have been monitored with automatic GPS equipment (Zeiner 2007).

GPS measurements function well through all seasons regardless of prevailing weather conditions. Not even a heavy snow can prevent carrying out measurements, although this would greatly hamper total station measurements. The greatest challenge in the use of GPS measurement is the positioning of measurement instruments in such a way that they stay in place in relation to the embankment. The antenna of the receiver is large, with a diameter of about 20 cm, and it might also be subject to vandalism.

Inclinometer

The inclinometer is an accurate sensor for angular positions in relation to the earth's gravity. Displacement measurements of soil layers are carried out via an inclinometer tube installed in the ground (Dunnicliff 1993). The tube can be pushed into the ground or installed in a borehole made for the purpose. Under Finland's soil and ground conditions, the tube must be installed to meet the stiff ground below the soft soil. This is necessary because measurements are carried out in relation to the tube's lower part in particular. Traditionally, these measurements have been manually conducted. For the measurement, the inclinometer is lowered into the tube, and the equally spaced measurement readings are taken from different depths. By repeating the measurements, information about the movements of the tube and thus also the lateral movements of the soil in relation to time are obtained from different depths.

An important step in the history of inclinometer development is their automation. There are applications in which the traditional inclinometer has been automated by constructing the mechanics to move the measurement device in the tube. This, however, was just a temporary stage; a clearly simpler way is to use several sensors simultaneously (Lemke 2006). Moreover, Finnish company FinMeas Oy has developed a measurement instrument based on a digital accelerometer sensor. The instrument enables real-time measurements (Ryhänen et al. 2007).

One of the significant advantages of an inclinometer is its capacity to reveal the horizontal movements of all the soil layers. In theory, the settlement of the soil layers can also be determined; however, there are inaccuracies in vertical installation because changes to the angle of the sensor caused by the settling soil layers are very small. To measure settlement, the inclinometer can be installed horizontally, in which case it will identify movements caused by the settlement very well. To measure the absolute settlement, one end of the inclinometer must be fixed to a motionless reference point.

Cable radar measurement

In Del Mar, California, USA, a track embankment located on a coastal bluff was instrumented with a coaxial cable and a cable radar (time domain reflectometer, TDR) (Kane et al. 2004). A nearly 1,000-m-long cable was installed at a depth of half a metre into a cable trench, longitudinally between the shore and the embankment. The sensor cable was covered with a concrete cast of dimensions approximately 200 × 300 mm (width × height). The measurement method is based on the assumption that the movements of the embankment will break the concrete beam, causing a deformation, observable with the cable radar in the coaxial cable. The cable radar emits a voltage pulse to the cable, and the pulse is reflected back from the end of the cable. If the cable has deformed significantly, the pulse will be reflected back from the source of failure, wholly or partially (due to damping). The method can thus detect the position of the moving embankment

but not the magnitude of the movement. Calibration might provide some indications about the magnitude of the movement, but the direction of the movement must be derived by other means.

Invar steel wire sensors

Invar steel wire sensors were designed for the measurement of soil movements in particular (King et al. 1976). In this method, the measurement instrument is fixed in a motionless location on a measurement site. An Invar steel wire can be drawn from the measurement instrument and attached to a moving object. The wire in the device is coiled, and the device measures the rolling motion of the coil. Thus, the device works as a kind of strain gauge. The idea behind the method is based on Invar steel, the heat expansion of which is very small. This allows one to make measurements of the embankment movements so that the effect of the wire's heat expansion will not significantly affect the result. The method, however, is suitable only for point-based measurements.

2.4.6. Monitoring methods for frost heave and frost penetration depth

The oldest methods for defining frost penetration depth are based on an observation about the colour change a liquid can undergo at a temperature of 0°C. The first version was the Gandahl frost tube based on methylene blue, which was developed in Sweden (Gandahl 1957). As a liquid, methylene is blue, but it becomes transparent on freezing. Later, Rickhard et al. (1972) developed their own frost tube, the operation of which is based on a fluorescein-saturated sand mixture. Its colour changes from green to pale yellow as a result of freezing. In both these methods, a plastic tube is installed into the structure. The actual measurement instrument must be installed inside the tube. The measurement instrument is a transparent tube, which contains material that changes its colour when freezing. The definition of the frost penetration depth itself takes place by removing the tube from the structure and measuring the location of the frost penetration depth on the basis of the colour.

In the method described, observation of the frost penetration depth is based on the zero-point temperature, which is a good estimation of the depth of frost in most cases. To be more precise, soil freezing occurs at slightly below 0°C, because in the partially frozen layer the water is supercooled (Koopmars et al. 1966). High salinity further lowers the freezing point of water. Thus, it is difficult to determine the location of the frost penetration depth solely on the basis of temperature. A more advanced way of defining the frost penetration depth on the basis of temperature is to use several temperature sensors for the estimation of the freezing point. The reading of temperature sensors can be automated, and thus it is possible to obtain real-time information from the monitored site about the frost penetration depth. Thermocouples were probably among the first sensors suitable for this purpose (Kinzie 1973). With them, it is possible to obtain an accurate temperature reading; however, the measurement of cold junction temperature required by its use is a challenge for measurements carried out at varying temperatures outdoors.

The frost penetration depth can be found not only with the help of temperature but also with electrical conductivity or by dielectric means. Hayhoe et al. (1986), among others, noted that the electrical conductivity of frozen ground is near zero, but the soil does not necessarily freeze at zero temperature yet. On the contrary, its electrical conductivity may increase even when the temperature is still below zero as the frost is thawing. The increase in the electrical conductivity of frozen ground is related to the existence of free water and generally to the flow of water through

the structure. Sun et al. (2012) compiled a literature review on the estimation of frost penetration depth based on electrical conductivity and dielectricity. The source regards TDR sensors as a method to be seriously considered for the estimation of frost depth, but notes that the layer-by-layer installation disturbs the ground in its natural state. Furthermore, instrumenting costs will increase if TDR sensors are extensively used in many cross-sections. Sun et al. (2012) proposed the installation of frequency domain sensors in an installation tube as a new method. These are economical, and they can be installed into the structure from the surface without disturbing the structure.

The ground-penetrating radar (GPR) is based on the measurement of soil dielectricity and on the reflection of the sent signal in layer boundaries. Saarenketo et al. (2000) proposed the possibility of determining frost penetration depth by a GPR, especially if no significant frost lenses have been formed. Ice lenses reflect the radar signal back and make it difficult to interpret the actual frost penetration depth (Silvast et al. 2012). With the ground-penetrating radar, one can determine the frost penetration depth along the whole line, which is something that cannot be done with point-based methods.

Frost heave is traditionally observed by levelling. Clearly more comprehensive measurements are achieved with laser scanning, with the help of which it is possible to measure the entire surface of a road or track (Jaakkola et al. 2008). By repeating the measurements during late winter and by comparing the autumn and winter measurements, the places of frost action can be located on the track. It is possible to find settlement using a similar principle (cf. Chapter 2.4.5). The use of the laser scanner for determining frost heave is a relatively new invention, but at least Roadscanners Oy in Finland has tested the method successfully (Saarenketo et al. 2012). Mill et al. (2014) amply describe the advantages of the method. Measurement from a moving vehicle requires a good positioning method, and RTK-GPS provides a solution to this problem. Basically, all the measurement methods for settlement are also suitable for measuring frost heave. Frost heave is a seasonal event however and to understand the reasons for the phenomenon and suitable maintenance actions, frost heave magnitude and frost penetration depth need to be known accurately.

3. Monitoring deformations

There are several methods to monitor deformations that are only well suited to their limited individual purposes. Geotechnical measuring sensors are often manufactured by commercial operators, but relatively few equipment manufacturers specialise in the measurement of vertical deformations in road and railway structures. Therefore, a number of research projects have been forced to construct such devices themselves to meet their requirements. This chapter describes some of the point-based monitoring methods developed for TUT's research projects. The measuring methods were developed into their current form described in this study by the author, although ideas for the methods were searched for with the help of literature and previous experiences. A shared feature between the measuring methods described in this chapter is that the measuring devices are installed inside a structure and used to measure the deformations in one or a few points. The methods have been divided into dynamic (Chapter 3.1) and static (Chapter 3.2). A dynamic method refers to a measuring arrangement that attempts to measure deformation while a vehicle is passing over a certain spot. A static method refers to measurements taken less frequently (e.g. once an hour) to analyse permanent deformations.

After the description of the measuring methods, each paragraph in Chapter 3.3 provides a case example of monitoring locations, where the measuring methods created have been utilised in practice and briefly describes the main findings regarding the method and the functioning of the structure.

3.1. Dynamic measuring methods

3.1.1. Acceleration sensors

Acceleration sensors have become significantly smaller and less expensive over the past few decades because of the developments in vehicle technology and consumer electronics. Acceleration sensors, which are used, for example, for drive stabilisation in cars, can also be used to measure movement in road and railway structures. In some applications, acceleration in itself provides ample information. For example, faulty train wheels or transition zones in the track cause significant accelerations, which place a stress on the track and the rolling stock. By measuring the vertical acceleration of an axle or a rail, it is possible to evaluate the condition of the track and the rolling stock.

Instead of acceleration, experts in geotechnical engineering are usually interested in the displacement of a structure. The measurement result from an acceleration sensor is converted into a displacement with a double integral (Equations (3.1) and (3.2)):

$$v(t) = \int a(t)dt \tag{3.1}$$

$$s(t) = \int v(t)dt \tag{3.2}$$

where

v	is speed [m/s]
a	is acceleration [m/s^2]
s	is displacement [m].

The acceleration signal is converted into vibration velocity with a specific integral so that the surface area between the acceleration signal and the temporal axis is added as differentially small slices in relation to time (Figure 3.1). The most natural period for calculating the integral is the sample interval determined by the measurement frequency. The integral is repeated for the calculated speed signal and the result indicates the displacement.

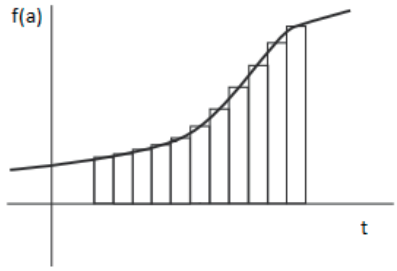

Figure 3.1. Calculating speed with the acceleration signal.

Acceleration sensors work indirectly because they are used to measure acceleration, which is then converted into displacement. A parameter is preferred to be measured directly, avoiding mathematical conversions. Usually, a displacement determined on the basis of acceleration is not completely accurate, because calculations inevitably contain errors. The reasons for errors include a sensor's offset error, which increases to the power of 2 during integration and causes the double integral to creep. The error increases in relation to the integration time, meaning that a displacement error will remain relatively small if the integration time is short enough. Therefore, acceleration sensors should only be used to determine the displacement in applications where the movement begins from a known origin and quickly returns to the same location. Such applications may include the measuring of a structure's recoverable deformation caused by a vehicle passing at high speed. A recoverable displacement from an individual wheel or bogie can be reliably calculated. Acceleration sensors cannot be used to measure slow movement, such as permanent settlement on a railway track.

Various filters can be used to reduce the creeping involved in double integrals. Signal processing software typically contains built-in filters, such as Bessel, Butterworth and Chebyshev (Gani et al. 2002), which can be used to conduct high-pass filtering for the acceleration signal before integration. A high-pass filter excludes all the frequencies below a set limit from the acceleration signal and simultaneously also any errors related to the sensor's offset. With filters, creeping is reduced significantly, but the use of too strong a filter will also remove some of the actual measurements. Using a filter requires some practice and experimentation, because the best way to

filter is a compromise between the interpretability of the measurement data and the correctness of the results, which depend on the speed of the movement and the object being measured.

There are many different acceleration sensors available, whose measuring range and principles vary. Sensors can be piezoelectric, strain-gauge-based or semiconductor sensors. Some sensors measure only dynamic events, while the lower frequencies are filtered due to sensor mechanics. Other sensors measure everything, starting from zero frequencies and these sensors can be used to detect inclination that occurs slowly.

Sensor SCA620 with an acceleration range of ±1.7 g, manufactured by Finnish VTI Technologies (later Murata Electronics), was used in this study in both road and railway applications (Figure 3.2). In addition, the same manufacturer's 3 and 12 g sensors from the SCA610 series with a slightly larger measuring range and a correspondingly more extensive frequency response were used. The acceleration range and frequency response increase proportionately, and an increase in the acceleration range may not yield any benefits. A sensor of a more extensive acceleration range will detect ever higher frequencies, which also produce increasingly large acceleration values. The detection of high frequencies hinders the detection of low frequencies, which are often more interesting with regard to the structure. High frequencies exceeding 50 Hz are usually unnecessary to detect movements in earth structures.

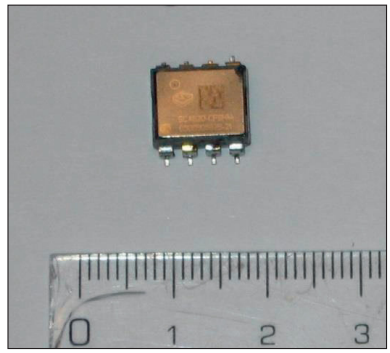

Figure 3.2. Acceleration sensor SCA620 used to monitor a road structure. The acceleration sensor components are very small. In practice, the size of a sensor depends on the way in which it is protected.

Sensors in road structures have been installed both on the pavement surface and completely inside the structure. The sensors are first protected against mechanical loads and water. Resin is used as the protection. The sensors are installed in holes drilled into the asphalt, when measuring deflection on the road surface (Figure 3.3).

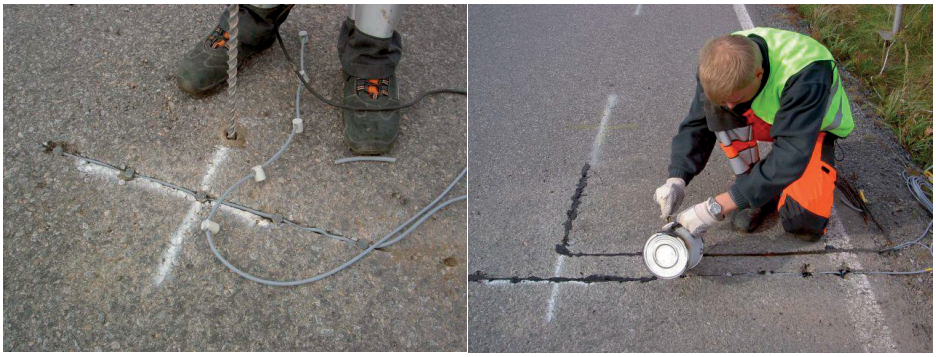

Figure 3.3. Installing acceleration sensors in the asphalt at a test location in Vesilahti.

In railway structures, the acceleration sensors are usually attached to sleepers (Figure 3.4). For this reason, the sensors are equipped with magnets that can easily be attached to a metal base during fieldwork. Metal plates are glued onto the sleepers for the sensors' magnets to attach firmly to. Measurements are conducted with these sensors from the sleepers, because measurements cannot be taken directly from the rail due to sensor saturation. Saturation refers to the offset of a sensor's zero point due to frequencies and accelerations that are too high for the sensor's measuring range (Wu et al. 2004). The accelerations on a rail are significantly higher than on a sleeper. In addition, in steel, shear waves travel from a distance to the measurement point, causing unnecessary interference when determining track deflection caused by a single axle. Strain-gauge-type sensors (e.g. Kyowa AS-20B) have been found to be the only useful sensor type for taking rail measurements (Figure 3.5). Measuring a deflection caused by a wheel that is in good condition is relatively easy with these sensors, but the accelerations caused by wheel flats interfere with the data interpretation. Some of the weaknesses of strain-gauge-type sensors include their limited lifecycle and a more expensive data collection system required to read the sensors.

Figure 3.4. An example of using acceleration sensors to take measurements of recoverable settlement of a sleeper. The sensors are located outside the rails at the ends of the sleepers.

Figure 3.5. Acceleration sensor AS-20B manufactured by Kyowa.

3.1.2. Deformation sensors

Structural deformations must often be measured from inside a structure at various depths. Acceleration sensors can also be placed inside the structure at varying depths, and then the compression of the layer as the difference of absolute displacements measured by two sensors can be calculated. An inaccuracy due to double integration may be too great when using this method, and therefore it will not yield reliable measurement results at a small displacement level.

Several development versions of deformation sensors have been constructed at TUT, measuring the distance of two points in an unbound structural layer (Figure 3.6). The first version was based on a sensor frame, shaped like a commercial sensor, but since then the designs have changed considerably (Kolisoja & Mäkelä 2002). However, all the sensors share the same basic principle. Two plates with a diameter of 100 mm are installed in the structure roughly 100 mm apart. A rod measuring their distance from one another connects them, and the rod's displacement in relation to the other plate is measured. The space between the plates is filled with the same material that has been used in the surrounding structure. The load from a vehicle or a loading arrangement will usually cause vertical compression in the structure, which can be detected as a decrease in the distance between the plates. In some cases, the deformation may also take the form of straining, especially if measurements for deformations are taken horizontally.

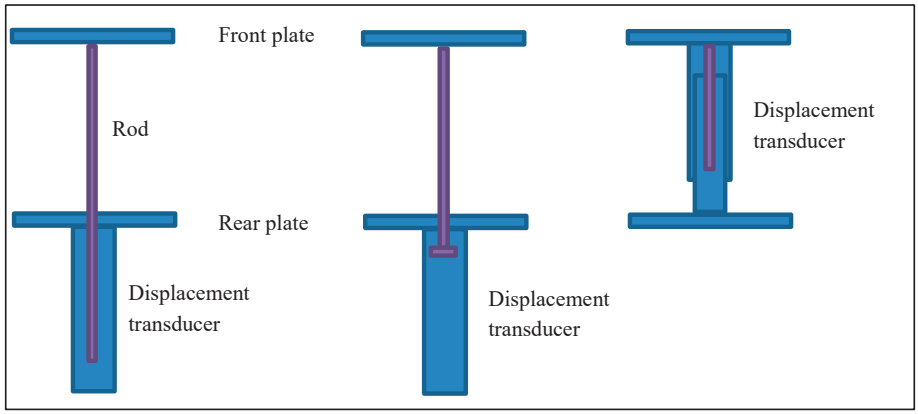

Figure 3.6. Principle of a deformation sensor and its various development versions.

Several sensor models have been developed, because each model has its pros and cons (Figure 3.7). Most of the measured deformations are relatively small, only a few hundred microstrains at their smallest. Typically, a measured displacement over a measuring distance of 100 mm is approximately 0.01–0.5 mm. In certain disadvantageous cases, however, the displacement level may be as much as 3–4 mm (Vuorimies et al. 2012). Deformation in the initial part of this range

could be measured with strain gauges; however, strain gauges made from steel will typically break at approximately 2,000 microstrains. Therefore, various types of displacement sensors and a structure that allows more extensive movement have been utilised in deformation sensors.

The sensor type used in the first deformation sensors was IAS-10-A13-IL. This watertight inductive proximity sensor enables non-contact measurements and long-term durability. Its measuring range is 0–5 mm, out of which only the range from 1.5 to 5 mm is completely linear. A sensor equipped with this particular displacement sensor will work well as long as the permanent deformations remain small. In several applications, there has been a problem with the permanent deformations increasing beyond 5 mm, due to which the sensors are no longer within their measurement range. There has also been a certain amount of noise in the sensors, which has hindered the interpretation of the measurement results.

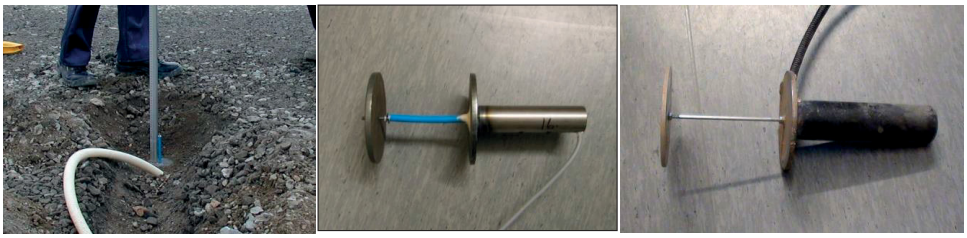

Figure 3.7. (a) Deformation sensors being installed, (b) a model equipped with an inductive sensor and (c) a model equipped with an LVDT sensor.

In the next development version, the sensor was changed into an LVDT sensor (Solartron S-Serie AS/15), which is also watertight and has a measurement range of 30 mm. There is almost no noise, and the sensor's accuracy is, in practice, based on the accuracy of the measuring device. The sensor will allow a measuring accuracy of approximately 1/1,000 of the measurement range. In other words, the displacement sensor technology cannot be used to measure the very smallest deformations that are only a few microstrains in size. No problems have been detected with this sensor model regarding large permanent deformations, because the sensor's measurement range is sufficiently extensive. However, the sensor's protective cover grew relatively large in size as the sensor itself was slightly larger than before.

The third sensor model was constructed so that the displacement sensor was placed inside the pipes connecting the plates. A potentiometer (Novotechnik KL 500 5K0/M SE), which does not have a completely watertight protective cover, was used as the sensor in this model. During the laboratory tests, the sensor's installation location was almost dry, which made the use of this sensor type possible. The sensor's range of motion is 50 mm, which enables extremely high displacement levels. The sensors were used in a small-scale bridge simulation modelling the interaction between a bridge and its approach embankment, in which the bridge was pushed towards the embankment, thereby simulating the thermal expansion of a long bridge (Laaksonen 2011).

The fourth sensor, which also consists of concentric steel pipes and operates with the same principle, was intended for measuring deformations in low-installed culverts. The pipes contain a

spring, which draws the pipes against the culvert while allowing the pipes to move inside one another. The actual displacement sensor (Novotechnik TRS50) was mounted on the side of the outer pipe. The sensor measures the pipes' movement in relation to one another. This measuring arrangement allows the measurement of movements as large as 50 mm, and the largest detected deformations in plastic, low-installed culverts in roads with a low traffic volume have been over 10 mm (Haakana et al. 2015).

3.1.3. Multi-depth deflectometer

The sensors described in Chapter 3.1.2 (the previous chapter) are only suitable for monitoring a thin individual layer. When it comes to road structures, it is often beneficial to observe relatively thin layers on the road surface, because the load from a tyre is focused on a single point and its loading impact to the structure decreases rapidly as the depth increases. The use of a similar measuring method in railway structures, directly below a sleeper, is justified, but otherwise the layers under observation may be thicker. Originally, a device measuring several layers simultaneously, a multi-depth deflectometer (MDD), was built in order to identify a layer caused by frost heave on a track (Luomala 2010). The same instrumentation is also suitable for measuring vertical deformation caused by traffic load.

MDD is not a new idea, as similar products have also been available commercially. At least Dynatest (MDD) and CTLGroup (Snap multi-depth deflectometer (SnapMDD)) market measuring devices that are installed from a structure's surface and intended to measure vertical deformations in an embankment. They operate in an almost identical way. A measuring rod consisting of a single piece is installed in a hole drilled to a structure, surrounded by LVDT sensors at pre-determined intervals. The ways in which the rod is anchored and the sensors are attached differ slightly. With MDD, the sensors are attached to the sides of the drilled hole with steel balls. Prior to this, the hole was covered with a rubber-like material. The advantage of this method is that the equipment can be removed from the hole after use. SnapMDD is mounted with glue. Both versions can only be installed above the groundwater level. In addition to factors related to the installation, the limitations include the sensors, which are not watertight. With MDD, the anchoring of the measuring rod is carried out with a mechanical grip, whereas SnapMDD uses a hydraulically expanding anchor (Figure 3.8).

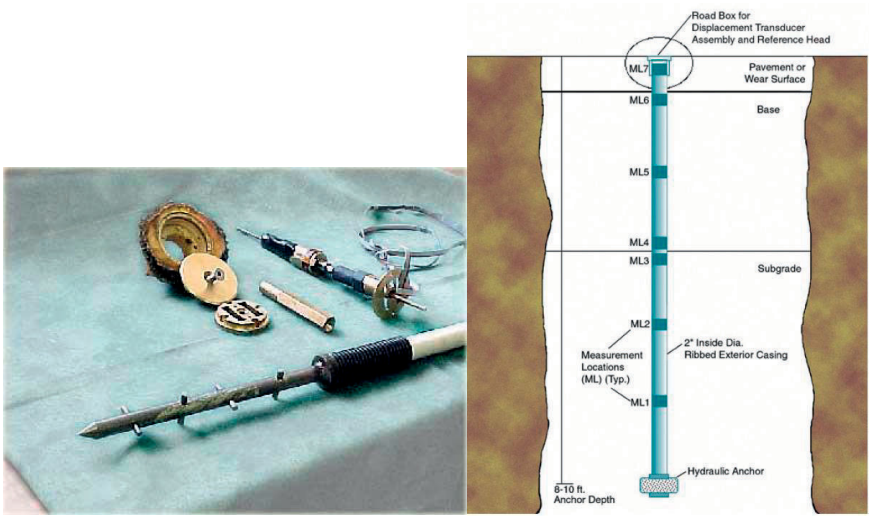

Figure 3.8. Two different MDD devices. On the left is the Dynatest version and on the right the schematic of CTLGroup's version (Dynatest 2014, Weinmann et al. 2004).

Neither device can be installed within just a few hours, which is often necessary in the railway environment. The installation of both devices usually takes two work days, according to information received from the manufacturers. Hence, neither of these devices can be installed in a track while there is traffic running. For this reason, a new version of a measuring device that works in a similar manner and that can be installed faster was developed.

The measuring method was initially tested in a laboratory by installing two LVDT sensors inside a flexible plastic pipe. The sensors were 400 mm apart and attached to the inside surface of the pipe with glue. The plastic pipe was easily compressible, and its outer surface was uneven, which was expected to help with its attachment to the embankment. The measuring rods of the LVDT sensors were attached to one another to form a single, long measurement rod. The sensor element was installed in the test embankment, which at the time was part of an embankment width study (Kalliainen et al. 2010). The installation was performed in a hole made into the embankment with a helical auger. The sensor element was installed in the hole, and the measuring rod was anchored in the ground with mortar dropped to the bottom of the hole. The flexible pipe was attached to the embankment with dry installation sand. The measured deformations corresponded with the other sensors placed in the embankment. It was considered possible to install the multi-depth measuring device with sand, even in a relatively short amount of time.

The actual measuring device that was intended for fieldwork contained five LVDT sensors, and the anchor rod functioning as a reference was 3 m long. The depth of the first measurement layer from the bottom up was 1 m, and the other layers were 0.5 m in thickness.

The LVDT sensors require electronics that can be placed near them or in a separate amplifier. The latter option was chosen for the field installations. Sensors without any electronics were less

expensive, and a separate amplifier may possibly be used later at some other test location. It is likely that the sensors installed into the track cannot be removed intact.

Solartron's S-series sensors were used. Two models that differ in their measurement range were selected. The measurement range of the two uppermost sensors was 50 mm, and the range of the other three sensors placed deeper was 30 mm. Although the sensors' measurement ranges were relatively extensive considering the dynamic deformations, it was likely that installing the sensors in the measurement area would be problematic. Efforts to remain within the measurement range included the use of a support rod, which was attached to the sensors' protective pipe with ceramic metal (Figure 3.9). The purpose of the steel rod is to keep the mutual distances of the sensors correct during the installation. The steel rod was removed after the sand installation by rotating the rod and simultaneously lifting it. Removal of the steel rod also served to compact the installation sand around the sensor's protective pipe in the drill hole.

The anchoring of the sensor rod was based on a mechanical grip, and the anchor itself consisted of round steel plates. The installation sand was expected to become compacted in the installation hole due to vibration and to create sufficient grip. It was decided not to use the concrete anchor, because even under laboratory conditions it took some time to make one. According to preliminary timetable information, working windows of approximately 20 min was available during the daytime at the installation location. The use of concrete was not considered a viable plan to in those time slots. In hindsight, dropping mortar in an installation hole only takes a few minutes, and it should have been used, because anchoring the rod with installation sand took months.

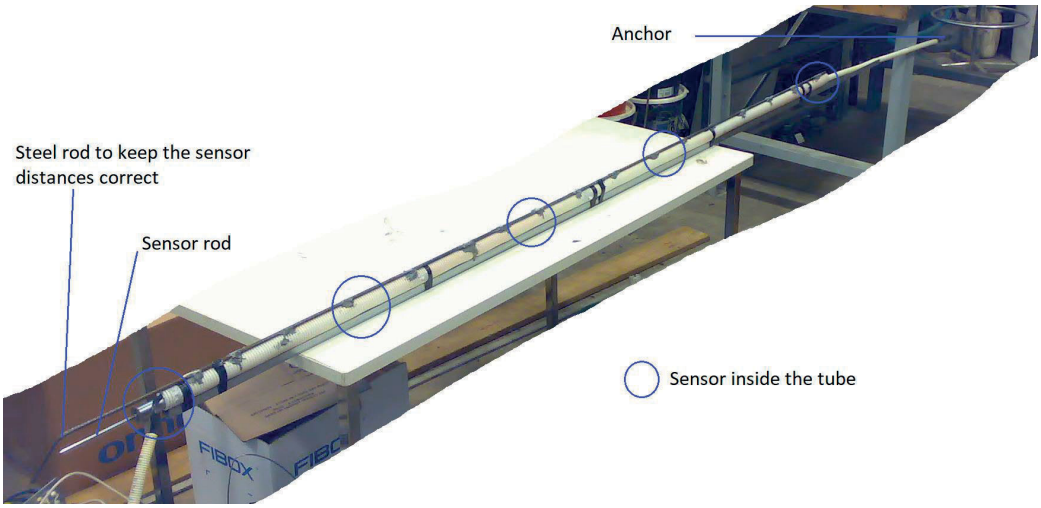

Figure 3.9. The MDD that is to be placed in the embankment is ready to be installed.

MDD was installed at the end of a sleeper in a 50-mm hole made with a drill rig. Swedish sounding drills were used to create the hole, but a boring head resembling a dynamic penetration test top was made for the drilling. The boring head was used to insert a plastic installation pipe through the ballast, with the aim of keeping the hole open during the installation work. The boring head was ultimately left at the bottom of the installation hole. The first hole was drilled down to the

target depth, but the hole was filled with sludge before installation of the sensor element. The groundwater level was at a depth of approximately 1 m; as a result, the drill hole quickly became blocked. During the second attempt, the installation hole remained open, and sensor was installed to the correct depth. The installation hole was filled with fine, uniformly graded sand (Figure 3.10). After the sand filling, the steel rod glued onto the sensor element was twisted apart and pulled out of the hole. The uppermost sensor was mechanically attached to the sleeper.

Figure 3.10. Installing MDD. The sensor element was installed in a 50-mm hole made with a drill rig (on the left) and fixed to its surroundings with installation sand (on the right).

3.1.4. Displacement sensors

To conduct frost research, several frost monitoring stations that monitor vertical movement in the sleepers have been constructed around the Finnish railway network. This measuring system uses displacement sensors that measure the vertical position of a sleeper in relation to a reference rod installed at a certain depth (see Chapter 3.3.6). A similar idea was applied at the test site in Vesilahti (see Chapter 3.3.1), where a system that measures the deflection of the pavement was selected, suitable for measuring recoverable and permanent deformation and frost heave. From the modelling perspective, this is considered to be a type of displacement measuring, because it does not measure deformation in any of the individual structural layers but instead covers the entire structure.

To carry out the anchoring, a hole 100 mm in diameter and approximately 15 mm in depth is first drilled into the pavement with a diamond drill bit (Figure 3.11). A 50-mm hole down to at least 300 mm is then drilled at the centre of the first hole, and a protective plastic pipe is installed in the second hole. The drilling rod is drilled through the protective pipe, either to a pre-determined depth or, if possible, all the way down to the hardpan. If the hardpan is stone or rock, the drilling rod may need to be removed or cut to a suitable length, as the top of the rod must remain roughly 200 mm below the road surface. The LVDT sensor's spindle is installed in the threads on top of the drilling rod with the adapter and tool built for this purpose. A protective pipe is placed around the sensor spindle and mounted onto the structure with bitumen and sand. A compact and even base approximately 15 mm below the pavement surface is prepared for the sensor. The actual sensor has been mounted on a steel plate, which will be installed in a recess made in the pavement and fixed in place with bitumen (Figure 3.11 in the middle). Finally, the sensor is covered with bitumen and installation sand. A diamond cutting wheel is used to make a groove into the pavement

for the sensor's signal cable, and the cable is attached to the groove with bitumen. Some of the sensor installation phases are shown in Figure 3.11.

Figure 3.11. Some of the installation phases of a sensor measuring deflections in the pavement.

A displacement sensor measuring the relation of the drilling rod functions similarly to an acceleration sensor installed on a road surface (i.e. it measures the deflection of the surface). Acceleration sensors can only be used to measure dynamic events, whereas a solution that is based on a displacement sensor works in all loading situations. The aim in Vesilahti was to measure compression caused by a vehicle and the recovering time after the load had passed. Acceleration sensors are not suitable for measuring the recovering time.

3.2. Static measuring methods

3.2.1. Settlement pipe

Finland has a large number of embankments built on soft soil, whose stability (i.e. confidence against shear failure) is low (Mansikkamäki 2015). To monitor such embankments, it was needed to develop a measuring arrangement that could monitor the movement of large areas. For example, an automatic inclinometer, which measures horizontal displacement, already existed for this purpose (see Chapter 2.4.5) (Ryhänen et al. 2007); however, because of the high cost, installing one is only possible in a cross-section that is considered to be the most dangerous. The aim was to develop a measuring system that would enable the monitoring of significantly longer sections of a track. A settlement pipe, installed parallel to the track and measuring the vertical movement of the track in several points with hydrostatic pressure, was deemed to be the most potential solution.

The operating principle of the settlement pipe is simple: several pressure sensors are placed in a single fluid-filled pipe, and these measure the sensor's vertical position with the hydrostatic pressure of the fluid column. One of the sensors functions as a reference and changes in the other sensors' vertical positions in relation to the reference sensor are calculated based on the pressure differences. When a settlement develops in an embankment, the hydrostatic pressure rises in the

settlement point in relation to points where settlements are not formed. Fluctuation in the air pressure affects all sensors, but the reference sensor will help to compensate for this. Sometimes, the reference sensor can be installed directly in a rock cutting or in another immovable location. Where this is not possible, an immovable point will be constructed for the reference sensor with drilling rods supported by hardpan, for example.

The functioning of the settlement pipe system was initially tested in a laboratory. A settlement pipe containing six pressure sensors was built for this purpose. Digital SCP1000 air pressure sensors manufactured by VTI Technologies were used. The pressure sensors were installed on a circuit board, onto which the necessary electronics were built for serial communication. A microprocessor was installed next to each sensor to record the sensor's measurements and transmit the values to a computer, when requested. This system allows an unlimited number of sensors to be connected with the four signal cables (Figure 3.12). In addition to pressure data, temperature data are also read from the sensor. A query for the measurement results of a single sensor takes just under a second; therefore, this method is not suitable for measuring dynamic phenomena.

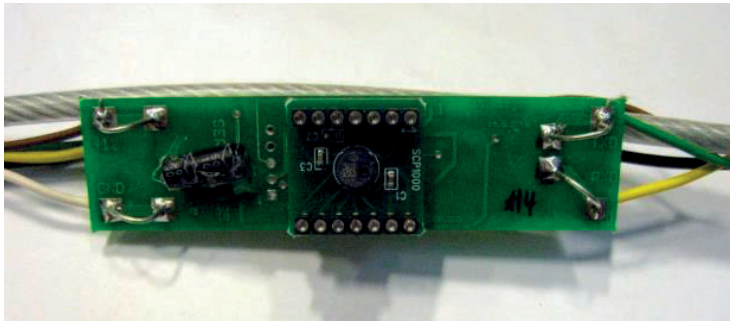

Figure 3.12. A pressure sensor circuit read through serial communication. The size of the circuit board is about 80 × 20 mm. The pressure sensor component itself is located at the centre of the circuit, and its diameter is only 6 mm.

Six sensors were used to test the sensors' measuring accuracy within the settlement pipe system. During the tests, the sensors measured the air pressure, while artificial temperature changes were simultaneously being made. The tests showed that the sensors react very similarly to temperature changes (Figure 3.13). During the observation period, the air pressure changed relatively little, albeit noticeably (top graph). The largest difference in the measurements taken by the sensors that measured the highest and lowest pressure was approximately 10 mm during the test, expressed as the height of the water column (middle graph). A fluctuating temperature of about 20 ºC (bottom graph) had an impact of a few millimetres on the pressure measurements. In addition, the measurements exhibited some slow creeping, the cause of which could not be identified. On the basis of the tests, it was concluded that the sensors require calibrating if the absolute vertical position must be known within 1 mm. However, if only settlement in relation to time is required, the sensors do not need calibrating. The noise of the sensors was equal to a water column of approximately 2 mm (20 Pa). With the average from 100 consecutive measurements, the noise was reduced at a level of 0.1 mm.

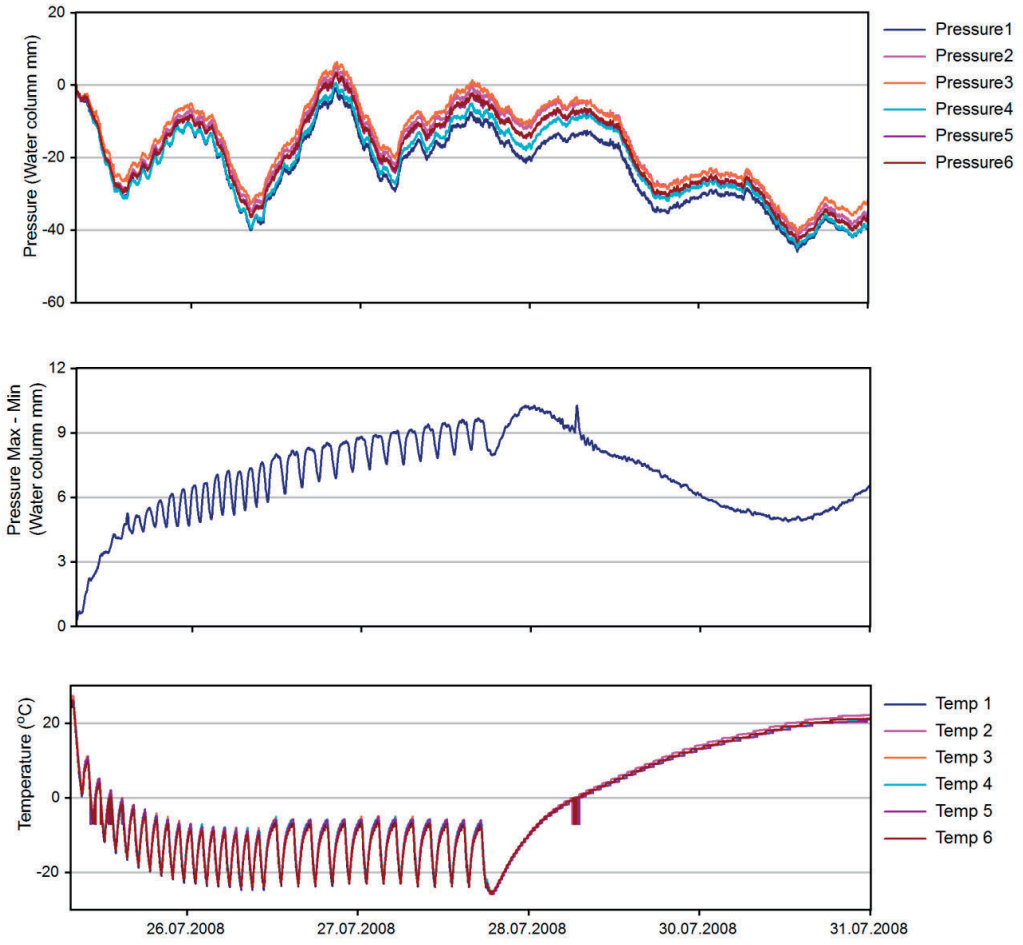

Figure 3.13. Measurement results from the test on the pressure sensors' dependency on temperature.

The most significant discovery regarding the settlement pipe was the choice of fluid creating the hydrostatic pressure. Traditional applications used water as the fluid, but it goes particularly poorly together with electronics. Discussion on the operation of large transformers had sparked an idea to immerse the sensors in oil. Electronics can function without any protection in clean oil. Therefore, the circuit boards were placed without protection inside the settlement pipe, and no expensive capsules were needed for the sensors. Biodegradable hydraulic oil, which is used in excavators and forest tractors for example, has also been used when conducting field measurements. In this way, the risk of environmental damage from an oil spill is minimised.

In addition to the sensor's temperature dependency, the accuracy of the measuring method is influenced by the thermal expansion of the fluid. Every liquid has its own coefficient of thermal expansion, which in the case of the oil used in this application is 0.00085/°C. The pressure difference between the measuring sensor and the reference sensor is directly proportional to the

fluid's density and fluid column height. Density changes in the fluid, caused by the temperature, result in pressure differences, which may be identified as movement of the embankment. This is particularly harmful if the sensors have a significant difference in their vertical positions. For example, a 3-m difference in the vertical position and a 20°C change in temperature already cause (3,000 mm × 20°C × 0.00085/°C) a 51-mm change in the measured settlement. An error resulting from the fluid's thermal expansion can never be completely eradicated, because the temperature will inevitably change at least during long-term measurements. Temperature differences are also created across the significant length of the settlement pipe, especially if there is variation in the installation depth. However, there are several ways in which the temperature dependency can be minimised:

- the sensors can be installed primarily at the same depth to prevent large differences in pressure
- the sensors can be installed as accurately as possible at the same depth in relation to the surface so that the temperature variations remain similar in all sensors
- the sensors can be installed as deep as possible inside the structure so that the temperature variations remain small
- momentary temperature variations can also be reduced by insulating the settlement pipe
- the effect of the fluid's thermal expansion can be compensated with a calculation, based on the measured temperature.

3.2.2. Measuring frost heave and frost depth

Measuring frost depth

To understand frost heave in embankments, the temperatures and frost heave in embankments have been measured at various locations around Finland (Pylkkänen et al. 2012). In accordance with the theme of this study, only the measurement of frost heave is relevant, but understanding the reasons behind frost heave requires the knowledge where the frost line is located. That is why this section will first describe the system for measuring frost depth, which is based on measuring the temperature.

Earlier experiences had taught (Vesilahti Instrumented Road, Chapter 3.3.1) that semiconductor sensors (e.g. LM335) are among the most cost-effective means of measuring temperatures. The components are cheap, and the total cost of the sensors comes from the work costs related to the instrumentation. These sensors were also utilised at frost monitoring stations.

The penetration depth of frost was assumed to be a maximum of approximately 2 m. Therefore, temperature sensors were installed in the structure up to a depth of 3 m to determine the temperature gradient of unfrozen ground as well. The temperature sensors were placed on two separate sensor rods that were installed at the centre of the embankment. One rod consisted of seven sensors and the other consisted of five. The sensors were divided into two groups for three reasons: transporting a 3-m sensor rod is difficult; any frost heave taking place will be more gentle for shorter rods; and if the installation of a rod in the full target depth fails, an allowance can be made with respect to the depth by installing the second rod in a different part of the structure. The sensor rods were installed inside a 16-mm plastic pipe, and the sensors were attached to the pipe

with resin. A plastic pole was formed of the sensor rod, which provided the sensors with a watertight cover.

To determine the frost depth, the measuring accuracy for the temperature must be at least 0.1°C. The main factor affecting the measuring accuracy is the calibration of the sensors. The calibration must be performed for the entire measuring system so that attention is paid to the features of both the data collection equipment and the sensor. Calibration is easiest to conduct with melting ice or snow, because this will allow a temperature that is realistic for the actual utilisation purpose and will remain constant for a long time.

Determining the frost line is often based on determining the zero point of temperature between two sensors with linear interpolation (Figure 3.14, B). This involves a method error, because the thermal conductivity of earth varies depending on whether the ground is frozen or unfrozen. The slope of the temperature gradient changes at the frost line so that it is greater in frozen ground than in unfrozen ground. This error is very small when using a large number of sensors. The frost line can be accurately identified if several sensors at various depths in the unfrozen ground are included in the observation and a line is drawn through their measurements in the coordinate system of temperature and depth (Figure 3.14, A). The line's intersection with the zero point of the temperature marks the depth of the frost line if the frost line is located at exactly 0°C. In reality, the frost line may be located slightly higher, because water only freezes completely at a temperature just under 0°C, depending on the material's specific surface area, salt content and other similar factors (Kujala 1991). Linear extrapolation on the frozen ground's side is also not as reliable as when done on the unfrozen side. Temporary changes in air temperature are clearly visible in the temperatures of frozen ground and may cause a significant error when determining the depth of the frost line.

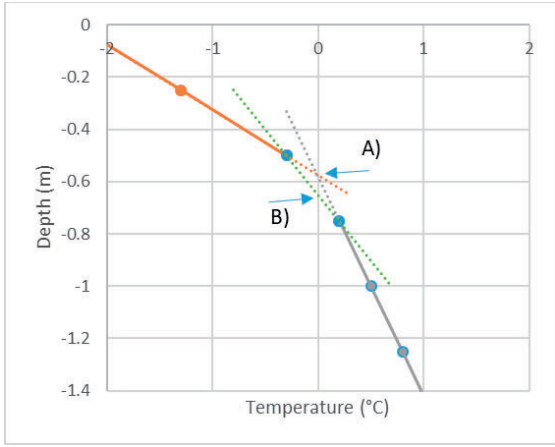

Figure 3.14. Ways of determining the frost line (i.e. the zero point of temperature). In option A, the zero point is determined based on the temperature gradient of unfrozen ground. This will yield a more accurate result compared with the more simple option B.

Measuring frost heave

A fixed reference point is required in order to measure frost heave, and one can be constructed with drill rods installed on the hardpan. Reaching the hardpan may be labour-intensive if the instrumentation targets are located in thick soft ground or high embankments. Vertical movements in an embankment caused by frost heave are created 0–2 m down from the surface, because the structure will usually only freeze down to approximately 2 m. A 3-m anchor rod, with a 2-m section from its top separated from the structure, was estimated to create a sufficiently accurately fixed reference point for measuring the frost heave (Figures 3.15 and 3.16).

The instrumentation of the railway track was conducted so that a 3-m steel rod was installed at the end of a sleeper through ramming. The rod was placed inside a protective pipe down to a depth of 2 m. An adapter was attached to the top of the anchor rod for the displacement sensor. The displacement sensor was mounted directly onto the sleeper. The sensor's protective plastic chamber was attached to the sleeper in a way that allows the sleeper to move dynamically a few millimetres without the chamber breaking. The sensor was installed in such a way that any frost heave will force the sensor's spindle to move, even if the sensor is slightly frozen. Maintenance can easily be performed on the sensor through the threaded lid (the lid is not shown in Figure 3.16). Sensors measuring frost heave were installed at both ends of the sleeper. Novotechnik TRS 50 sensors were used as the displacement sensors. Later, it was discovered that this same measuring arrangement is also suitable for measuring other embankment deformations in addition to those caused by frost. For example, a compaction and settlement of the supporting layer due to ballast degradation and the effect of tamping can be identified with this same measuring system.

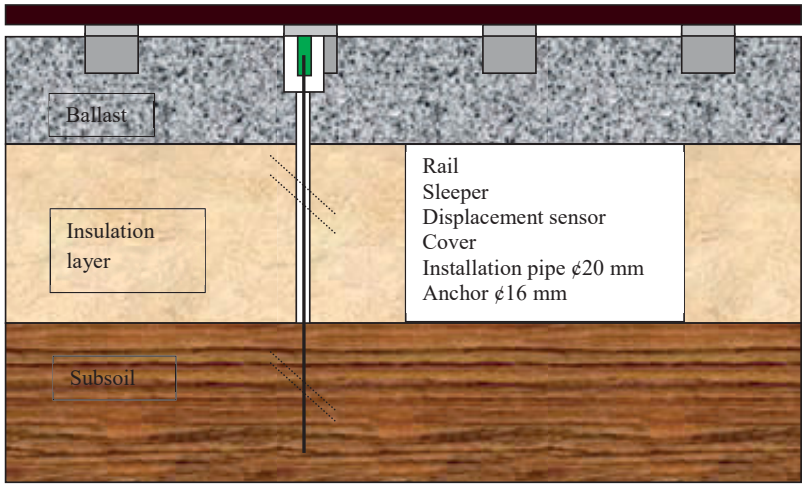

Figure 3.15. Schematic of the automated measuring of frost heave in the structural layers of a track.

Figure 3.16. Measuring system built to measure frost heave in the structural layers of a track.

3.3. Case examples of monitoring sites

3.3.1. Vesilahti Instrumented Road

The Vesilahti test site was the first instrumentation where the author was involved as a primary researcher. The aim of the instrumentation was to develop a new measurement technique for estimation of the service life of a road structure. The Vesilahti test site Mt 2983 is located 30 km southwest from Tampere. The road section was heavily instrumented in the project 'Pavement service life management by new technology' in 2006. The test site is described in more detail in Luomala & Kolisoja (2008). Some of the instruments are still in place, but the real-time monitoring on the site stopped in 2015.

Deflection measurements

Several accelerometers were installed in the road structure in 2006. Five of them were located side by side perpendicular to the lane, and the distance between them was 300 mm. Two installation depths, 180 and 300 mm, were used. A vehicle passing by the lane induces acceleration to the road surface. The measured acceleration can be converted to movement by integrating the signal twice with regard to time (Figure 3.17). The movements of the parallel accelerometers were interpolated as a surface in Figure 3.17. The deflection basin on the left side of the picture is caused by the front axle of a truck. In this case, the tandem axle produces a much larger deflection (right side of the picture).

The depth of the deflection basin seems to be very high compared with the width of the basin. Such a deflection basin is often related to a very low elastic modulus value on the base layer or on the subsoil. However, the moving load can be seen to push a wave ahead, which appears as a heave. The heave makes the shape of the deflection basin very sharp in front of the load.

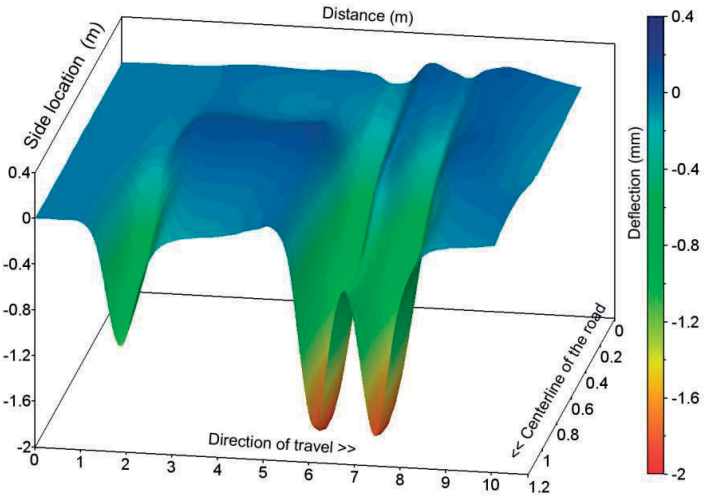

Figure 3.17. Deflection of the road surface caused by a truck and measured by accelerometers

Effect of seasonal variation on pavement stiffness

The main objective of the Vesilahti project was to study management methods for the service life of road structures by measuring the pavement properties. The computational modelling was one of the most important parts of the project. The measurement results can be used as parameters in the calculations. For instance, the use of accelerometers opens up new opportunities to monitor the effects of seasonal variations of the materials.

Deflections of the pavement surface can be determined automatically for every passing axle. Information regarding axle-specific deflections is very important in cumulative traffic loading calculations. In Finland, the pavement stiffness also changes dramatically during a year. Deflections are very small in the winter when the pavement is frozen. Because the asphalt layers are relatively thin, deflections in the summer are rather large. The effect of seasonal variation is readily noticeable from the measurement results of the accelerometers. Even if there were no information on the axle loads, the trend of peak deflection indicates the stiffness properties very clearly.

To determine the actual seasonal variation, the axle loads have to be known. When the loading is random traffic, the axle load must be measured. Unfortunately, in the Vesilahti test site there was no such sensor installed that would measure the axle load reliably enough. For this reason, all the vehicles could not be used for evaluation of the effects of seasonal variation. On the contrary, the Vesilahti test site is a low-volume road, and only a few heavy trucks pass by daily. One of them is a school bus, which passes the instrumentation site on weekdays, and the loading of the bus is very similar day after day. The research was focused on this bus.

The daily deflections caused by the bus were calculated during a three-month period. The observation was made from 23 October 2006 to 17 January 2007. The period included three unfrozen and frozen seasons. Data from the sensors installed at a depth of 330 mm were used in the calculations. The highest deflection on the lane caused by the bus was taken into account. The

distance between accelerometers was 300 mm, which seemed to be slightly too much for detecting the highest possible deflection peak for every passing. This caused some scattering in the results. The peak deflections during the time period are shown in Figure 3.18. The peak deflections caused by the front and the rear wheels of the bus were separated.

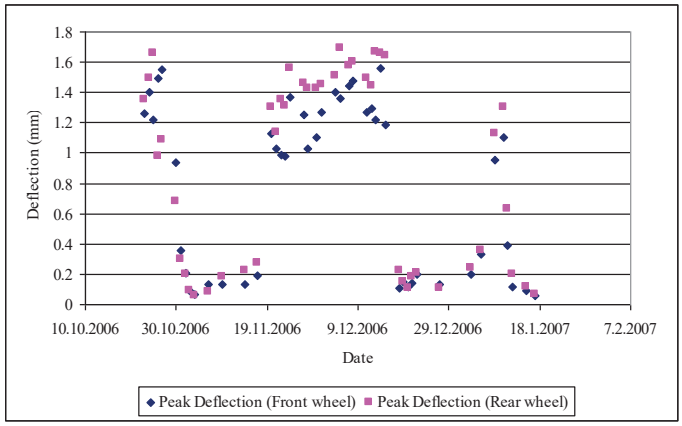

Figure 3.18. Deflection of the road surface during the time period caused by a school bus.

The peak deflections varied considerably during the time period in Figure 3.18. Decreasing deflections are a consequence of frost. The thawing in mid-November and the freezing in mid-December occurred during the weekends as the school bus did not run. This is why the thawing and freezing appear to occur abruptly.

The temperature data were used to estimate the frost penetration depth and had a very similar trend to those of peak deflections. The peak deflections and the estimated frost depths from the temperature measurements were placed in the same plot in Figure 3.19. The effect of freezing in the upper unbound aggregate layers was very clear and strong.

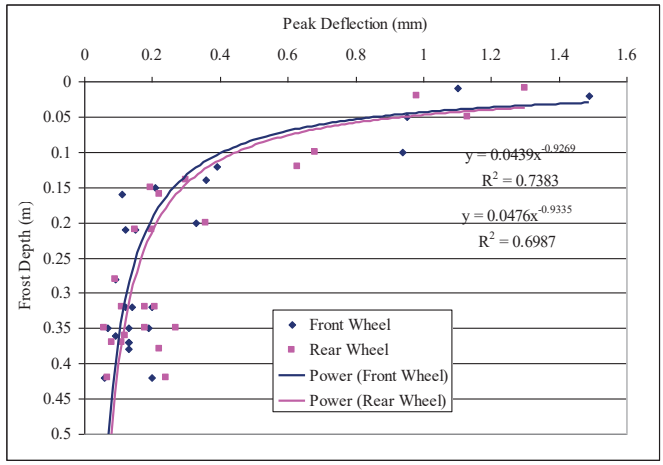

Figure 3.19. Effect of frost depth on peak deflection caused by a school bus.

According to Figure 3.19, the peak deflection decreased rapidly while the frost depth increased. The deflections at unfrozen time were around 1.25 mm under the front wheel and 1.5 mm under the rear wheel. A 0.15-m-thick frozen layer decreased the deflections to a very low level compared with the unfrozen time. The number of measurement points was not large enough to make any specific models of the effects of seasonal variation. However, these measurements definitely show that frost improves the bearing capacity significantly.

Because the lanes at the Vesilahti test site are very narrow and are not marked, the wheel path of the bus varies considerably. The vehicles usually use a little of both of the lanes, unless there is oncoming traffic. Because of the narrow cross-section, the stiffness of the pavement also changes in the side location. Variation of the side location and the properties of the cross-section cause some scattering in the deflection measurements. The edge of the lane is softer than the centre of the road.

The freezing pavement affects not only the peak deflections but also the wideness of the deflection basin. The thicker the frozen layer, the wider the deflection basin. This phenomenon is illustrated in Figure 3.20, where three different deflection basins are shown. The loading is the same in all cases, but the depth of the frozen layer changes.

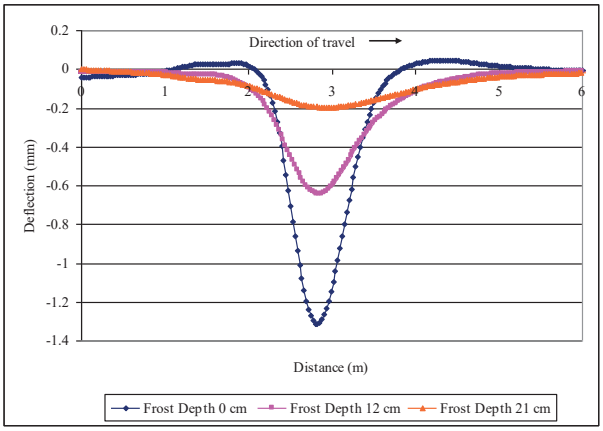

Figure 3.20. Shape of the deflection basin of the road surface with different frost depths measured by accelerometers.

While the pavement is unfrozen, there is also some heave before and after the wheel. Soon after the pavement freezes, the heave disappears. The frost makes the pavement stiffer, which expands the deflection basins and decreases the magnitude of the heave.

In theory, the elastic modulus of the frozen aggregate could be backcalculated. In practice, the backcalculations for partially frozen materials are not that simple due to the remarkable differences in layer stiffness (Simonsen & Isacsson 1999). The elastic modulus of the frozen aggregate is comparable to that of the asphalt layer or even higher. According to the calculations, the elastic modulus of the frozen aggregate in short-term loading can be even more than 10,000 MPa.

Vertical strain

In the Vesilahti test site, the vertical strain of the base course was instrumented at two depths, 200 and 300 mm, using the sensors described in Chapter 3.1.2. The most remarkable finding of the measurement results was that the wheel path has an enormous effect on strains. If the wheel path goes directly over a sensor, the strain is compression most of the time (as is reasonable to assume), and all the strain is recoverable. In such cases, when the wheel path goes next to the sensor, the measurement result may occur as expansion of the layer. Expansion is probably caused by dilatation of the aggregate, and this is due to loosening of the base course material. The expansion also accumulated after every passing axle.

The phenomenon is illustrated in Figure 3.21, which presents the strain signals of one wheel pass from three sensors installed parallel on the lane. The distance between the farthest sensors is 150 mm. In the orange signal, measured underneath the load, the strain is resilient; however, in the other two signals, a part of the strains becomes permanent.

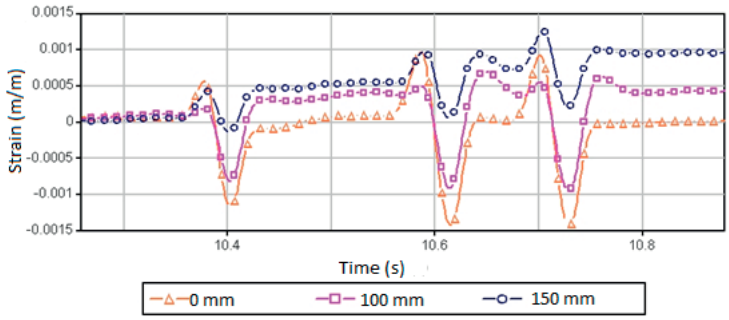

Figure 3.21. Measurement results of the strain sensors from the Vesilahti test site.

Another significant finding in the measured strains was the expansion of the layer in front of the wheel. It was systematically seen that expansion in front of the wheel occurred in the sensor at a depth of 200 mm, but not at a depth of 300 mm, or the effect in the latter case was almost negligible. In sensors located underneath the load, the expansion in front of the wheel could be as large as the overall expansion in sensors next to the load (Figure 3.21). The expansion can be explained by the rotation of principal stresses, which causes shear strain in front of the wheel (Kolisoja 1997).

While the test runs were conducted, the wheel paths varied significantly and several variations of wheel paths were performed. The magnitude of the strain was strongly dependent on the previous loading history. If the previous loading went next to a sensor, the strain caused by a perfect hit on the same sensor caused a much larger deformation than the latter of two subsequent perfect hits. The variation of the results was almost 40%. The variation of the results was largest underneath the first axle of the vehicle, because it loosened and compacted the layer the most.

The detected variation in deformations and the behaviour of the material under various loading conditions caused by differing driving lines place a small question mark on the comparability of the laboratory tests when modelling the materials. For example, the stiffness modulus determined

with a triaxial test is probably higher than that mobilising on a real-life road with a low traffic volume. This is because the loadings in a triaxial test are always the same, and no turning of the principal stresses occurs. The effect of driving lines on base course deformation behaviour is likely to be significantly reduced on roads with heavier traffic and thicker asphalt layers. With thicker structures, the stiffness determined in a laboratory will also be more comparable with that mobilised due to traffic loading.

Main findings

- Acceleration sensors can be used to easily measure deflections on a road surface.
- Frost will reduce deflection significantly: the size of the deflections on a low-volume road that is affected by frost down to a depth of 0.15 m is only a fraction compared with the unfrozen structure. The magnitude of deflection decreases, and the deflection curve's width increases due to the frost.
- The deformations in the upper parts of a structure depend significantly on the location of a load in relation to the sensor. The upper part of a road structure will compress under a load, but shear stresses cause expansion in front and to the sides of a tyre. This observation can partly explain the rutting and widening of a road.
- The loading history affects the mobilising deformation level. Consecutive passes by vehicles on top of a sensor cause a markedly smaller compression compared with a situation in which the previous pass took place slightly to one side of the sensor.

3.3.2. Railway bridge transition zones

A railway bridge approach is often a spot of an uneven track. The transition zone requires more maintenance, and the problems caused by the settlement may lead to the need for speed restrictions. Several types of structures are being built to minimise the effect of the bridge approach. In Finland, the most common type of structure is a transition slab. TUT together with the Finnish railway maintenance company VR Track Ltd. has conducted stiffness measurements on several bridge approaches. The study contained a total of 20 bridges on the Tampere-Seinäjoki (9) and Seinäjoki-Oulu (11) railway lines. The vertical displacement of the sleepers at the end of the bridges was measured by means of accelerometers. On some bridges, the measurements were carried out both before and after the maintenance, and the effect of the maintenance was compared (Luomala & Nurmikolu 2012).

The measurement arrangement consisted of 16 accelerometers, a datalogger, a laptop computer and a power supply unit. The accelerometers were installed on top of the sleeper near the end of the sleeper. Only the vertical displacement was monitored. One sensor was located on top of the first bridge opening (1), one on top of the abutment (2) and the other 14 (3–16) on the embankment (Figure 3.22).

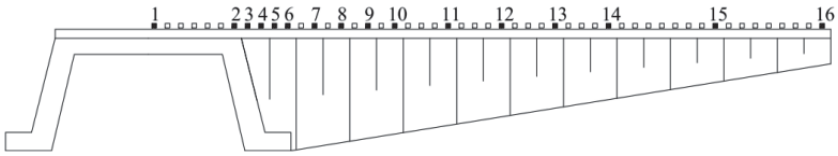

Figure 3.22. Principle of instrumentation and sensor locations.

Tampere-Seinäjoki line

The first phase measurements were conducted on the Tampere-Seinäjoki line in 2008. The line was under rehabilitation, and the aim was to lift the speed limit up to 200 km/h. Several bridge approaches were improved by installing transition slabs to both the bridge ends. Some bridge approaches with better performance were only strengthened by corner retaining wall elements (Table 3.1). The monitored bridges were concrete bridges, including a ballast layer. The sleepers were also made of concrete, and the rails were continuously welded. In these bridges, the design engineer wanted to ensure that the variation of track stiffness was small enough. For this reason, the instrumentation was conducted after the increase in the speed limit, and the effect of Pendolinos (Finnish high-speed passenger trains) at a speed of 200 km/h was monitored among other train services.

Table 3.1. Monitored bridges in 2008.

Location (km + m)	Bridge	Type	Tamping	Procedure
205 + 984	Hirvijärvi	Cont. slab	2003, 2006	Corner ret. wall elem.
222 + 649	Hyönälä	Frame	2005, 2006	Corner ret. wall elem.
199 + 127	Keijärvi	Frame	2006	No procedure
252 + 662	Marjalampi	Cont. beam	2 times a year	Sheet pile wall
251 + 370	Rasinkuja	—	1 time a year	Corner ret. wall elem.
247 + 522	Vahojärvi II	Cont. holl. slab	2005, 2006	Corner ret. wall elem.
231 + 651	Vahonkoski	Slab	2003, 2005	Corner ret. wall elem.
196 + 233	Vihattula	Frame	2004, 2006	Corner ret. wall elem.
229 + 315	Viitaharju	Frame	2 times a year	Corner ret. wall elem.

The measurement results showed that on the bridge abutment, the vertical displacement of the sleeper was very small, 0.1–1.0 mm (Figure 3.23), as the axle load was 14 t. The displacement was usually slightly smaller on the bridge than on the embankment. The first sensor was installed on the deck, but the readings are not shown in Figure 3.23, because the length of the bridges varied.

The main concern was the embankment, where the vertical displacement of the sleeper was typically 0.3–1.3 mm. The track stiffness varied on the transition zone, but the variation was not considered substantial. The variation between bridges was also very small; only on one of the bridges, Marjalampi bridge, the northern transition zone was considerably softer than the other measured 17 transition zones, the vertical displacement being almost 3 mm.

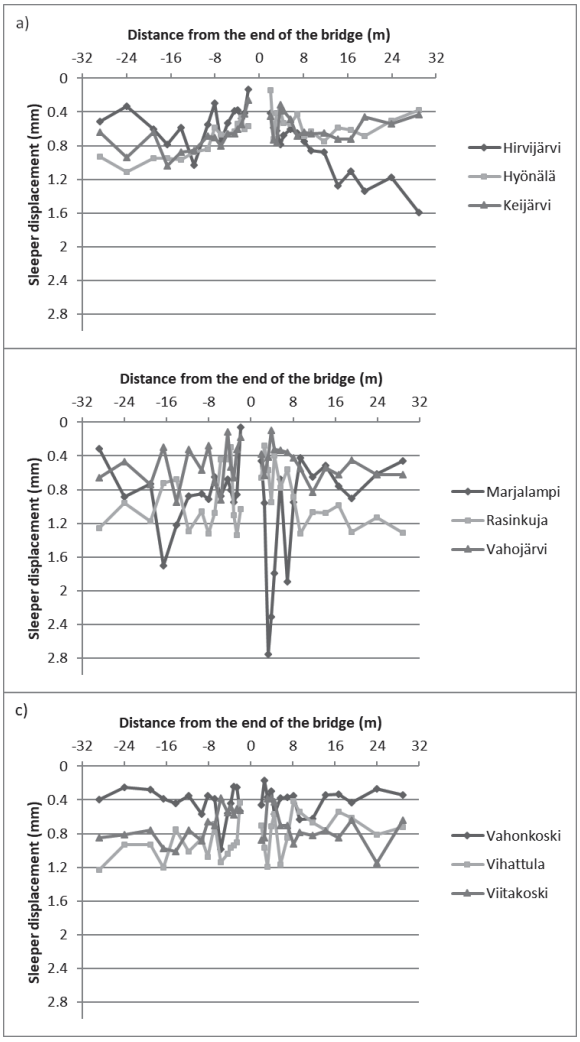

Figure 3.23. Measurement results of the Tampere-Seinäjoki line. The axle load was 14 t.

Seinäjoki-Oulu line

The track improvement work moved up north on the Seinäjoki-Oulu line in the year 2009. There are several river bridges that are made of steel, and the bridge deck is ballastless. Wooden sleepers are connected directly to the bridge beams, but elsewhere on the line, concrete sleepers are in use. Figure 3.24 shows an example from a typical steel bridge over the river Ähtävänjoki. Some properties of the monitored bridges are given in Table 3.2.

Table 3.2. Monitored bridges in 2009.

Location (km + m)	Bridge	Usage	Type	Procedure before the 2011 measurements
524 + 675	Ähtävänjoki	Over river	Steel	Corner ret. wall elem. + transition slab
523 + 156	Dalabäcken	Over river	Conc. frame	
520 + 277	Katternö	Underpass	Conc. frame	
524 + 757	Kolppi	Underpass	Conc. cont. beam	Corner ret. wall elem. + mass replacem.
538 + 311	Kruununkylänjoki	Over river	Steel	Corner ret. wall elem. + transition slab
688 + 337	Ohtuanoja	Over river	Steel	
729 + 847	Ruotsinoja	Over river	Steel	
705 + 751	Siikajoki	Over river	Steel	
730 + 568	Temmesjoki	Over river	Steel	
524 + 339	Torppi	Underpass	Conc. frame	
537 + 213	Tössbacka	Underpass	Conc. cont. beam	

The river embankments are typically located on soft soil, and permanent deformation accumulation on the transition zone is common. The abutments are made of stone blocks, and sometimes they are supported by piles. Seven bridges of this type were monitored. The other four bridges were underpass concrete bridges. All the bridges were monitored by similar instrumentation, as shown earlier in Figure 3.22.

Figure 3.24. Example of a typical Finnish steel bridge, Ähtävänjoki bridge, over a river.

The monitoring was made before the maintenance actions. The purpose was to locate bridges that need heavier improvement and those that possibly do not need any maintenance. The measurement

results are shown in Figure 3.25, where the loading vehicle is electric locomotive SR2 with an axle load of 21 t.

It was found that the magnitude of sleeper displacement was generally remarkably higher than on the Tampere-Seinäjoki line. The most important factor increasing sleeper displacement was the higher axle load and also an old and fouled ballast. The elastic modulus of the ballast was probably only slightly smaller (Nurmikolu & Kolisoja 2011), but the support of the sleepers was extremely poor on some bridge approaches. Especially on Ruotsinoja, Torppi, Kruununkylänjoki and Siikajoki bridges, the scattering of the measurement results on consecutive sleepers was very large. An unevenness on Kruununkylänjoki bridge was noticed on everyday service, and locomotive drivers had reminded the authorities of the maintenance need of the bridge.

The maintenance record was not available, and the timing of the latest tamping was unknown. The measurements were conducted soon after spring thaw, and it was assumed that tamping was not made after the latest winter. It was also found that the support of the sleepers had large variations. Some of the sleepers were supported well, but some of them were hanging from the rails. The void under the sleeper was probably more than 5 mm in the worst-case bridge.

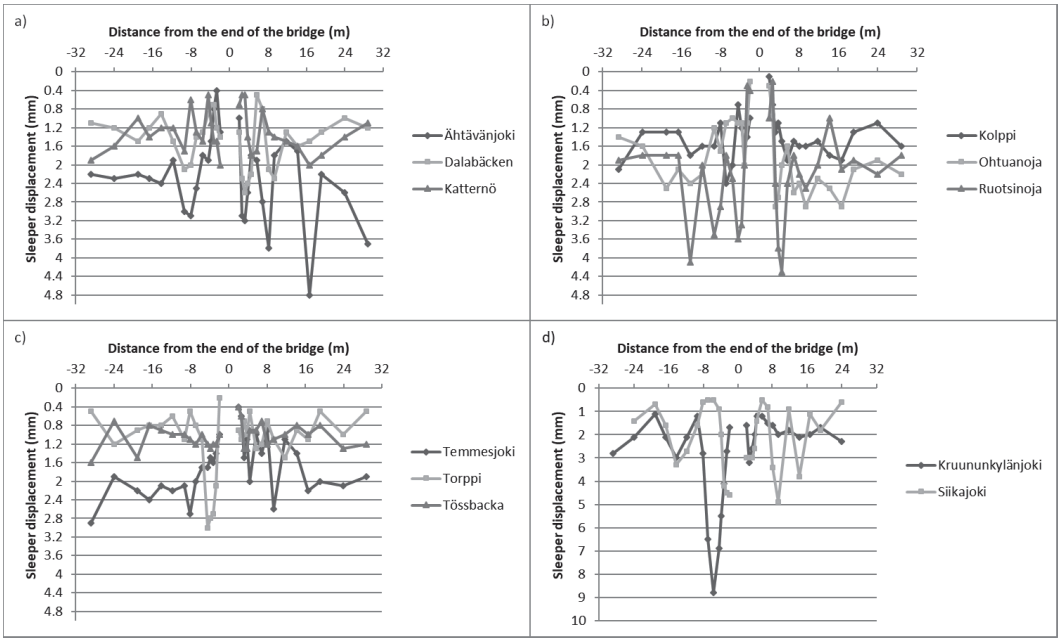

Figure 3.25. Measurement results of bridge approach monitoring in the Seinäjoki-Oulu line. The axle load was 21 t.

Second measurement round

Three of the bridges were monitored again two years after the improvement work in the year 2011. The Kruununkylänjoki and Ähtävänjoki bridges were repaired by installing corner retaining walls next to the abutment and by installing transition slabs on new drilled piles. Geogrids were also used. Kolppi bridge was improved by installing corner retaining wall elements next to the abutment and the earth material was replaced.

The measurement results of both the measurement rounds are shown in Figure 3.26. The loading vehicle was an electric locomotive with an axle load of 21 t. The transition zone improvement work seemed to be working very well on Kruununkylänjoki bridge south end, but it was the only place where sleeper displacements were actually smaller after the maintenance than before. The results were rather confusing: why did the expensive improvements not work? There are several reasons that may cause higher sleeper displacements:

1. The new ballast layer may deform easily soon after the replacement.
2. Tamping was not conducted in 2011.
3. Winter 2010–2011 was rather severe and this may have caused permanent deformation accumulation during spring thaw.

Probably, the most important factor that reduced track stiffness near the bridge ends was the new ballast layer that compacted over time. It has been shown (Nurmikolu & Kolisoja 2010) that ballast will clearly defragment and compact after installation. After tamping, the speed of compaction is rather rapid too (Pylkkänen et al. 2012). According to the results shown in Figure 3.26, it is clear that the bridge approach needs maintenance soon after the improvement work.

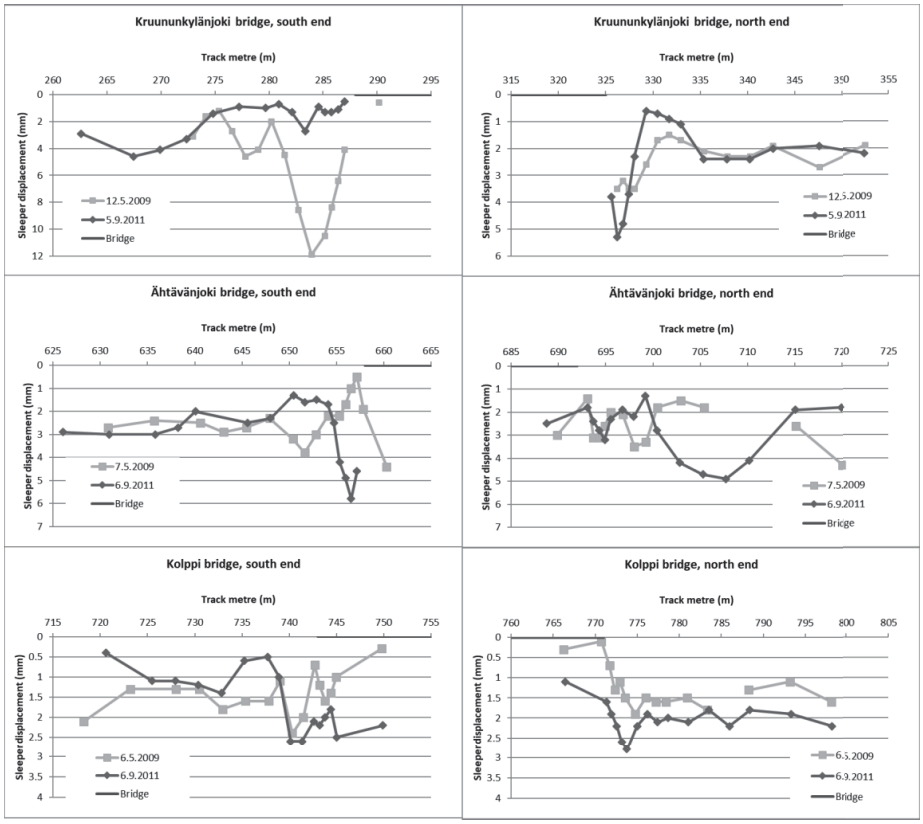

Figure 3.26. Measurement result comparison of two measurement rounds. Measurements were taken before maintenance in 2009 and after maintenance in 2011.

Main findings

- The accelerometers are suitable for measuring recoverable track deflection and sleeper displacement caused by rolling stock.
- A ballasted railway track bridge does not usually cause significant stiffness variation. Stiffness problems occur first as hanging sleepers next to the bridge. This is due to the different speed of permanent deformation accumulation between the bridge and the embankment.
- A ballastless bridge may cause some stiffness variation between the bridge and the embankment; especially the bridge abutment is often a spot of small elasticity.
- The stiffness variation and permanent deformation accumulation are often smoothed by transition slabs and by corner wall elements. These structures decrease maintenance need in the long run, but installation of transition slabs will increase maintenance need in the short run due to compaction of the ballast and structural layers.

3.3.3. Instrumented track in Viiala

A monitoring site was constructed in 2008 in Viiala, 30 km south of Tampere, mainly for frost monitoring purposes. The aim was to measure frost heave and permanent deformation in the railway structure. The monitoring also observed the developments in track deflection during

different seasons. One MDD and three displacement sensors measuring the relation of a drilling rod reaching all the way to the hard bottom were installed in the embankment. MDD was mounted at one end of a sleeper and the displacement sensors to both ends and the middle of the adjacent sleeper. In addition, the temperature of the embankment, the deflection of the sleepers and the axle loads of trains were measured at the site (Figure 3.27).

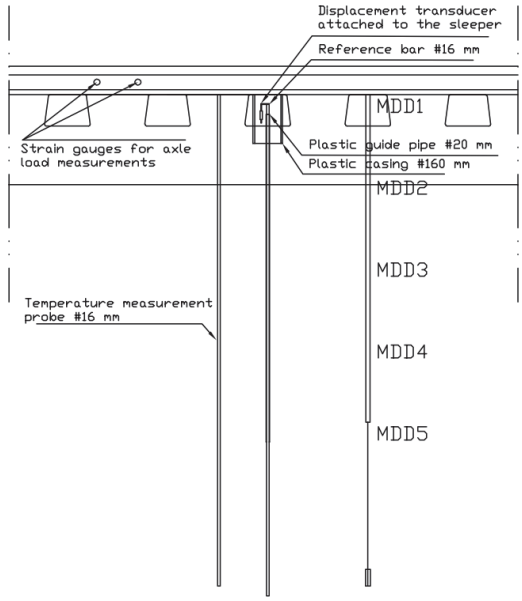

Figure 3.27. Instrumentation plan for Viiala's test site.

According to MDD's measurements, nearly half of the vertical movement of a sleeper was caused by compression of the supporting layer, and the rest was due to compression of the understructure. Figure 3.28 illustrates the vertical deformations at various depths in a railway structure caused by 14 t axles. The relative magnitudes of the compression of different layers are realistic, and the deformations decrease in size when observed deeper in the structure.

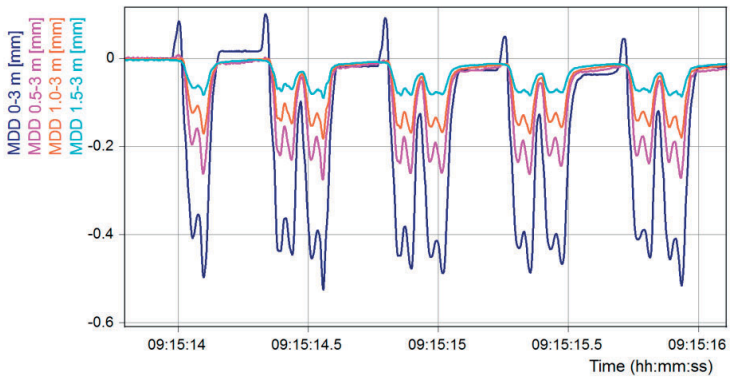

Figure 3.28. Layered compression of the embankment in relation to an anchor at a depth of 3 m, determined with MDD.

MDD was also used to measure frost heave. The total frost heave calculated based on the measuring results, the frost heave occurring at a depth of 0.5–1.0 m, and the frost heave measured with a displacement sensor from the adjacent sleeper in relation to time are presented in Figure 3.29. The total frost heave measured from adjacent sleepers using different methods was very similar. The figure shows that the frost heave occurred almost completely at a depth of 0.5–1.0 m. The same conclusion can be drawn from the frost line calculated based on the temperature measurements. The frost heave mostly took place when the frost line was located at a depth of 0.8 m. Permanent deformation was also accumulated in spring, which was mostly the result of compression of the supporting layer. The sleeper's position after the frost thawed in spring was 4 mm lower than in autumn.

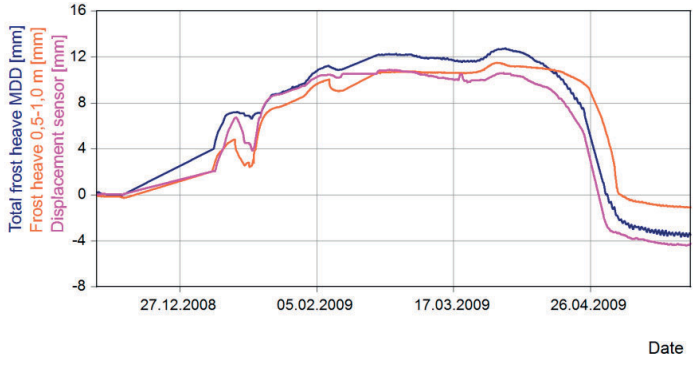

Figure 3.29. Total frost heave and frost heave between 0.5 and 1.0 m measured with MDD, and the adjacent sleeper's total frost heave measured with a displacement sensor.

Main findings

- The MDD sensor is suitable for measuring layered vertical deformations in a railway track or a road.
- The same sensor can be used to measure both recoverable and permanent deformation as well as frost heave.
- At Viiala's test site, this measuring method enabled to identify the layer that causes frost heave.
- The permanent deformation detected in spring thaw was largely due to deformations in the supporting layer.

3.3.4. CTI test, Stynie Wood, Scotland

It has been shown that a vehicle's tyre pressure has an impact on stresses on a road. The impact on permanent deformation accumulation may be significant, especially on low-volume roads and on forest truck roads, which have thin structural layers. The effect of tyre pressure on stresses and deformations was studied with a demonstration test in Stynie Wood, Scotland.

The test site in Stynie Wood was located on a forest truck road that has relatively thin structural layers. The structural layers constructed using good-quality sandy gravel were approximately 0.2 m thick, whereas down to 0.35 m the material was considerably poorer in quality. Below this, the structure consisted of a 0.05-m layer of humus, underneath which was the subsoil of sandy silt. The aim of this monitoring was to investigate the effect that CTI has on the stress level mobilised on a road structure and thus study the benefits of low tyre pressure in reducing permanent deformations in road structures. Four pressure cells were installed in the structure at varying depths, and one strain gauge was placed in the base course layer (Figure 3.30).

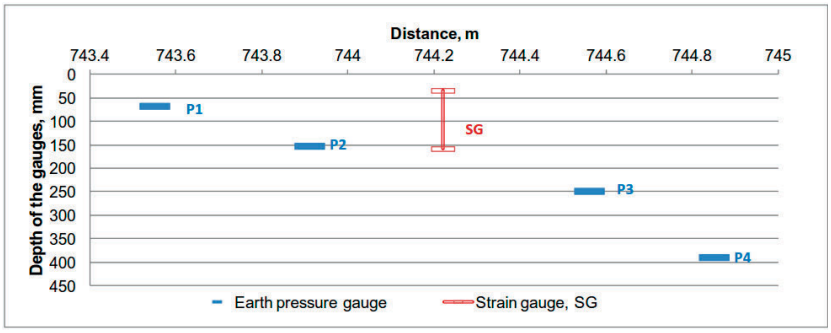

Figure 3.30. Sensor locations at the beginning of the Stynie Wood tests (Vuorimies et al. 2012).

The strain gauge was only installed for test purposes so that the results could provide some interesting findings on the behaviour of the base course layer. The main focus of the test was on the stresses, not on deformations. However, the monitoring revealed that permanent deformation was developed in the instrumented layer with nearly every pass (Figure 3.31). The distance between the strain gauge plates before the test was approximately 120 mm. After the test and 84

passes of the six-axle truck, the permanent deformation near the road surface was almost 10% (11 mm) (Vuorimies et al. 2012).

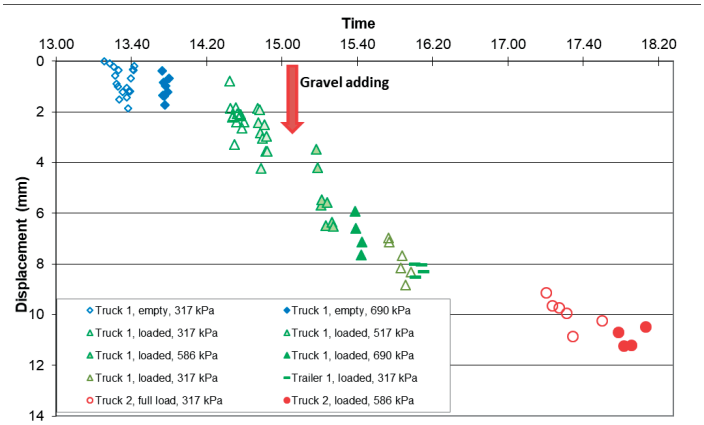

Figure 3.31. Displacement between strain gauge plates after each pass of the trucks (Vuorimies et al. 2012).

Figure 3.32 illustrates the recoverable deformation in the strain gauge caused by the passing front wheel of the truck. The driving line has a significant effect on the magnitude of a deformation. With single wheels, it is clear that when a load hits a sensor, this results in the highest measurement values. An increase in the wheel load of a single wheel also increased the number of deformations very quickly. The number of loadings with different wheel loads varied, as did their drive paths, which may lay emphasis on the effect of the increase in the wheel load. According to the results, a 22% increase in the wheel load also increased the number of deformations by as much as 50%.

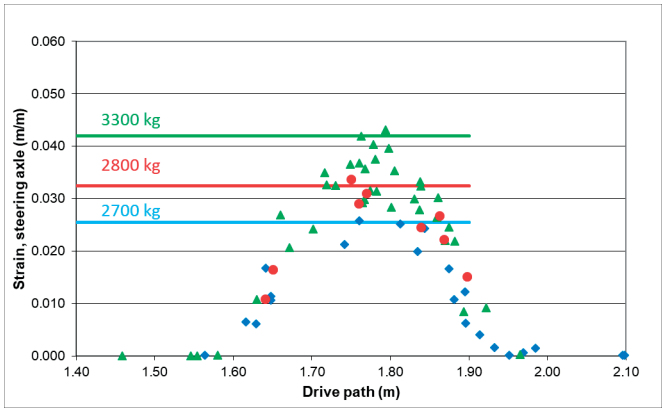

Figure 3.32. Effect of the driving line on strains caused by the steering axle wheels. The colours indicate different wheel loads (Vuorimies et al. 2012).

With dual wheels, interpreting the deformations may be more difficult, because due to rutting, the wheels next to each other may produce a wide range of measurement results (Figure 3.33). Four different tyre pressures were used with the dual wheels and from the lowest to the highest these

were 317, 517, 586 and 690 kPa. Tyre pressure did not have a significant effect on recoverable deformations. The most significant effect from tyre pressure was detected during the first test conducted with an unloaded vehicle, in which the lowest tyre pressure also significantly decreased the strains compared with the high tyre pressures. The rest of the results were mixed, as they were significantly influenced by the increase in road rutting. With dual wheels as well, the driving line as a single parameter had the largest impact on the measured deformations.

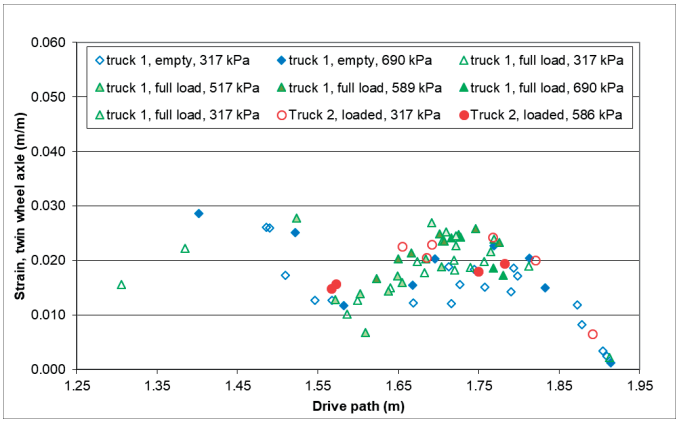

Figure 3.33. Effect of the driving line on strains caused by the dual wheels with variable loads and tyre pressures (Vuorimies et al. 2012).

Main findings

- A strain gauge is well suited to measuring deformations in an individual structural layer.
- The strain gauge can be used to study the magnitude of both recoverable and permanent deformations.
- A vehicle's driving line will have a significant effect on the measurements. With single wheels, a recoverable deformation is at its greatest when the wheel is directly above the sensor. With dual wheels, the ruts on the road affect the measurements considerably. A measured deformation will be smaller than the true deformation if the sensor is located at the bottom of a rut and a dual wheel next to the rut bears a greater proportion of the load.
- On a low-volume forest truck road, permanent deformation is developed with each passing of a vehicle. Changing the driving lines will slow down the accumulation of a permanent deformation.

3.3.5. Settlement study in Paimio

Paimio was chosen as the location for full-scale testing of the settlement pipe (see Chapter 3.2.1). The track section was undergoing upgrade maintenance and levelling had therefore been performed there. Near track milestone km 175 + 000, a clear settlement had been detected, compared with the situation during the track's construction. The settlement, visually estimated to be approximately 50 m in length, was apparently partly created due to the consolidation settlement of subsoil, but also partly because of the poor stability of it. According to the levelling, a settlement of approximately 200 mm had formed in the embankment in 20 years. The total settlement was

notably larger than this, because more ballast had been added several times. A section 150 m in length was selected as the test site, beginning at km 174 + 900 and ending at km 175 + 050. The test section starts from a rock cutting, which quickly changes into a clay bed of approximately 10 m in thickness. The height of the embankment at the end of the test section is roughly 2.5 m.

The settlement pipe was installed at the edge of the embankment to approximately 300 mm in depth. A groove for the pipe was dug with an excavator. The track's supporting layer had recently been sieved, and the sieving residue had been unloaded on the embankment slope. During this process, the embankment became slightly wider. The settlement pipe was placed almost on the original slope's outer edge (Figure 3.34).

Figure 3.34. The settlement pipe being installed.

A settlement pipe can also be installed by ploughing with a cable plough, which can best be done with an excavator equipped with railway wheels. Installing a settlement pipe by ploughing is relatively quick. Ploughing allows 100–200 m of settlement pipe to be installed within a work window of 2 h. This method was later tested at another site with good results. With ploughing, the settlement pipe can be installed right next to the supporting layer. In this way, movements in the embankment are more likely to be transferred to the settlement pipe.

To evaluate the functioning of the new measuring method, measuring points were also installed at the site, measuring the settlement in the embankment by levelling. These measuring points were placed approximately 10 m apart. The steel measuring points consisted of a 250 × 250 mm stand and a 600 mm stem (Figure 3.35). The stand was placed underneath the settlement pipe. The stem was left about 200 mm above the ground.

Figure 3.35. One of the embankment settlement's measuring points for levelling.

The researchers managed to obtain the settlement pipe to take continuous measurements on 9 January 2009. At that time, the ground was still almost completely unfrozen and without snow cover. The installation depth of the settlement pipe varied slightly, so that the initial section of the pipe was closer to the surface of the embankment, whereas towards the end of the monitoring site the pipe had been installed somewhat deeper (Figure 3.36). Measured from the embankment's surface, the depth difference was approximately 0.3 m. The relative vertical position of the settlement pipe was determined based on the pressure inside the pipe. The first ground-installed sensor was chosen to represent the vertical position 0. The first section of the settlement pipe and the reference sensor were attached to the rock cutting, as it was known to remain immobile.

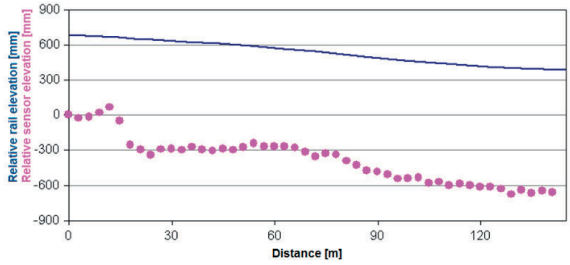

Figure 3.36. Vertical position of the settlement pipe's sensors in relation to the rail.

The settlements were studied in relation to the initial situation. In this way, even the smallest vertical differences could be made more visible. During a small period of frost in mid-January, the temperature dropped very quickly and the embankment froze. The cold temperature lasted for a few days, after which it rose back above 0°C. Owing to the variation in the installation depths, the temperature initially dropped lower in the first section of the pipe than in the last section. When the temperature began to rise again, the situation was reversed. This caused a clearly noticeable change in the pressure. It seemed as if the end of the pipe had first risen a few millimetres in a very short time and then sunk by the same amount later. A thorough analysis showed, however, that the change had been caused mainly by the changes in the fluid density inside the pipe. At the beginning of the pipe, the fluid was colder and therefore heavier at the start of the frosty period. As the temperature gradient turned, the situation was reversed.

After the ground was covered with snow, the situation stabilised for nearly three months, and no large temperature differences or pressure variations were detected until the frost thawed in mid-April. During this three-month period, the end section of the embankment suffered from a settlement of 4–5 mm, according to the settlement pipe (Figure 3.37). It should be noted that there was some deviation between the results from individual sensors; however, after the midpoint in the pipe, the settlement map showed clear areas indicating a settlement. In Figure 3.37, the pipe begins at the bottom of the figure and ends at the top. The yellow or red colour indicates a settlement, and the blue colour indicates a rise. The timeline in the figure goes from left to right. The figure also displays the short frosty period that took place in mid-January. The pressure variation caused by the temperature changes equalled a few millimetres in the vertical position. The measurements were taken every 2 min, but Figure 3.37 shows a 4-h moving average.

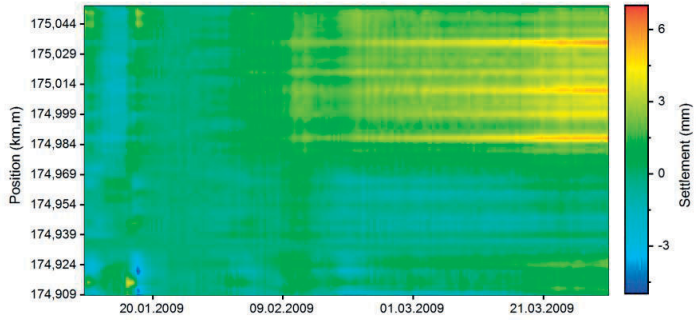

Figure 3.37. Winter-season settlements according to the settlement pipe.

After the frost had thawed, the daily temperature variations in the embankment were large and caused pressure variation inside the pipe. The largest daily temperature changes measured inside the pipe were approximately 10°C, and they caused changes of a few millimetres in the vertical position (Figure 3.38). The figure shows that the rising temperature in the afternoon can be seen as a rise in the vertical position in the sensors near the embankment's surface (km 174 + 909–174 + 924) and similarly as settlement at night-time. Sensors at the end of the pipe, farther down from the embankment's surface, picked up the phenomena caused by the temperature changes later, because in this section the temperature responds to the outside temperature with a delay. The settlement observations were made in relation to sensor No. 10, which is located at approximately track metre 174 + 933.

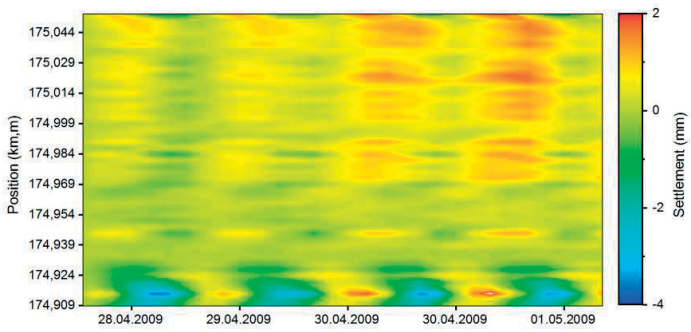

Figure 3.38. Effect of a sizeable daily temperature variation to the settlement pipe's measurements.

True settlement of the embankment

The settlement pipe was in operation until 2017. The levelling was also continued once a year, until the summer of 2013, when the reference points were broken while the coppice was being cut. By that time, the embankment's settlement had become mainly uniform, according to the levelling and the settlement pipe (Figure 3.39). Three of the measuring points differed notably from the levelling results, but because the levelling points were farther apart compared with the sensors, the accuracy of these points is difficult to verify. For example, compaction may have occurred in the embankment after the installation, which would explain the larger settlement in the settlement pipe.

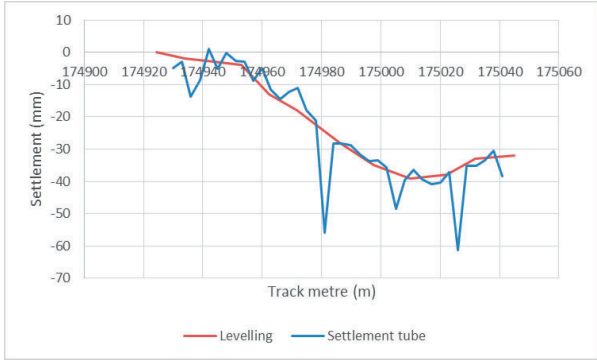

Figure 3.39. Comparison between the results from the levelling and the settlement pipe between 6/2009 and 6/2012.

The settlement pipe has continued to provide measurements after this period (Figure 3.40). The settlement pipe functions still very reliably, apart from those three sensors that indicated a significantly faster settling, compared with the rest of the sensors. The variation in individual sensor readings does not mean that the measurements cannot be used if the sensor network consists of a sufficient number of sensors.

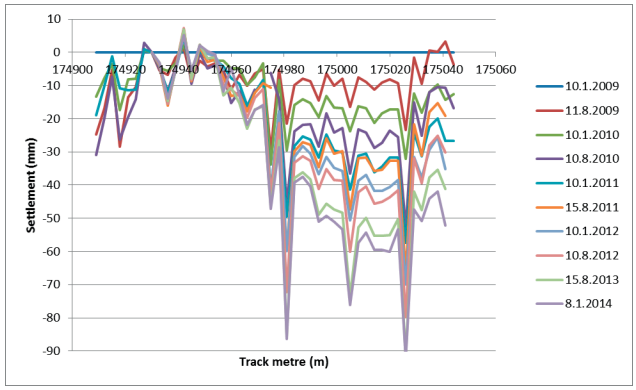

Figure 3.40. Measurements from the settlement pipe at Paimio's monitoring site after five years of monitoring.

Main findings

- An automated settlement pipe has been found to be a functioning method to monitor embankment settlements. In addition, it can be used to measure frost heave.
- The thermal expansion of the fluid inside the settlement pipe affects the measurements, and therefore the installation method should ensure that all the sensors are located in temperatures as close to one another as possible.
- The most accurate measurements can be achieved when the absolute depth of the sensors is as uniform as possible.
- Even old embankments with foundations on soft soil will experience settlement, even though the consolidation settlement should have already ended. In such cross-sections, the resistance to shear failure is low and the settlement is partly caused by shear stress.
- The settlement pipe is also suitable for monitoring embankments with poor stability.

3.3.6. Frost monitoring stations

Frost monitoring stations have been constructed around Finland's railway network in order to study the reasons behind frost damage (Pylkkänen & Nurmikolu 2015). A total of six frost monitoring stations were built in the autumn of 2008. The following year, another six of these stations were added. The measurement findings made at this point created a need to increase the number of temperature sensors, in addition to which water content measurements were deemed necessary in order to gain an understanding of the magnitude of the frost heaves. Similar sensors and measuring arrangements were used to measure the temperature and frost heave as before, but the temperature sensors were installed at shorter intervals depthwise and also on the sides of the embankment.

A Decagon EC-5 sensor, whose operation is based on measuring dielectricity, was used to measure the moisture in the structure. The sensor is intended to be installed by pushing it directly into the ground that is in its natural state, but this cannot be easily achieved in a railway environment. Sensor elements were built inside plastic pipes with holes to measure the moisture content (Figure

3.41), and these pipes were inserted in holes made on the railway structure with drilling rods, similarly to the temperature sensors. The plastic pipe containing moisture sensors was pre-filled with sand. A piece of fabric was inserted into the plastic pipe, thus preventing sand from coming out of the pipe's holes. In other words, the moisture content sensors measure the water content formed in the sensor element's sand material.

When analysing the moisture content measurements, the potential difference between the water content of the installation sand and the true water content of the structure should be noted. The assumption was that the suction of the sand would settle at the same level as in the surrounding material. Even if this did not actually happen, the sensor would indicate the relative change in the water content. By using the materials' soil water characteristics curves (Fredlund & Xing 1994), the sensors were calibrated to indicate the water content in the surrounding material. The installation method used allowed reliable installation and for the sensor to have a known installation material and density level surrounding it.

Figure 3.41. Water content sensors, ready-to-install sensor elements and the installation hole being filled with sand.

In 2010, a further five monitoring stations were built. The highest number of frost monitoring stations in use was 17. Frost findings have been made around Finland's railway network during several winters, and at the time of this dissertation's writing, there are still 12 frost monitoring stations in operation (Figure 3.42) (Pylkkänen et al. 2014).

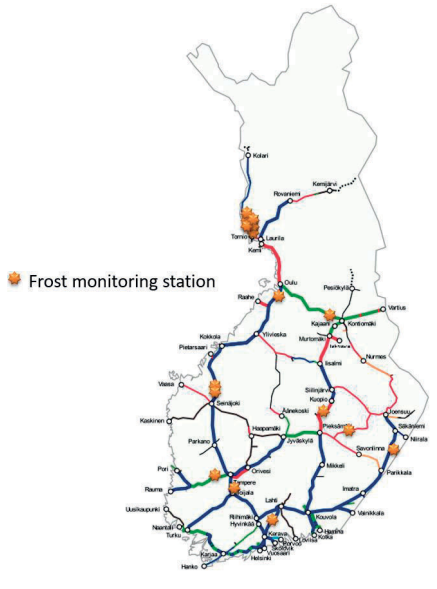

Figure 3.42. Locations of the frost monitoring stations (Pylkkänen et al. 2014).

There are so many frost monitoring stations and presenting all these measurements is not practical in this study. The following figures present some of the measurements taken at three frost monitoring stations, Kitee, Varkaus and Tornio. Data regarding the frost depth (black curve), the vertical position of sleeper ends (blue and red curves), and the water contents in relation to time have been combined in a single figure. Kitee's measurement data (Figure 3.43) on the frost heave measured from either end of a sleeper differ notably. This means that one of the track's sides suffers from frost action considerably more than the other, which causes a certain amount of inclination defect on the track. The winter of 2010–2011 was the coldest of those presented in the figure, and the frost penetrated down the farthest. The frost heave was also at its severest that winter. The following winters were slightly milder, and there was also less frost heave. The white perforated lines illustrate the borderlines between the structural layers and show that every winter the frost penetrated into the embankment filling where the frost-susceptible layer is also located. The colours in the figures represent the relative water content of the sensors' installation sand. The blue colour means dry material, and the red colour indicates material that is completely water saturated. Sensors measuring dielectricity cannot detect frozen water, which is why frozen ground is also shown in blue. On the basis of the measurement data, the structural layers seem to have been slightly more moist in the summer of 2012 than in the summer of 2011. This may indeed have been the case, because the latter summer's precipitation was considerably higher. The moisture content measurements also show that the water content in a structure begins to increase as the structure begins to thaw. The water released when the snow melts seeps through the structure, and therefore a frozen railway structure is by no means impervious to water. Each year, the frost heave begins to develop at very different times: 3 January 2011, 12 February 2012 and 24 March 2013. Every time the frost heave begins, the depth of frost is approximately 1.8 m. The

maximum frost depth is reached in late March or early April, after which the structure begins to thaw, starting primarily from the top but also to a certain extent from the bottom.

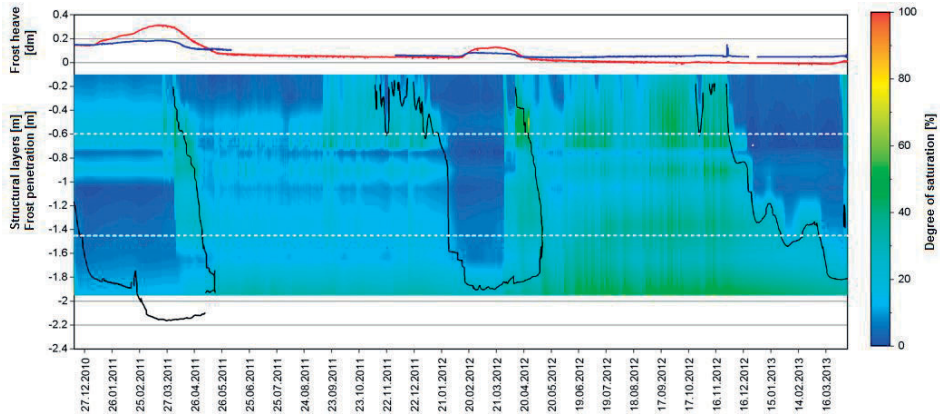

Figure 3.43. Measurement results from Kitee's frost monitoring station.

Measurements taken at the frost monitoring station in Varkaus share many of the properties with those taken in Kitee (Figure 3.44). The frost heave begins to develop when the frost line reaches the subsoil. The winter of 2010–2011 was the coldest, and the greatest amount of frost heave also occurred then. However, the penetration depth of frost was significantly smaller compared with that of Kitee. This can be explained by the site's location in a cutting and the relatively high groundwater level. With the moisture contents, the groundwater level is shown in red, and at its highest it reaches all the way to the structural layers. As winter progresses, the groundwater level drops, but rises rapidly once the frost thaws. The thawing increases the water content most at a depth of approximately 1.2 m, which is also where the layer causing frost heave is located.

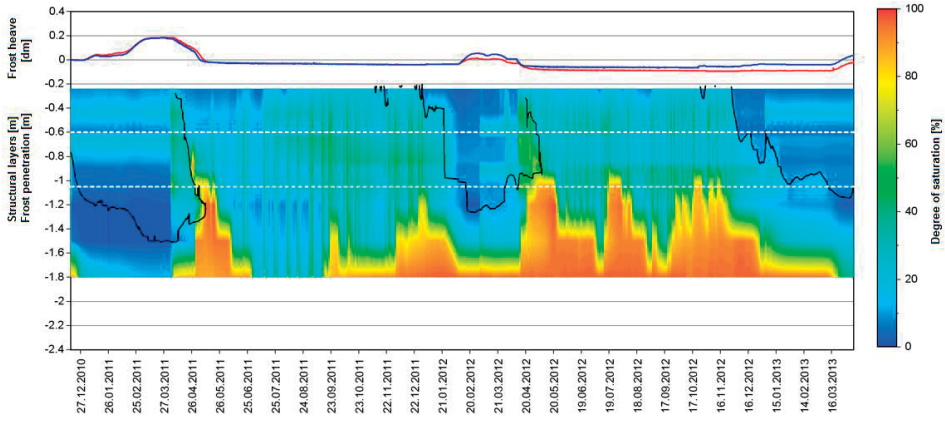

Figure 3.44. Measurement results from the frost monitoring station in Varkaus.

The data from Tornio's frost monitoring station, presented in Figure 3.45, show that this site does not suffer from frost heave, although for three winters the frost penetrates deep into the subsoil. Furthermore, the subsoil at this site was not frost susceptible, based on the frost heave tests. The

constant slow drop in the sleeper's vertical position should be noted in this figure. The same observation was made at all the sites, although distinguishing between the thawing frost heave and the constant settlement is difficult at frost-susceptible sites. The settlement is mainly caused by degradation of the ballast and the resulting increase in the supporting layer's bulk density. The degradation effect is continuous, and its severity depends on rock strength and amount of traffic (Nurmikolu 2005, Pylkkänen & Nurmikolu 2015). Sleeper settlement that is more severe than the degradation occurs at sites that experience a large amount of frost heave. Particularly during the thawing period, the strength of the embankment material or the subsoil decreases due to excess water, causing permanent deformations as a consequence of traffic loading (Metsovuori 2013).

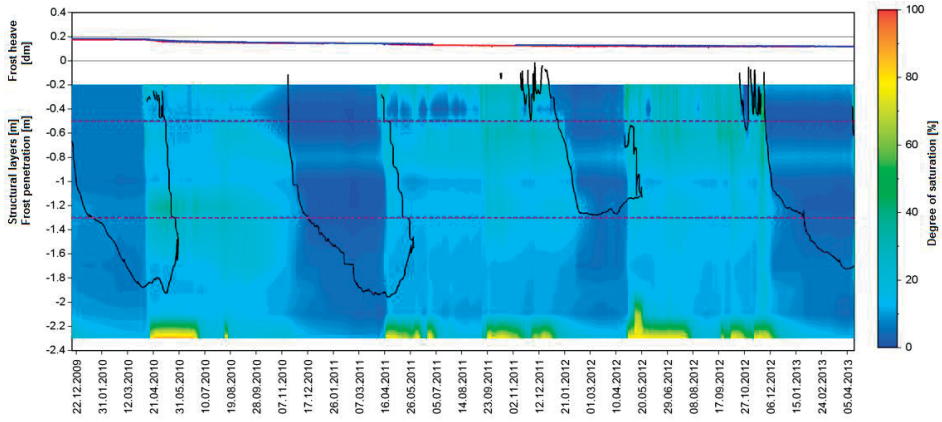

Figure 3.45. Measurement results from Tornio's frost monitoring station.

Another significant finding at this site, built with non-frost-susceptible materials, was that the water content in the embankment decreases below the frost line throughout the winter. Sensors measuring moisture content cannot detect frozen water; however, below the frost line they should produce correct measurements. The water content decreases in unfrozen ground until snow begins to melt on the surface of the structure and the melt water almost immediately seeps through the whole structure, causing a rise in the groundwater level. It is typically assumed that melting water cannot properly leave the structure downwards from the top, because the embankment is frozen. Yet, these examples show that water can find a way through an embankment even if the structural layers are frozen. In other words, a frozen embankment will have pores that are not completely filled with ice. If ice lenses form in a structure due to frost, they will significantly hinder water flow. In these monitoring sites, this does not seem to be the case.

In Tornio's example, the melting does not cause a significant increase in the water content of the structure because of frost, because the structures do not have any melting frost lenses. However, heavy rainfall will show as a momentary increase in the water content.

Main findings

- It is possible to conduct frost line assessment by measuring the temperatures, but special attention should be paid to the measurements' accuracy.
- Frost heave in Finnish railway structures is primarily created rather deep in the insulation layer, embankment fill or subsoil.
- Notable frost heave only occurs during winters that are above the average severity, which supports the finding that the frost-susceptible layer is located deep inside the structure.
- When frost thaws, the track settles notably more in locations that are frost susceptible than in locations that are not. This indicates a decrease in the load-bearing capacity of frost-susceptible materials and the resulting accumulation of permanent deformations in the supporting layer, embankment and subsoil.
- The track's elevation line will continue to drop throughout the year. This is due to the permanent deformation resulting from traffic loading, caused by the degradation of ballast and, to a lesser degree, any permanent deformations occurring in the embankment and the subsoil.

3.4. Challenges related to the utilisation of monitoring methods

The primary aim of the development of all the measuring methods described above was to gain an understanding of the reasons why recoverable and permanent vertical deformations occur in road and railway structures. Different measuring methods can accurately measure the behaviour of one or a few points, but unfortunately these point-based monitoring methods are not sufficiently effective in analysing a large-scale road or track section. For example, acceleration sensors can be used to instrument and monitor simultaneously a maximum of a few dozen points, but this will only cover a small section of a road or track.

Measurement results have shown that traffic loading causes unevenness in bridge approaches: for example, if there is significant variation in the recoverable settlement of different sleepers. Because of structural differences, permanent deformations usually developed slower on a bridge than in an embankment. This easily results in hanging sleepers, which in turn will cause significant unevenness over time. Some of these transition zones can be easily detected by engineers; however, it is also reasonable to assume that transition zones exist in places where they are not so easily identifiable. Therefore, developing a continuous method for measuring track stiffness was believed to be a crucial step in discovering these transition zones more easily.

Of the monitoring methods, perhaps the ones that can be utilised most effectively are those instrumentations that measure both permanent and recoverable deformation. These will help to identify accumulating permanent deformations, which can then be compared with the recoverable deformation and traffic loading in order to determine the load-bearing capacity of a cross-section. With a recoverable deformation alone, it is not possible to deduce the load-bearing capacity or susceptibility to permanent deformations, unless there is a reference with which recoverable deformations can be compared. For example, a combination of both dynamic and static measurements taken over a year-long monitoring period just begins to produce useful data on a

structure's load-bearing capacity. The measurement results from a few cross-sections can be expanded to cover the entire length of a track or road by measuring its stiffness with a continuous method.

A settlement pipe can be used to analyse permanent large-scale or long-wavelength deformations, which cannot necessarily be detected with a track inspection car, for example. However, using a settlement pipe is not a cost-effective solution if the aim is only to monitor the development of permanent deformation. Inexpensive and direct approaches exist for this, including the use of a track inspection trolley (Engstrand 2011). These can quickly and accurately measure a track's geometry without instrumentation. A settlement pipe can, however, add a time dimension to the measurements, and the measuring will turn into monitoring. Real-time measurements are possible, if necessary, and a limit can be determined for the settlement depth to receive a warning if movements are occurring at a dangerous rate. The settlement pipe is one of the few methods available for extensive monitoring conducted for safety reasons.

4. Continuous track stiffness measurement

Track stiffness is a quantity that describes how large deflection of rail is caused by a certain loading inserted into the track. In this Section, a term deflection is used when discussed of the magnitude of stiffness. The axle load in the measurements was 14 t and the dynamic loading was considered insignificant. A small deflection means a high track stiffness or a stiff track. A large deflection means a small stiffness or a soft track. The amount of deflection is easier to comprehend, as the unit is millimetre.

4.1. The Stiffmaster measuring device

Continuous measuring methods for the total stiffness of a track can be divided into two groups based on their operation: methods that measure deflections caused by the rolling stock and those that measure deflections caused by oscillating loads. The methods pertaining to loading by the rolling stock measure a track's geometry, both loaded and unloaded, and the track's total deflection is calculated as the difference between these two measurements. A loading axle is a stock unit's axle with a known axle load, and in some cases the axle load can also be adjusted with a separate loading system. With the methods based on an oscillating load, the load varies within a selected range and frequency, and a track's total deflection is measured with acceleration sensors.

The difference between the loadings in the different measuring methods is considerable, although in theory this should not have a significant effect on the measurement results themselves. With the methods of measuring the loading from rolling stock, the load is comparable to a real-life train load, but the adjustability of the loading is limited. With the methods measuring oscillating loads, the loading can be freely adjusted but differs somewhat from a real-life loading. Another difficulty is determining a suitable loading range. On the one hand, starting the loading range from zero and ending it in a selected axle load is a justifiable approach. In this way, all the properties of the track from the support condition to subsoil properties are included in the observation. On the other hand, the loading range could begin just above the rail seat load that is required to remove the void under a sleeper and end in a selected axle load. This would provide more data on the properties of the embankment and the subsoil. One option would be to use only a load range from zero to the seating load, in which case the observation would focus primarily on the condition of the supporting layer. Regardless of the measuring method, different types of loadings require their own measurement runs, meaning that the choice of method will not completely exclude the different loading ranges from the observation. However, an adjustable loading would be easier to achieve in a measuring method that is based on an oscillating load. This comparison led to a construction of a device that measures deflection caused by rolling stock and operates similarly to another device in use in Switzerland (RIVAS 2013). The device had to be built, because the track gauge in Finland is wider than normal, 1.524 mm. The measuring device was named the Stiffmaster. (Luomala et al. 2015, Peltokangas et al. 2013).

4.1.1. Operating principle

The Stiffmaster's operation is based on the measurement of vertical deviation in a track's height, from both a loaded and an unloaded track. The measuring device consists of three light-weight axles that measure a track's vertical geometry, first under a stock unit's axle load and then without a load (Figure 4.1). The track deflection is the difference between these two measurements, and if necessary, the track's total stiffness can be calculated based on the deflection.

Figure 4.1. The Stiffmaster, a continuously operating measuring device for track stiffness.

The wheelbase of the measurement car was set at 3 m, which was calculated to be sufficiently long to allow a deflection caused by a heavy axle to recover before the light axle. The BOEF model (Chapter 2.2.2) was used for the calculations, according to which the deflection curve of measures performed with a 14 t axle weight will not reach beyond 3 m from the centre of the load. This determined the total length of the device to be 9 m and the height to be approximately 1.3 m. The device height was affected by the wheel diameter and the structural height of the device. The device frame was designed to be triangular in shape in order to make it as light and steady as possible. Structural height was also needed for the actual measuring, because the measuring accuracy of a device improves in proportion to the structural height due to the fact that the sensor measuring the geometry is located at the top section of the device. The wheel diameter was set at 500 mm, because this meets the minimum requirements for the rolling stock (diameter ≥ 400 mm) (Rato 21, Table 21.5:1). In the first prototype, the wheels had separate bearings, which gave a possibility to change the wheels to rubber tyres and to run and test the device on a road, as well. A straight cone, instead of an S1002 profile, was initially selected as the shape of the steel wheel's profile. The test measurements taken at the turnouts showed that the wheels' separate bearings and the simplicity of the wheel profile had an excessive effect on its movement, and the device could not be safely pushed without a risk of derailing. Therefore, another prototype of the device was constructed, using an S1002 wheel profile and a fixed axle, in accordance with standard EN

13715:2006+A1. The measuring device was made as light as possible, and the final axle load was approximately 2.5 t.

The measuring device is attached to a selected stock unit's unsprung mass below the axle for measurements (Figure 4.2). The heavy axle loads the track, causing deflection, the magnitude of which on a track in good condition is normally 0.5–2 mm. The first two axles in the measuring device function as reference points when determining the loaded vertical geometry of the track. The unloaded geometry, in turn, is determined based on the measuring car's first axle, with the second and third axles functioning as reference points. This results in two relative vertical elevation lines. The measurement results are accurately tied to a location, which is done with the help of a pulse sensor measuring the wheel rotation. The spatially tied signal of the unloaded geometry is moved 3 m forwards so that the numerical values of the different elevation lines represent the same location. The deflection of the track can be calculated by subtracting the loaded geometry from the unloaded geometry.

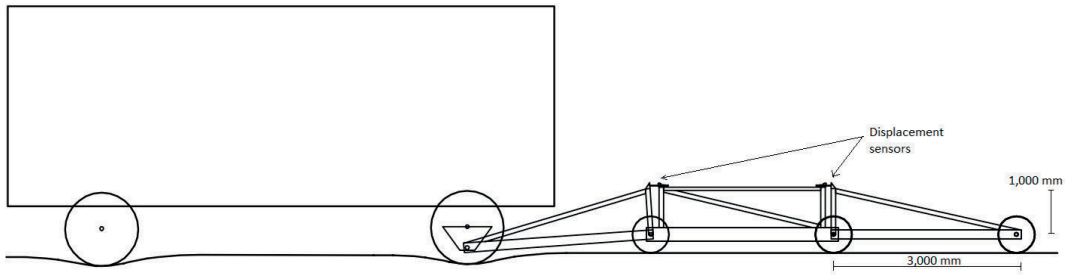

Figure 4.2. Schematic of the continuously operating stiffness measuring device.

The displacement sensors taking the actual measurements are located above a light axle, 1 m from the axle (Figure 4.2). The sensor on the left measures the loaded geometry, and the sensor on the right measures the unloaded geometry. The pulse sensor is located on one of the light axles. The vertical position of a heavy axle is calculated using the level formed by the first and second light wheels (Figure 4.3). This is then compared with the situation created by the light wheels in the same part of the track.

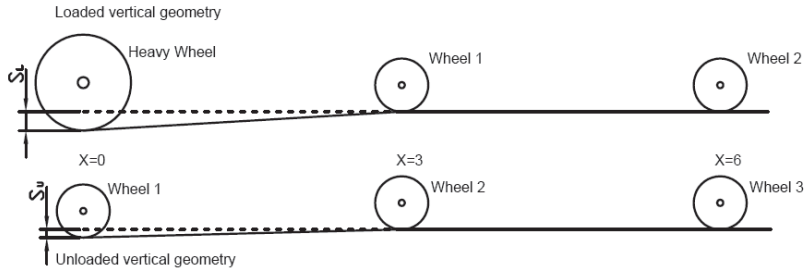

Figure 4.3. Schematic of calculating recoverable deflection.

Track deflection is determined by the following calculation. During the loaded measuring, x is chosen as the location of the first (i.e. heavy) axle, x + 3 as the location of the second one and x + 6 as the location of the third one. Similarly, during the unloaded measuring, the three light axles have the locations x, x + 3 and x + 6. The vertical position y(x) of a loaded axle in relation to an unloaded one is calculated with Equation (4.1). The reference point for the calculation is at x + 3, in relation to which the difference in the vertical positions of the loaded and unloaded axles is determined using the equation of a straight line with respect to the reference surface formed by the second and third axles. The track deflection is the difference between the vertical positions.

$$y(x) = \left[S_L(x+3) + 3 \times \left(-\frac{S_L(x+6) - S_L(x+3)}{6-3}\right) - S_L(x)\right] - \left[S_U(x+3) + 3 \times \left(-\frac{S_U(x+6) - S_U(x+3)}{6-3}\right) - S_U(x)\right] \quad (4.1)$$

where

y(x)	is the track deflection at point x [mm]
S_L	is the vertical position of a loaded wheel [mm]
S_U	is the vertical position of an unloaded wheel [mm]
x	is the distance along the track [m].

Usually, a track's absolute geometry is unknown, and this is why the equation contains several unknown parameters. Only S_L and S_U at x are measured. If assumed that the track deflection has been completely recovered at the first light measurement wheel's position, the terms S_L and S_U receive the same numerical values at points x + 3 and x + 6. This reduces Equation (4.1) to

$$y(x) = S_U(x) - S_L(x) \quad (4.2)$$

Simply put, the track deflection is the difference in sensor readings when transferred to the same location.

The measuring device requires a calibration, which can be used to determine the absolute reading of the sensors in relation to one another and thus the absolute magnitude of the deflection. The calibration can be performed by measuring the track's deflection with acceleration sensors, for example. The use of levelling is also possible. In practice, focusing the calibration methods accurately at a single location in the measuring data may cause problems. Therefore, one more calibration method was designed, in which the measuring device is demounted from the rolling stock but left on a separate support so that the rails support the attachment point. After this, the load is removed, meaning that the rolling stock is moved farther away. In this way, the device will measure the loading effect directly, and the zero level of the deflection can be determined. During the prototype phase, the calibration must be performed separately for each measuring, because the sensors are detached between the measurements. The vertical position of the measuring device's attachment point on the rail service vehicle may also vary, in addition to which it is possible for the device to begin suffering from wear and tear or even have permanent deformations.

Initially, a TKA7 was used as the loading stock unit, and the measuring device was mounted onto its axle with a specifically made attachment (Luomala et al. 2014). TKA7 was chosen after careful consideration, because it would be readily available around Finland. TKA7's axle weight is only 14 t, but finding a heavier axle loads for measurements around the country is considerably more challenging. Later, measurements were also taken with a measuring device mounted on a ballast wagon, which enables the use of a 22.5 t axle weight for the measurements (Luomala et al. 2017).

4.1.2. Testing the prototype

For the first measurements, the measuring device was mounted on the TKA7's unsprung mass at Ylöjärvi's rail yard, where the device was also calibrated (Figure 4.4 and Figure 4.5). The calibration was performed with a video camera, which filmed the rail's deflection during the pass of a heavy axle. The test run was conducted between the operating points of Lielahti and Ylöjärvi, mostly at a speed of 10 km/h. At the midway point, the speed of 20 km/h was tested, but it caused unexpected interference with the measurements, and therefore the running speed was reduced back to 10 km/h. During the measurement run, the functionality of the stiffness measurement was not able to evaluate, as the actual calculation procedure was conducted afterwards.

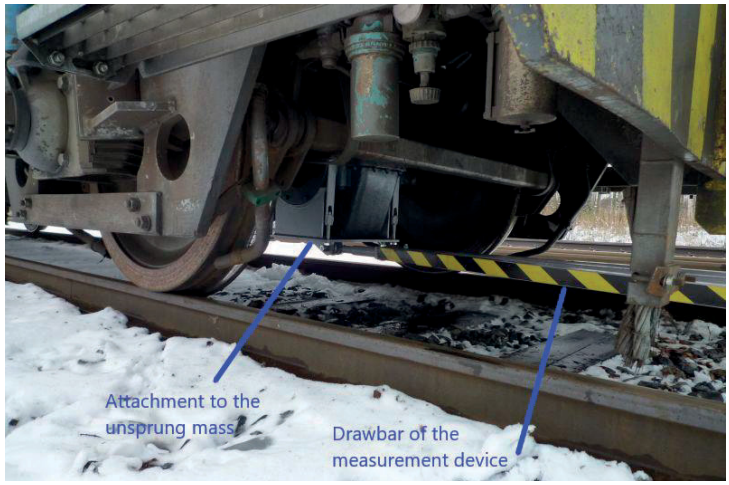

Figure 4.4. The measuring device's attachment to the TKA7's axle on the unsprung mass. A specifically designed mounting adapter is used, attached to the locomotive's transmission.

Figure 4.5.Calibrating the measuring device with a video camera. For this measurement, the device was calibrated by filming the deflection caused by a heavy axle at a known point in the track.

Distance measurements, based on a pulse sensor, and GPS positioning were used to position the measurement results. In addition, lasers were installed in the measuring device to measure the distance to targets located on the sides. Lasers enabled an accurate positioning using, for example, the overhead line poles and mileage markers. In addition, rock cuttings, bridge railings and appliance cabinets could easily be seen in the laser measurements. The measurement run was also filmed. Together with the video, the pulse sensor and laser measuring, the positioning was managed to perform with an error margin of less than 1 m.

4.1.3. Sources of errors

The absolute accuracy of the measuring sensors is approximately 0.015 mm. A coefficient of 3, caused by the device geometry, reduces the sensors' accuracy to approximately 0.045 mm, which can be improved, if necessary, by using a low-pass filter or a moving average. In addition, vibration was initially detected in the measuring wagon attached to the stock unit, and the maximum magnitude of this vibration was over 1 mm at a frequency of 12 Hz. At a speed of 10 km/h, used during the test run, this equals a wavelength of 0.23 m. The effects of vibration can be reduced with low-pass filtering, which does not significantly impair the measurement results, because the deflection of a continuously welded rail cannot vary significantly between two adjacent sleepers. The relative accuracy of the measuring device, factoring in the noise and filters, is therefore somewhere around 0.1 mm.

Naturally, the rails must be clean to allow reliable measurement. Snow causes a notable hindrance to measuring, particularly on a side track, where the rails may be covered in snow. The way in which the rolling stock rides on the rail affects the measurement results as well. A wheel that is in poor condition and has a false flange may have a significant effect on the numerical value of a recoverable deflection, particularly in curves.

The out-of-roundness of the measuring device's wheels shows in the measurements as an approximately 1.6-m wavelength. This error is inconsequential in large-scale stiffness analyses, because the error is cyclic and zero on average. The error caused by the wheels' out-of-roundness is small compared with the other sources of errors.

The most puzzling feature in the measurement results was the negative deflection occurring at some individual points in the Lielahti's test area. Physically, this would mean that the rail was rising upwards underneath a heavy load. Naturally, this cannot be true, and an explanation was searched from the measuring method itself. The phenomenon was connected to the fishplate joints and presumably to the fact that deflection caused by a heavy load is more widespread than the expected maximum of 3 m from the axle (Figure 4.6). Let us assume that a track's vertical geometry is a straight line. Because of the wide shape of the deflection curve, the measuring device can detect a deflection smaller than the true deflection during loaded measuring, and the unloaded geometry erroneously also includes a small deflection caused by the load at the location of the first unloaded wheel. If the latter is greater than the former, the calculated deflection becomes negative.

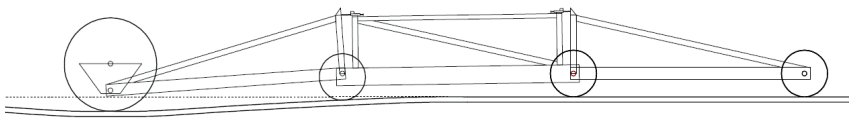

Figure 4.6. Effect of a wide deflection curve on the measurements.

Let us assume that the deflection has time to recover over a distance of 3 m and that the track's absolute geometry is known. The imaginary numerical values are inserted in Equation (4.3) so that the vertical position of the heavy wheel is $S_L(x) = 1$ mm (0.001 m) and the other wheels are at a height of 6 mm. This results in a deflection of 5 mm.

$$y(x) = \left[0.006 + 3 \times \left(-\frac{0.006 - 0.006}{6 - 3}\right) - 0.001\right] - \left[0.006 + 3 \times \left(-\frac{0.006 - 0.006}{6 - 3}\right) - 0.006\right] = 0.005 \quad (4.3)$$

If the deflection curve is more extensive than expected and the deflection continues to affect the area where the wheel $S_L(x + 3)$ is located by 2 mm, it will receive the numerical value of $S_L(x + 3) = 4$ mm. A constantly wide deflection curve will also affect the wheel $S_U(x)$, which is likewise travelling 2 mm lower. The other wheels are still travelling at the level of 6 mm. That is why the formula's result is −1 mm.

$$y(x) = \left[0.004 + 3 \times \left(-\frac{0.006 - 0.004}{6 - 3}\right) - 0.001\right] - \left[0.006 + 3 \times \left(-\frac{0.006 - 0.006}{6 - 3}\right) - 0.004\right] = -0.001 \quad (4.4)$$

Another situation in which negative deflection may occur is when there are frequent fishplate joints, the ballast at the joints has suffered from degradation, and there is a short and notably stiffer section between the joints. In this case, the stiffer section might function as a support and the rail as a lever so that a heavy load lifts the adjacent fishplate joint in the air. This would cause negative deflection in the support section, because the loaded geometry produces little deflection whereas the unloaded geometry detects significant deflection in that spot (Figure 4.7).

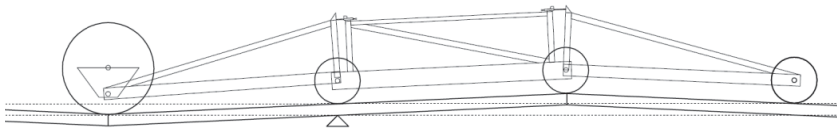

Figure 4.7. Effect of fishplate joints and a degraded supporting layer on the measuring.

The numerical values for the wheels' vertical positions (mm) could be 2, 3 and 3, for example, in the loaded geometry and 3, 5 and 3 in the unloaded geometry. In that case, the result of the formula would be −2 mm.

$$y(x) = \left[0.003 + 3 \times \left(-\frac{0.003 - 0.003}{6 - 3}\right) - 0.002\right] - \left[0.004 + 3 \times \left(-\frac{0.003 - 0.005}{6 - 3}\right) - 0.003\right] = -0.002 \quad (4.5)$$

On the basis of what has been described above, it is mathematically possible that a measured deflection receives an incorrect algebraic sign. Removing this feature from the current measuring device is nearly impossible. The only solution to correct the situation would be to extend the wheelbase, which would require building a whole new device. The error can be reduced by half by adding an extra set of wheels in the measuring device. This would allow the unloaded geometry, determined farther away from the load, to be measured correctly every time. This extra set of wheels has since been added when taking measurements with a heavier axle load (Luomala et al. 2017).

4.2. Measurement examples from the track section of Lielahti–Ylöjärvi

The first actual measurements were taken on the main track, between the operating points of Lielahti and Ylöjärvi. This track section is 7.4 km long and is on the second-best maintenance level, 1A. This section was selected as the test track due to its conveniently close location, suitable work windows and diverse properties. This track section has both high embankments and rock cuttings, even embankments in water. This was the extent of the information intended to gain on the track's features, because the aim was to test the functionality of the measuring device under varying conditions on a good track. The first measurement run was conducted on 29 October 2012. At that time, there was some snow on the ground, but severe freezing temperatures had not yet occurred and the railway structure was still completely unfrozen. The second measurement run took place on 5 March 2013 when the railway structure was frozen.

4.2.1. Measurement results

The measurement results from the winter measuring sessions on the entire section of the track are presented in Figure 4.8. The blue curve represents the deflection signal, filtered with a 2-Hz low-pass filter, which at a measurement speed of 10 km/h equals a wavelength of approximately 1.4 m. In other words, variations shorter than this will not be completely visible in the signal, and very short variations, such as track joints, will not show at all. The effects of different filters on the measurement results are discussed in more detail in Chapter 4.3.1, once the measuring arrangement has been further developed. The pink curve is the 20-m moving average calculated from the signal described above and better illustrates the local variation in stiffness. The calibration points have been marked in the figure with orange dots.

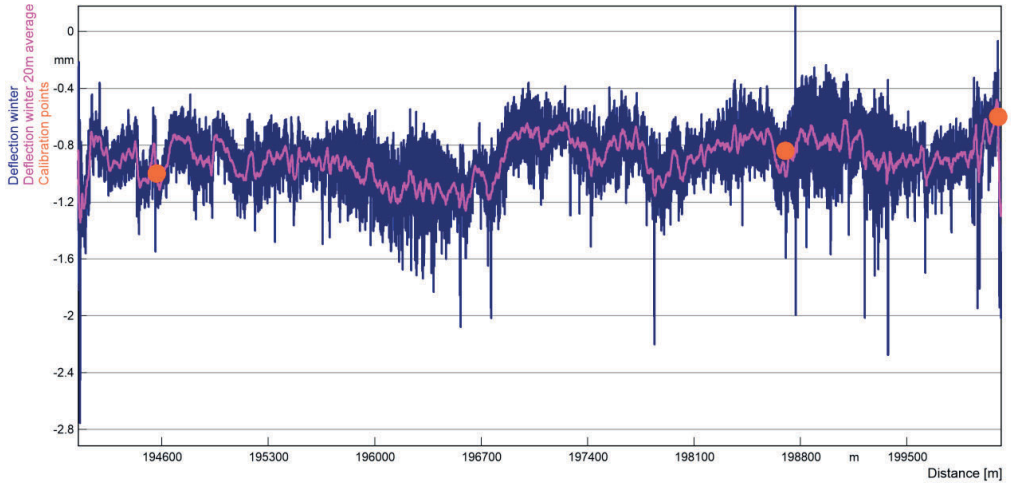

Figure 4.8. Measurement results from winter measurements on the Lielahti–Ylöjärvi track section.

The measurements show large individual deflections in various parts of the track. To analyse these, the scale of the figure must be increased considerably. The average curve shows most clearly the turnout located at km 194+060 and beyond that an area of larger deflection caused by something else (possibly a frost insulation board). A bridge is located at km 194+545, which can be seen in the graph due to the frost insulation on both sides of the bridge, which increases deflection. At km 196+900 a rock cutting begins, which shows up as a decrease in deflection in the winter as well. The rock cutting ends completely at km 197+850, where the shorter average signal clearly shows the weak support of sleepers as a large focused deflection. An analysis of the video material provides an explanation for most of the individual large deflection spikes, because these are associated with points of discontinuity on the track, such as a balise, a hot axle-box detector or an insulated joint. Some are also the result of other factors deeper in the railway structure, such as bridges, frost insulation boards, culverts or rock cuttings.

To compare the measurements taken in autumn and winter, the 20-m moving averages of the measurement data were drawn in the same diagram (Figure 4.9). The details in a corresponding figure illustrating the shorter average signal were lost in the noise, and that is why the 20-m moving

average was found to be the most suitable for comparison. The noise level was similar in magnitude during the different measurement sessions. The distance was determined sufficiently accurately to be able to compare the measurements taken during different runs. Problems were experienced with the calibration of the autumn measurements, and the absolute level of the measurement results remained uncertain. The winter measurement calibration was more reliable. Deflection should, on average, be smaller in winter due to the track's freezing. There are, however, areas, such as rock cuttings and bridges, where frost presumably does not have a great impact on the measurement results. Hence, the autumn measurement level was set so that the deflections from different measurement runs are near each other in the rock cuttings and bridges.

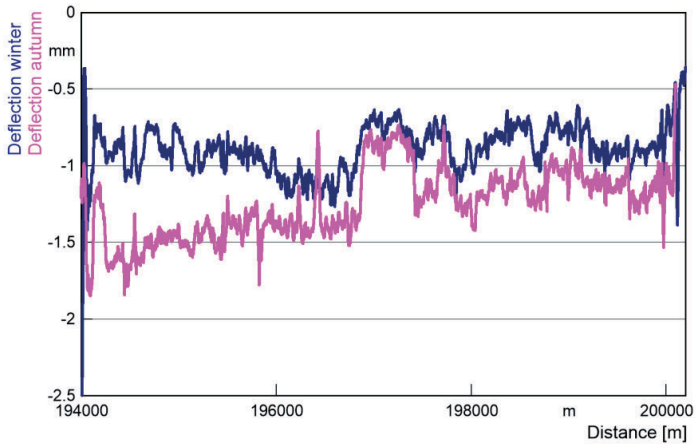

Figure 4.9. Winter and autumn measurement results from between the operating points of Lielahti and Ylöjärvi, using a 20-m moving average.

The moving average of the deflection (Figure 4.9) shows several similarities on both measurement runs. For instance, the rock cutting at km 197 is visible in the graph, and after km 198 the deflection curves look very much alike. On average, the deflection in the winter measurement is 0.88 mm, and that in the autumn measurement is 1.25 mm. In the winter measurement, the deflection is more even throughout the entire measurement area, whereas in the autumn measurement, the average deflection decreases slightly as the kilometres increase. A clear reason was not found for this, but it was suspected that a curve in the track (km 194 + 251 to 195 + 354, R = 2,000) caused a measuring error. For example, the bridge located at km 194 + 550 should produce an almost identical deflection during both the autumn and winter measurements; however, in the autumn the deflection is 0.8 mm greater.

4.2.2. Main findings

The measurement results were initially analysed by finding the transition zones in the registers and investigating whether they affected the deflection values. The comparison included both measurement runs.

Track culverts

The culverts were the first object that were analysed. Out of these, only the culvert at km 199 + 378 was clearly visible as a larger deflection (Figure 4.10). The other culverts were, in practice, non-visible amid the noise. The greater deflection detected at the culvert is likely caused by poor support, and there are a few hanging sleepers at the culvert's location.

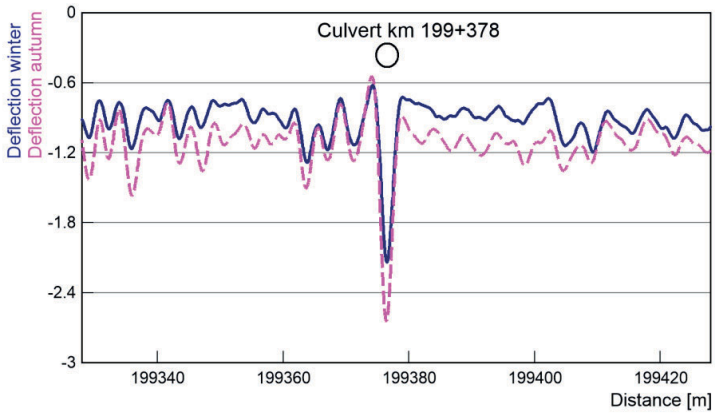

Figure 4.10. Measurement results from the culvert at km 199 + 378.

Bridge approaches

Some of the bridge approaches are clearly visible due to significant deflection (Figure 4.11). For example, the recoverable deflection on the Epilänharju bridge at km 194 + 547 was slightly smaller in magnitude on the bridge deck when compared with the surrounding track; however, this is at least partly explained by the frost insulation boards surrounding the bridge. The increased deflection at the northern end of the bridge, likely caused by hanging sleepers, was notably larger during the autumn measurement than during the winter measurement. At the southern end, changing seasons do not have an equally significant effect. The smaller deflection in the transition zone in winter is a little surprising, because it means that freezing reduces deflection. If a deflection larger than usual was entirely caused by poor support, the recoverable deflection should not decrease in magnitude in the winter. However, a frozen structure does spread the load in a new way, which may explain some of the reduction in the deflection. Well-supported sleepers around hanging sleepers receive a larger load in winter, and the railway structure underneath them is stiffer, which partly reduces deflection. However, with this particular bridge, the need for tamping in the relatively near future is obvious. The difference in the deflection level between two measurement runs is much greater at this bridge than at the culvert illustrated in Figure 4.10. The measurement arrangement may have a feature that causes error in the levels in the measurement results.

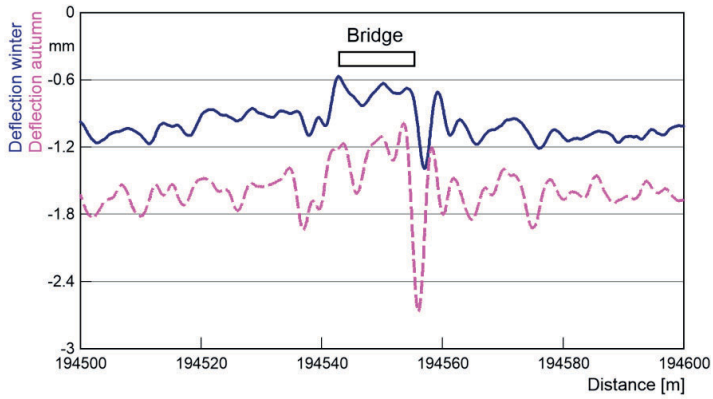

Figure 4.11. Measurement results from Epilänharju's underpass at km 194 + 547.

Turnouts

At the turnout V001 in Ylöjärvi, the winter measurement was conducted as a through run over the turnout, but during the autumn measurement run, the measuring device stopped at the turnout to pick up an assistant (km 200 + 100). Therefore, the autumn measurement may contain a small measurement error caused by the deceleration and acceleration. At the switch panel, sections that were clearly more flexible were detected and the crossing is also slightly visible. The turnout in Ylöjärvi is partially located on top of a bridge (Koulupolku's underpass at km 200 + 128), which contributes to the problems in interpreting the data (Figure 4.12).

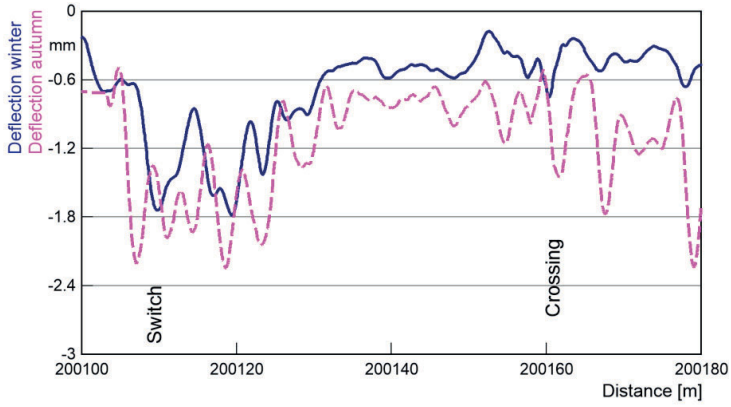

Figure 4.12. Measurement results at the turnout V001 in Ylöjärvi.

The measurement section has two turnouts with wooden sleepers. In those, the track's stiffness is somewhat less in magnitude than the average where the switch panel and, in particular, the actuators are located. A similar observation can be made for the crossing, although the effect is smaller there. When it comes to the switch panel, the cause is probably poor support, because the

actuator spots cannot be properly tamped. At the crossing, the support is probably also poor, but this is likely due to the dynamic loading created because of the crossing.

One interesting observation is that the deflection is almost equal in magnitude in both autumn and winter where the switch panel is located, whereas at the crossing, it is clearly smaller in winter. A hypothesis exists, which explains that at the switch panel, the switch heating keeps the track mostly unfrozen during winter. Frost would seem to significantly reduce the stiffness variation detected at the crossing and towards the track that separates at the crossing.

Frost insulation boards

Frost insulation boards affect a track's stiffness in a number of ways. The deflection increases by approximately 0.1–0.2 mm on average in frost insulation board locations. However, the deflection does not clearly increase in all the expected board locations, and the maximum increase is approximately 0.3 mm. The thickness and material of the boards will, of course, influence the magnitude of the deflection (Nurmikolu & Kolisoja 2005). Detailed information on the frost insulation boards' properties in the track section is not available, and comparisons on, for example, whether deflection increases in relation to the board thickness cannot be done.

Another clear finding regarding frost insulation boards was that approximately half of the places where the board edges are located exhibited localised deflections greater than average in magnitude. There can be several reasons for this, but presumably the phenomenon is at least partly connected to a sudden transition zone, resulting in a similar increase in permanent deformations at both the board edges than the bridge approaches.

Figures 4.13 and 4.14 present the measurement results from the track sections with insulation boards. In the first figure, the effect of the boards is clearly visible as a level change, at least in the autumn measurement. In addition, the second example shows the reduced support connected to the beginnings and ends of the insulation boards, which is a phenomenon similar to the one occurring at bridge approaches. In fact, Figure 4.14 contains a bridge in the middle of the graph at km 194 + 550. It is likely that a large recoverable deflection is connected to the beginning of frost insulation at km 194 + 440.

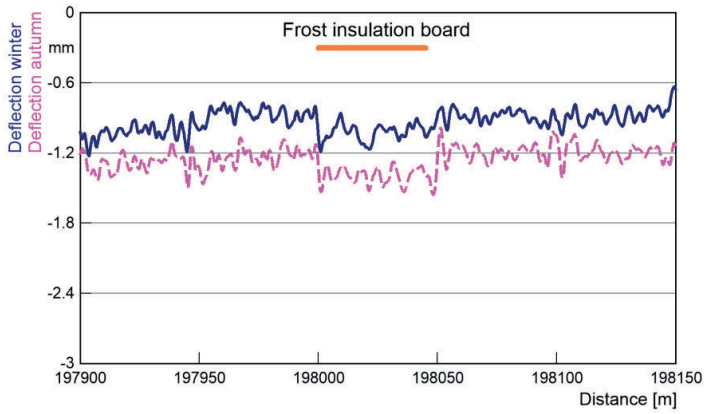

Figure 4.13. The frost insulation board's effect on track deflection at km 198 + 000 to 198 + 050.

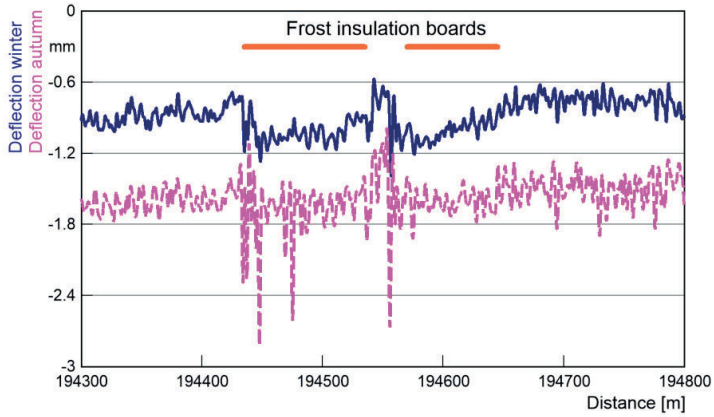

Figure 4.14. The frost insulation board's effect on track deflection at km 194 + 440 to 194 + 650.

4.2.3. Connection to geometry defects

One of the driving forces of this study has been the assumption that geometry defects are developed in those parts of a track with stiffness variation. Here geometry defects do not refer specifically to categorised errors but to geometric variation in general. The supposition is that after maintenance, the geometry is in a good state and no significant unevenness exists.

The measuring device measures the vertical geometry as an interim result, using the chord measurement technique with a wheel interval of 3 + 3 m. The author of this study is fully aware that the method places varying emphasis on different wavelengths and that a symmetrical wheel interval is an especially poor choice in this regard (Esveld 1978). For example, the measuring does not detect the 3-m wavelength of the vertical geometry at all, but doubles the 6-m wave's amplitude in comparison to the true value. Therefore, transfer functions should definitely be used when

scaling the results in relation to the wavelength. Even a slightly skewed measurement result shows the location of the geometry defects, and because the measuring device is not used to identify geometry defects, in particular, no more attention was paid to the absolute accuracy of the geometry.

A comparison between vertical geometry and deflection shows that the supposition of a correlation existing between geometry defects and stiffness variation is true in many places, albeit not everywhere. Usually, stiffness variation is also accompanied by geometry defects, as in Figure 4.15, although not always to a significant extent, as illustrated by Figure 4.16. On the contrary, geometry defects also occur in places without a large variation in stiffness (Figure 4.17).

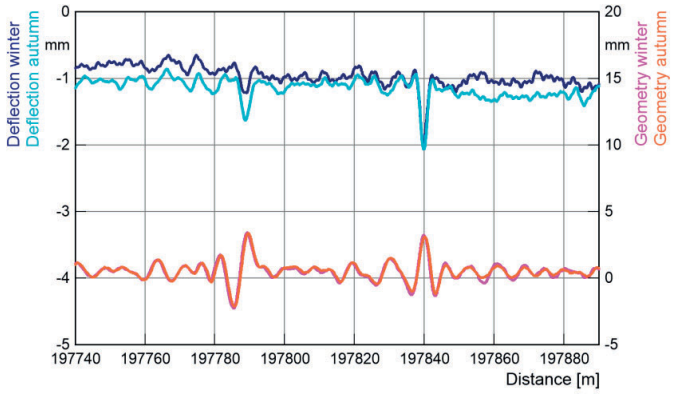

Figure 4.15. Some variation areas of track stiffness, which also exhibit defects in the geometry.

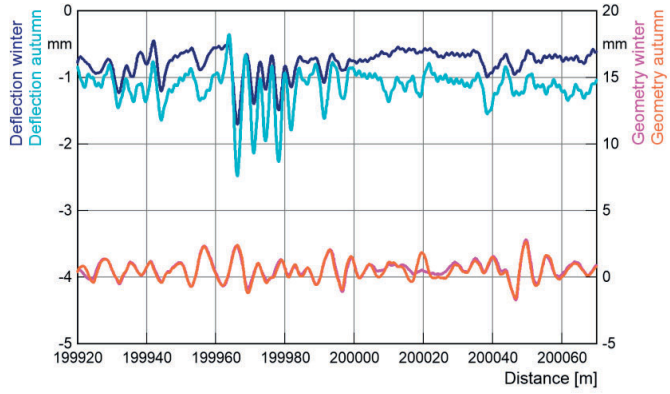

Figure 4.16. Some variation areas of track stiffness, without clear geometry defects.

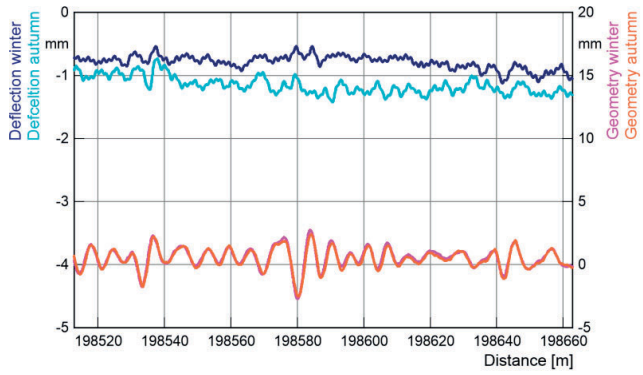

Figure 4.17. Some track geometry defects in areas without a clear variation in stiffness.

The interplay between stiffness variations and geometry variations is not straightforward, but some hypotheses can be made. An occurrence of stiffness variation without a geometry defect indicates recent maintenance, meaning that the track has been levelled and that the geometry will deteriorate over time.

An occurrence of a geometry defect without stiffness variation may originally be caused by an unevenness created during maintenance. Moreover, the dynamic loading resulting from this may increase the uneven degradation of the ballast or the number of permanent deformations in the embankment, which in the long run will produce an ever-growing geometry defect.

When interpreting the graphs presented above, it should be noted that the scales in the figures for the geometry and deflection are different. The unit for both parameters is a millimetre; that is, the geometry defects are roughly 5 times larger in comparison to the stiffness variations.

Generally speaking, the variation in the geometry between autumn and winter measurements is very small. Of all the examples above, only Figure 4.16 shows even the smallest difference between these measurement runs. Based on this observation, the geometry does not change much over winter, unless there is frost heave.

A direct comparison between geometry variation and recoverable deflection, performed measuring point by measuring point, will not yield a completely unambiguous result. For correlation, both parameters were divided into 10-m sections, and the sections' standard deviations were calculated (Figure 4.18). The graph of the distance parameter shows that some of the large variations in the geometry and stiffness occur in the same locations. There are also a large number of places where the geometry varies, but the deflection's variation is smaller. Only in a few places is the stiffness variation relatively greater than the geometry variation. The stiffness variation and, to a certain extent, the geometry variation increase towards an increase in kilometres.

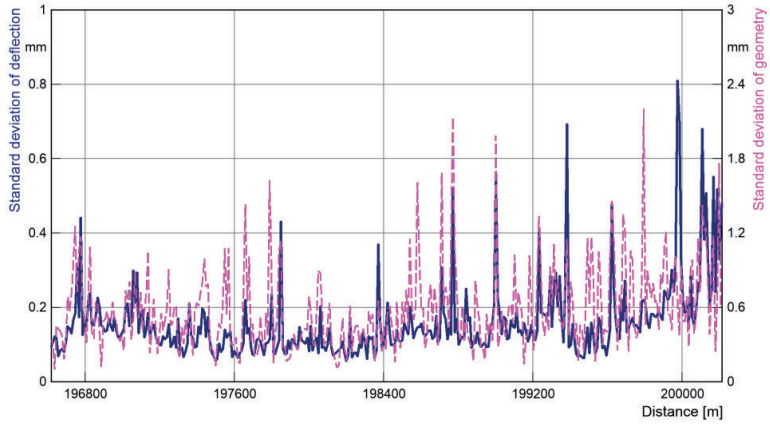

Figure 4.18. Standard deviations of the geometry and deflection, calculated for the 10-m sections.

A similar correlation could also be drawn so that the deflection's standard deviation was on the horizontal axis and the geometry's standard deviation was on the vertical axis (Figure 4.19). With this method, there is significant deviation, but a more general group with a slope of approximately 6 can be seen in the graph. This is likely to be the most common group of observations, in which the geometric variation is 5–6 compared with the variation in recoverable deflection. In addition to this, the graph shows a slightly different group, in which the geometric deviation is equal in magnitude to the deviation of the recoverable deflection. This group probably represents a situation where hardly any geometric variation occurs, but the stiffness variation is significant in comparison.

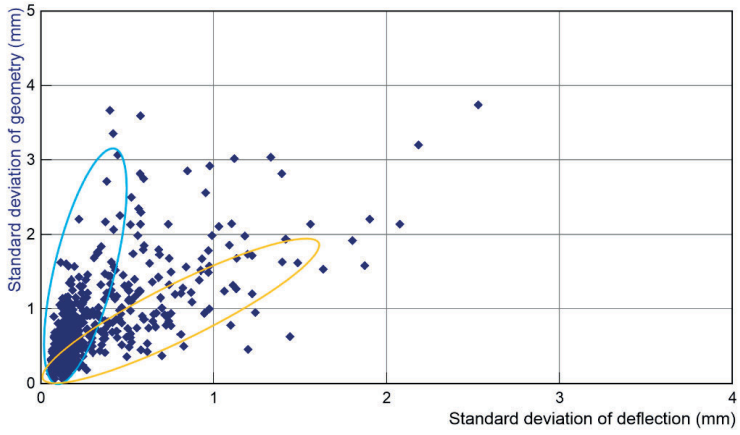

Figure 4.19. Correlation between the standard deviations of geometry and deflection.

4.3. Processing measurement data and analysing the results

After conducting an analysis on the track section between Lielahti and Ylöjärvi, and on the operating principle of the measuring device, described above, the Stiffmaster has been used on several track sections in various studies and for project quality controls. On the basis of the measurement findings, a number of small improvements have been made to the device. This chapter discusses the measurements conducted with the measuring device version from 2015.

4.3.1. Filtering measurement data

As described before, the operation of the Stiffmaster is based on two displacement sensors that measure a track's vertical geometry. Other assisting parameters are also measured, mainly to aid in the positioning. The deflection signal is calculated as the difference between two separate displacement sensors and the sensor noise, the vibration originating from the measuring device and the wheels' out-of-roundness are summed up with the deflection signal. Measurements taken on a single track section in opposite directions have shown that the curves are slightly visible in the deflection level. A change in the level is shown as a change in the algebraic sign in curves turning in opposite directions. The effect of curves can be minimised by measuring the rail section in both directions and calculating the average of the measurements. To detect errors caused by curves, sensors that measure curves have been installed in the Stiffmaster to make a curve correction, if necessary. The necessity and size of the correction varies slightly, depending on the location. This could be a result of the features in the rolling stock in use and especially how worn its wheels are, or the eccentricity of the measuring device's attachment point location. In addition, the radius of a curve has some role in the error. However, the problem is not yet fully understood and it has not been able to eradicate.

The error source during measurement runs conducted in only one direction was attempted to reduce by performing a curve correction to the deflection signal. This is done by adding the curve sensor's measurement result to the deflection, multiplied by a suitable constant. This constant is location specific, and its accurate determination requires a measurement run performed in both directions. The error created in curves is not symmetrical in relation to the direction and size of the curve. For example, if the necessary curve correction in curves turning to the left is positive, it may be zero in curves turning to the right. The smaller the curve's radius, the larger the correction; however, very small radius curves do not increase the need for correction anymore.

Using this third signal in calculating deflection increases the deflection's noise. A sampling rate of 5 kHz is used in the measuring, mainly because the acceleration of a heavy axle was also measured with acceleration sensors during the measuring. A sufficient amount of measurement data was wanted to be available for performing various types of filtering. A considerably lower sampling rate would suffice to study deflection. The deflection is calculated based on the distance measured by the pulse sensor in relation to a fixed location. The pulse sensor sends out a pulse every 35.7 mm, and the second displacement sensor's signal is delayed in the measurement programme by 84 pulses ($84 \times 35.7\ \text{mm} \approx 3{,}000\ \text{mm}$) so that the signals represent the same location in relation to time. Naturally, this means that the deflection signal output is in relation to distance, with a sample interval of 35.7 mm. This longer sample interval is beneficial when

analysing long measurement areas, because it prevents the measurement data from becoming excessive. For example, the data output from every seventh sample (i.e. every 0.25 m) contains all the data necessary to analyse the deflection, but the amount of measurement data is reduced to a fraction of the original.

Often, the measurement runs have been performed at 50 km/h, which is the maximum allowed speed for railway work. This means that the sampling rate of measurements taken in relation to time is approximately 400 Hz, and reading this result requires a minimum of 800 samples a second, preferably 1,600, to ensure correct calculation of the pulses. The extra measuring frequency can also be utilised to filter the signal even before the deflection is calculated.

When considering the types of deflection changes that can occur in a track, can be assumed that the first cyclic phenomenon is the approximately 0.61-m wavelength resulting from the sleeper division. In other words, the rail displacement is greater between the sleepers than directly on top of them. A rough estimate of rail deflection between the sleepers can be made by using, for example, the beam deflection formula (4.6):

$$y = \frac{Q_d a^3}{48EI} \tag{4.6}$$

where

y	is the deflection between sleepers [mm]
Q_d	is the wheel load [N]
a	is the distance between sleepers [mm]
E	is the modulus of elasticity [N/mm^2]
I	is the moment of inertia [mm^4].

By inserting the 70 kN wheel load, the 210,000 N/m^2 modulus of elasticity of steel, and the 3,055 × 104 mm^4 moment of inertia of a 60 E1 rail in the formula, the resulting rail deflection between sleepers is approximately 0.05 mm. This is at the lower limit of the measuring method's detection capacity, possibly even below it. All the deflection changes of a wavelength shorter than the distance between two sleepers on a continuously welded rail are therefore too small to be detected. The fundamental question is: What is the minimum level of deflection that the measurement method can still detect? One approach to the subject would be to use the above-mentioned Equation (4.6) and calculate how a rail will become deflected if assumed that the track has one, two or three hanging sleepers. The supposition is that the hanging sleepers bear no load and that the first well-supported sleepers receive all the load. This results in rail deflections of 0.39, 1.33 and 3.14 mm, respectively. In this scenario, the displacement in the load-bearing sleepers is not taken into account, and only the deflection of the rail is observed. If the track stiffness changes so that all the sleepers are supported, the change in the deflection must be smaller than what has been described above. On the basis of the calculation, can be concluded that the measuring method is able to detect deflection variation that is caused by a single hanging sleeper. Merely two or three hanging sleepers will cause a significant dent in the deflection graph, as in Figure 4.10, for example.

On the basis of the above calculation, track deflection cannot significantly change over a distance of less than 1 m on a continuously welded rail. Therefore, it is justified to use filtering that removes the wavelengths of less than 1 m from the measurement data. This can be done by filtering the signal in relation to either time or distance. A method where the raw measurement signal is first filtered with a 50-Hz low-pass filter, intended to remove electric disturbance from the measurement data, was found very useful. Simultaneously, it removes wavelengths of less than 0.28 m if the measurement has been taken at a speed of 50 km/h. After this, a phase shift was performed: that is, focus the signals of the loaded and unloaded geometries in the same position and calculate the deflection. Finally, a 2-m-long moving average (56 samples) was calculated from the resulting deflection signal, which will further reduce the amount of noise in the signal. The resulting deflection signal will contain the deflection's wavelengths from approximately 1 m up, but any shorter waves will have mainly been filtered. Occasionally, a 3-m-long moving average (84 samples), which will reduce short-wavelength variation in the signal even more, was found useful. However, this will also reduce the variation in the measurement signal caused by individual hanging sleepers.

In the first test runs, a low-pass filters as low as 2 and 5 Hz was used. At a speed of 10 km/h, their effect as wavelengths was 1.39 and 0.56 m, respectively. These filters reduce noise very efficiently. Later, the run speed was increased to 50 km/h, which increased the filtering effect expressed as wavelengths to 6.94 and 2.77 m. The 2-Hz low-pass filter, in particular, was found to have too large an effect on the measurement result, as the short-wavelength variation caused by hanging sleepers disappeared from the deflection signal almost completely.

Therefore, there is no single right way of filtering the signal, and instead the selection of the filtering method is based on a comprehensive picture formed by trial and error on the best approach. If the aim is to identify hanging sleepers, an overly strict filtering cannot be used. Instead, if the aim is to study phenomena originating in the subsoil or to classify a track section based on its underlying structure, the use of a long-wavelength filter is justified. A moving average of over 10 m will remove any errors caused by the out-of-roundness of the measuring device's wheels, among other things, and simultaneously the effect of hanging sleepers decreases. Hanging sleepers pose a problem when using a moving average, because even when using longer distances to calculate deflection they significantly raise the average. The effect of hanging sleepers can most effectively be minimised with a filter operating based on the wavelength, with which the selected short wavelengths can be excluded from the deflection curve.

4.3.2. Absolute deflection level

On the basis of the literature, the absolute deflection level seems to be the most important parameter to be analysed when measuring stiffness. For example, Selig & Li (1994) discovered in their calculations that subsoil has the greatest effect on track deflection. The magnitude of deflection has been found to be directly linked to a road's load-bearing capacity (Huang 2004), although this link may not necessarily be linear. Regardless of a deflection's magnitude, it does not in itself create longitudinal unevenness on a road or railway. Unevenness is developed in areas with stiffness variation, where the magnitude of deflection changes.

At measured sites, the average absolute level of deflection varies from just under a millimetre on a track that is in good condition to approximately 5 mm on side tracks. It should be noted that the largest changes develop in areas where the entire structure changes. For example, when moving from a concrete-sleeper track to a wooden-sleeper track, a clear level change in deflection can be detected. Similarly, when moving from one rail type to another on a side track, the deflection level changes notably (Figure 4.20). However, when moving along a main track, subsoil changes do not significantly appear in the measured deflection. Instead, in some cases, the additional deflection caused by a frost insulation board is visible as a level change as extensive as 0.5 mm. A general conclusion based on the measurements taken so far (650 km of measurement runs, 400 km of different track sections) is that the deflections measured with the Stiffmaster primarily display deflection in the superstructure and the structural layers rather than deflection caused by the subsoil. It should also be noted that Finland's railway structures contain a thick insulation layer constructed from sand. Typically, the thickness of the track structure is at least 1.4 m.

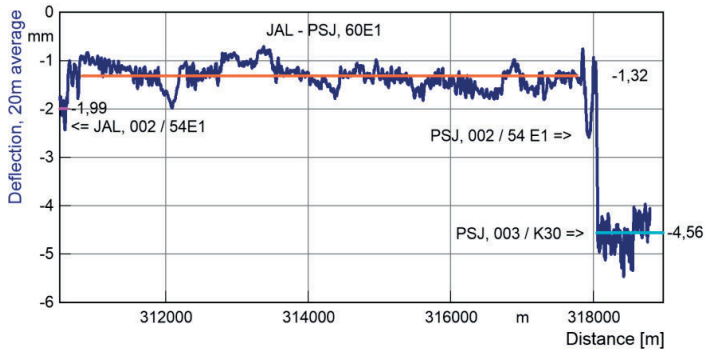

Figure 4.20. Effect of different rail types on the recoverable deflection level at the operating points of Jalasjärvi and Peräseinäjoki.

Why is the deflection of subsoil indicated as the most important factor affecting track stiffness (Selig & Li 1994) if measurement of a track's stiffness cannot even properly identify changes in the subsoil? The main unique feature in Finnish tracks is probably the thick railway structure, designed for the cold climate, which efficiently spreads the axle load of 14 t used in the measuring across the various structural layers. On the main tracks, deformations in the subsoil are not notably visible, because the deflection variation caused by the subsoil is genuinely small. However, the situation is different when measurements are taken on tracks with thin structures, as shown in Figure 4.20 from the operating point of Peräseinäjoki (PSJ). On the contrary, a 14 t axle load is relatively light, even though it corresponds to the axle load found in passenger trains. Using a heavier axle load could make the subsoil's properties more visible on the main tracks as well. Heavy axles are often used in bogies, and the combined effects of the axles increase the deflection significantly when the subsoil is soft. The third factor is connected to the selected measuring method, which assumes that at a distance of 3 m, the deflection caused by the load has completely recovered. In some cases, the deflection curve is wider in shape than this, and the measuring method therefore cannot detect deformation deep in the subsoil. However, variation occurring

close to the structure's surface is visible in the measurement results, because the properties of the top part of a structure are emphasised near the centre of a load.

What can be deduced from a deflection's absolute level? At least it provides information about the surface structure's properties and the type of track. If the deflection level is more than 2 mm, the track in question likely has wooden sleepers, and if the deflection level is over 3 mm, the rail weight is very small and the structural layers are thin. On the most interesting main tracks, the level changes can be extremely small: a deflection at a turnout may be 0.3 mm less than at the rest of the track, and the same goes for concrete bridges with support layers. However, transition zones that connect to these structures often create a few hanging sleepers, which can be seen as a dip as deep as 2–3 mm in the deflection graph. On the basis of these examples, the difference in deflection does not need to be very significant before permanent deformation begins to develop at varying rates. Over time, a few hanging sleepers develop at these transition zones, amplifying the dynamic effects of the load. This is why newly developed unevenness will spread at an accelerating pace.

4.3.3. Variation of deflection

As described in Chapter 4.3.2, the Stiffmaster measuring device can best detect deflection variation in a superstructure. The primary origin of a superstructure's deflection variation is the condition of the track's support. In practice, the rail stiffness or bending will not change much over a single type of rail. The properties of sleepers may vary somewhat, particularly if they are made of wood; however, as long as the sleeper type and the age of the superstructure remain the same, this is also very small in scale. The stiffness of a support layer may vary, but the variation will not be so extensive as to cause a significant number of deflection variations. Thus, the most important factor will be the way in which the sleepers are supported by the support layer, which may have considerable local variation.

To study stiffness variation mainly originating from the superstructure, the simplest way is probably to use a similar presentation method, based on a chord, as with the track recording vehicle. The effect of a deflection's level variation can be reduced by calculating the deflection's moving average over a selected distance and subtracting this from the original deflection signal. For example, Figure 4.21 was formed by calculating a 5-m moving average for the deflection signal, which was then subtracted from the original signal. This will reveal the deflection variation's wavelength range that is thought to represent the support condition. The signal describing the deflection variation can be utilised as is, or a standard deviation can be calculated from it, either as moving or by using the section division method. For example, sections of 25 or 50 m will enable the detection of poorly supported areas instead of poorly supported individual sleepers. Figure 4.22 illustrates the standard deviation of deflection calculated over a 10-m distance at a location on the track between Kirkkonummi and Turku receiving maintenance. The figure shows the results before and after the tamping work.

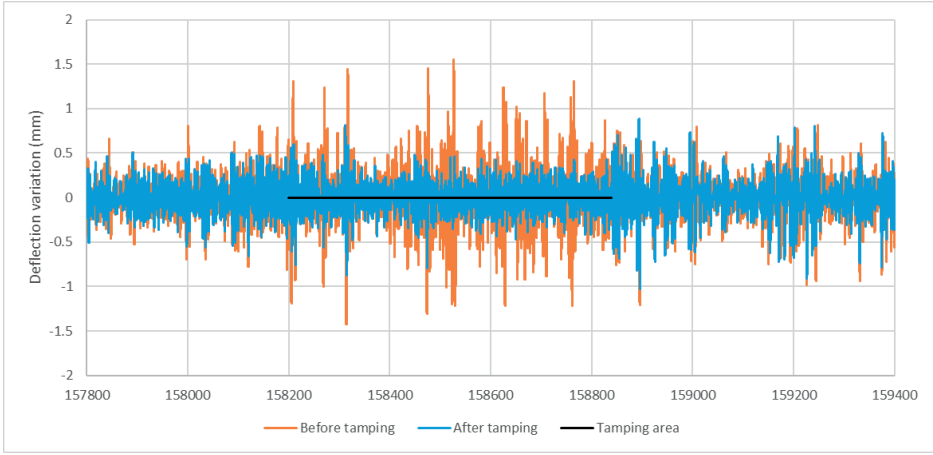

Figure 4.21. Effect of tamping on the deflection variation on the track section between Kirkkonummi and Turku.

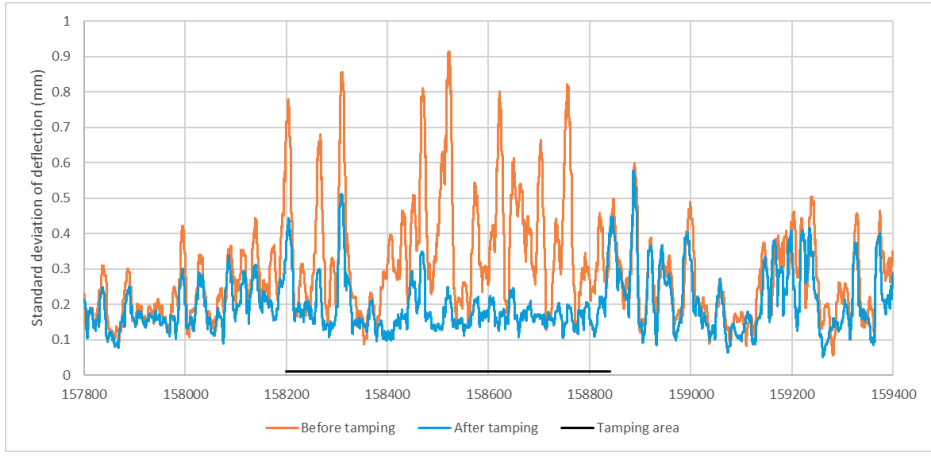

Figure 4.22. Effect of tamping on the standard deviation of the deflection. The standard deviation has been calculated as moving over a 10-m distance.

On the basis of the measures taken, the hanging sleepers may be relatively common and improving the track in those sections would often be prudent. Fixing deflection variation is generally easy, because tamping that immediately removes stiffness variation will work at least as a short-term solution. Further measurement need to be conducted to define how long this effect will last. According to measurements, tamping does not have a significant impact on the absolute level of the deflection. Rather, tamping increases the average deflection temporarily, because it decompresses the old support layer.

An absolute numerical limit for when tamping should take place based on stiffness variation has not yet been determined. The limit value cannot be a single numerical value covering all the parts of a track; instead, the limit must probably be set separately for each maintenance level. The selected measuring and filtering method will also have a fundamental effect on the limit values.

However, these values must be universally applicable and it should be possible to measure them with other devices besides the Stiffmaster. The aim of further research on this subject is to develop limit values, which can be used as a basis for improving track support proactively. The purpose of proactive tamping is to reduce stiffness variation and the need for tamping during a track's lifecycle. A geometry defect detected by a track recording vehicle is already an advanced-stage lack in support, which on a single-line railway track will affect a large area in both directions from the actual problem source.

A study based on deflection variation is a simple way of identifying poorly supported sections, caused mainly by the superstructure. The effects of a track's structural solutions on track stiffness are considerably more difficult to detect. For example, track deflection on a bridge that has a support layer should in theory be slightly smaller than on an embankment. It could be asked how quickly and over what distance could a deflection variation occur without causing any unevenness on the track. Measurement runs have crossed dozens if not hundreds of bridges, and most of them do not cause detectable variation in track deflection. However, some bridges are primarily detected due to a hanging sleeper formed at a bridge approach. What makes the matter difficult is that hanging sleepers become highlighted during measuring. The actual deflection level difference between an embankment and a bridge may be as much as 0.3 mm, but hanging sleepers at a bridge approach can easily cause a 2-mm variation in the deflection signal. Even an experienced researcher will focus attention on a 2-mm variation instead of a small difference in the levels. To detect the level differences, the effect of the hanging sleepers must be eliminated with filtering.

Another option, which requires method development as well, is to perform the measurements with two-axle loads that are greater than the seating load. This would require either two measurement runs with different axle loads or a whole new measurement arrangement, in which the measuring device was considerably heavier. The support condition should not be visible in measurements that measure, for example, the difference between the deflection caused by an empty and a full freight wagon, instead of the total deflection.

The most challenging task is to determine how fast a deflection may vary from the perspective of the structure's functionality. Measurements have shown that the geometric variation is approximately 5–6 times larger in comparison to the deflection variation. In addition, most of the deflection variation is caused by the support condition and hanging sleepers, not the underneath track structure. For example, the deflection variation due to a bridge is about 0.3 mm, which is only 4% compared with a demanding geometry defect that requires immediate action. Therefore, the stiffness variation seems to have little effect on a train's running properties, and limiting the stiffness variation should not be based on the safety aspects. The limit values for the variation of deflection are first and foremost an asset management issue.

A profound problem in determining these values is the lack of information regarding the rate of deflection change. Measurement results from frost monitoring stations (Pylkkänen et al. 2015) show that a track's elevation line drops typically 2–4 mm a year. This information is only based on a small sample from the Finnish railway network, but provides the direction for further study. The speed at which permanent deformations develop depends on amount of traffic, structure,

materials and conditions, but track stiffness also has its effect. If assumed, that the range of permanent deformations is entirely based on track stiffness (e.g. between a bridge and an embankment). The track settlement is 4 mm/year on the embankment, and 2 mm/year on the bridge. The 7-mm difference, calling for immediate maintenance, would be reached within four years. Therefore, the limit value for the stiffness variation should be determined on the basis of a similar thought process. It is a balance between the cost of maintenance and the cost of reducing stiffness variation. The minimum lifecycle cost can only be determined once understood the connection between track stiffness and the speed at which permanent deformations develop, and a link is formed from this to the costs incurred from maintaining the desired geometry.

One possible topic for further research could be a carefully monitored track section where permanent deformations are measured at least annually, preferably several times a year. The best way to measure permanent deformations would be to do so with a track inspection trolley by using a tachymeter. Combined with the measuring of stiffness, a model could be formed between track stiffness, the rate at which permanent deformations develop, and traffic volume. To conduct such research, the monitored track section would need to have a significant number of permanent deformations developing at varying speeds. Assuming that a correlation with stiffness exists, the model could be used to determine proper limits for the rate of stiffness variation, which would be based on the desired maintenance intervals.

4.4. Verifying the measurement method

Verifying the accuracy of the continuous stiffness measurement results is very challenging. The Stiffmaster can take measurements at 50 km/h, and the results are obtained as a continuous curve. The point-specific measuring method used to verify the absolute accuracy can only cover a few measurement points during a single work shift. Typically, 16 acceleration sensors have been used to calibrate the Stiffmaster by measuring the movement of sleepers or the rail at one or two spots within the measurement area. Problems have occurred already when focusing these measurement results accurately at the same location. More extensive absolute-level verification measurements have been taken at turnouts and on a wooden-sleeper track with a low traffic volume.

Assessing the repeatability of the measuring method is a slightly easier verification method to conduct, because it compares two measurements taken with the same method. This method has been used to study both repeatability and reproducibility, in accordance with standard EN-13848-2.

4.4.1. Repeatability

The repeatability of a measuring method means that two measurement runs performed under the same conditions, by the same driver and with the same settings, are similar. Repeatability is calculated, in accordance with standard EN-13848-2, from the distribution of the difference between two measurement runs at the 95th percentile. Because the distribution will have both negative and positive numerical values, the percentile is calculated from the distribution range of 2.5%–97.5%. If the distribution is symmetrical, the absolute value of both fractiles is equal, and the result can be expressed as ±0.1 mm, for example. If the second measurement's deflection level

differs from the first one, the distribution will be asymmetrical in relation to zero (Figure 4.23. Distributions of the deflection measurement points of three consecutive measurement runs and an example of the repeatability calculation points.Thus, the repeatability will be ± the average of the absolute value of the difference between the fractiles and the median, and the median's absolute value will be expressed as the systematic error. Standard EN-13848-2 does not comment on the systematic error caused by the different ways of presenting the results. When measuring track stiffness, it is extremely important to be aware of the systematic error: that is, the change in the deflection level between separate measurements.

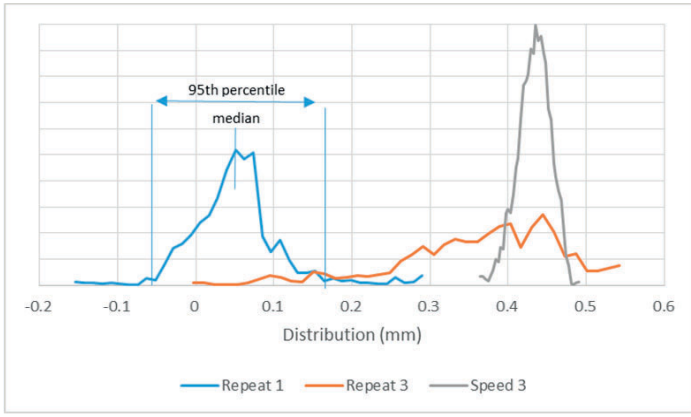

Figure 4.23. Distributions of the deflection measurement points of three consecutive measurement runs and an example of the repeatability calculation points.

The calculation corresponding to the standard also assumes that the first measurement run represents the real properties of a track and that the second measurement contains all the random errors. Another way would be to assume that both measurements deviate an equal amount from the true track properties, which would result in an approximately 40% smaller numerical value for the repeatability. However, in this study, the calculations were carried out using the first method.

No actual test track exists to test the repeatability of the Stiffmaster's deflection measurement. Nor have all the measurement runs used in the repeatability calculation been performed at the same location, and the sampling therefore varies. For this reason, the standard deviation of the deflection in addition to the repeatability is also reported for the measurement period, because the unevenness of a track may affect the repeatability. A 200-m measurement section was used for the sampling when calculating the repeatability, selected randomly from the measurement data. Each measurement run consisted of approximately 5,600 sample points. Two separate measurement runs were focused on the same location manually. Doing this successfully has a great impact on the analysis, and its importance is further increased on tracks with a significant variation in deflection. On a track that is in good condition, the standard deviation of the deflection variation is small (0.18 mm), and an error of 1 m in the location will increase the repeatability to approximately double in magnitude. Furthermore, if the standard deviation of deflection is extensive (0.56 mm), an error of 1 m in the location will increase the repeatability to 5 times the magnitude in comparison to the best possible positioning.

In all the analyses, a 5-Hz low-pass filter was used in relation to time and a 3-m rolling average in relation to distance as the filtering method. The repeatability calculation results from four separate pairs of comparison runs are presented in Table 4.1. The repeatability of the deflection measurement varies slightly, depending on the sampling, but is ±0.1 mm on average. Track properties (the magnitude of a deflection's standard deviation) or running speed do not seem to have an influence on repeatability. However, the analysis method revealed a systematic error in the measuring method. The absolute deflection level may change as much as 0.5 mm between two consecutive measurements. However, this does not affect repeatability unless the level change occurs within the section being studied.

Table 4.1. Calculation results for the deflection measurement's repeatability.

Test	Measuring speed (km/h)	Repeatability, 95th percentile (mm)	Systematic error (mm)	Standard deviation (mm)
Repeat 1.1	10	±0.135	0.050	0.556
Repeat 1.2	10			0.559
Repeat 2.1	10	±0.041	0.434	0.165
Repeat 2.2	10			0.159
Repeat 3.1	30	±0.220	0.378	0.152
Repeat 3.2	30			0.130
Repeat 4.1	50	±0.075	0.140	0.174
Repeat 4.2	50			0.187
Average		±0.118	0.251	

The analysis of the repeatability confirms the belief that the measuring method detects deflection variations well, but its absolute accuracy could be better. This is also evident in Figure 4.10 and Figure 4.11, in which the first level is almost identical between the two measurements; however, in the second figure, the level is clearly different even though these measurements were both taken during the same run. Both figures mainly show the same variations in stiffness. The measurements were taken during different seasons and the track stiffness was genuinely changed, but the level difference between the locations is greater than expected.

4.4.2. Reproducibility

The reproducibility of measurement results refers to the repeatability of these results at varying driving speeds, by different drivers, measured in different driving directions and with a different measuring device orientation, and the effect of other similar factors on repeatability. The direction indicates whether the measuring is performed by pulling or pushing. The orientation indicates whether the measuring is done towards the increasing or decreasing number of kilometres, although in both cases the measuring device is being pulled. Table 4.2 illustrates the effects of orientation, driving speed and direction on reproducibility. Compared with the repeatability described above, the results of reproducibility are significantly poorer. The greatest effect comes from the direction of the measuring device. The measurement results from pulling and pushing differ to such an extent that performing measurements by pushing the device is not sensible. In addition, the measuring device's orientation may have a notable effect. On a track that is in good condition, the reproducibility of the different directions is only about double in comparison to the repeatability, but on a track that is in weak condition, the reproducibility is relatively weak. This

may in part be due to the fact that track deflection varies slightly depending on the direction, and therefore it may not necessarily be a method error alone. Hanging sleepers and track joints may produce a slightly different output depending on the direction, and hence the measurements cannot be focused on the same location completely accurately. This reduces the repeatability mathematically, even if the absolute deflection variation is similar but a mirror image regarding the track joint, for example. The driving speed does not seem to have a significant effect on the reproducibility, as the effect of speed on reproducibility was only approximately 1.5 times in magnitude compared with the repeatability.

Table 4.2. The measuring method's reproducibility.

Test	Measuring speed (km/h)	Orientation	Direction	Reproducibility, 95th percentile (mm)	Systematic error (mm)	Standard deviation (mm)
Orientation 1.1	50	Up	Forwards	±0.228	0.010	0.105
Orientation 1.2	50	Down	Forwards			0.125
Orientation 2.1	10	Up	Forwards	±0.891	0.502	0.435
Orientation 2.2	10	Down	Forwards			0.524
Speed 1.1	10	Up	Forwards	±0.225	0.070	0.511
Speed 1.2	50	Up	Forwards			0.529
Speed 2.1	10	Up	Forwards	±0.140	0.017	0.139
Speed 2.2	50	Up	Forwards			0.125
Speed 3.1	10	Up	Forwards	±0.175	0.303	0.146
Speed 3.2	30	Up	Forwards			0.135
Direction 1.1	30	Up	Reverse	±1.088	1.282	1.131
Direction 1.2	10	Down	Forwards			1.007
Direction 2.1	10	Down	Reverse	±0.436	0.749	0.236
Direction 2.2	10	Up	Forwards			0.191
Direction 3.1	30	Down	Reverse	±0.338	0.021	0.191
Direction 3.2	30	Up	Forwards			0.158

The systematic error becomes amplified between the different directions, and it is assumed be caused by the running properties of the measuring device. Sensors measuring curves detect that the measuring device is twisted during pushing. The measuring device's axles move from one side of the rail to the other in an alternate pattern to maintain steerability. The conicity of the wheels results in a level change in deflection, because the loading axle remains at the centre of the rail during pushing. The fact that the measuring device is moving in a twisted position causes greater tractive resistance, which likely increases the deformations of the measuring device itself, which may also be visible as a level change in deflection. In addition, in this direction, the deflection curve itself is steeper in front of a wheel than behind it.

Some accelerations and brake applications were also found to create random level changes, which indicates the existence of the same measuring device deformations or movement of the attachment point in the locomotive, mentioned above. This annoying problem can probably be removed from later production versions of the measuring device.

4.4.3. Comparability with other methods

An instrumentation, based on displacement sensors, is in use at Kouvola's operating point, covering a few sleepers at turnouts V055 and V056. The vertical position of a sleeper is measured

with a displacement sensor in relation to a rod installed 3 m deep (the same principle as in Figure 3.16), and the motion between the sleeper and the rail is measured with a second displacement sensor. Monitoring is conducted on both sides of the track. By adding the sleeper's movement and the rail pad, the motion of the rail at that particular sleeper's location can be discovered. The Stiffmaster measuring device measures the total deflection of a track (i.e. rail motion). These results obtained with different measuring methods have been combined in Figure 4.24. The figure shows that recoverable deflection varies significantly in the turnout area during the measuring, but the deflection measured with the displacement sensors varies only slightly between the measuring points. This is because the number of displacement sensors in use is small, and the sensors are placed on similarly behaving sleepers. However, the measurement results obtained with different methods correlate rather well. Only at the fourth instrumented sleeper is the deflection slightly less in magnitude according to the displacement sensors, when compared with the deflection measured with the Stiffmaster. The filtering method also affects the correlation between different methods. If the Stiffmaster's measurement result is intensely filtered, the large individual stiffness variations disappear from the graph.

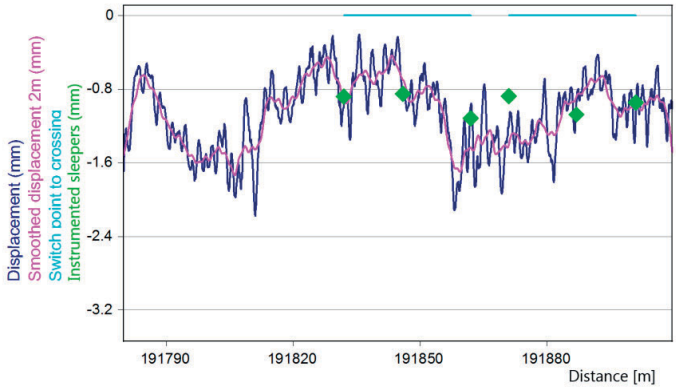

Figure 4.24. Comparison between the continuously measured deflection and the recoverable settlement of instrumented sleepers at turnouts V055 and V056 located at Kouvola's rail yard.

The measurements conducted at Tampere's rail yard compared the recoverable settlement determined with acceleration sensors to the Stiffmaster's measurement results. There is excellent correlation between these different methods pertaining to the recoverable settlement of turnout V062 (Figure 4.25). The acceleration sensors were placed directly onto the rail at the switch rail and crossing areas. The acceleration sensors' measurement result was constructed from four measurements; the sensors were attached to the right and left sides of the rail in an alternating pattern, and the average from these was calculated for the figure. Here too, the absolute level of the continuous measurement is based on the acceleration sensors' measurement result, but the stiffness variations correlate well too. The continuous measurement curve rises above zero twice, which cannot be correct. The deflection with an incorrect algebraic sign is a measurement error, which is likely caused by a deflection bowl that is more extensive than the measuring device's wheelbase of 3 m. The insulated joint behind the crossing (in the figure at track metre 38) might

have caused this behaviour if hanging sleepers had formed at the insulated joint's area. However, this type of transition zone does not exist in the switch rail area (in the figure at track metre 8), and the reason for the negative deflection is therefore unknown.

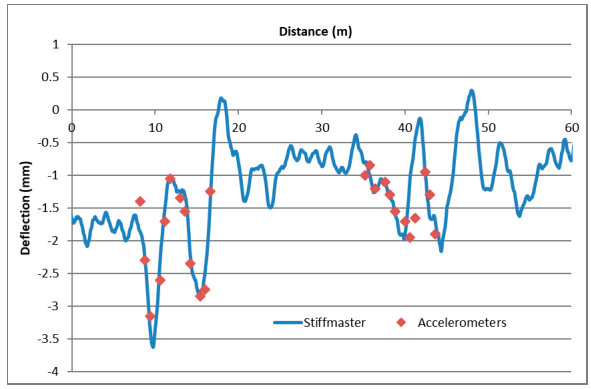

Figure 4.25. Comparison of the measurements taken with the Stiffmaster and the acceleration sensors at turnout V062 of Tampere's rail yard.

4.4.4. Effect of load on measurements

The load that is used will also have a notable impact on the deflection measurement result. The static axle load of the TKA7 is assumed to have been the same during each measuring run, and the dynamic force created by the track's unevenness was not measured separately. The measuring is thought to represent a normal loading situation that the track experiences when a train is passing over it. However, the acceleration of a loading axle was measured during the stiffness measuring. The high-frequency acceleration increases significantly as the measuring speed increases, but the high frequencies likely have no significant impact on the stiffness measurements (Remennikov et al. 2008). Transition zones, such as fishplate joints and poor welds, add considerably to the dynamic loading (Remennikov et al. 2008). The high-frequency acceleration mainly focuses on the unsprung mass and the rail, but the loading effect on the track is estimated to be small. Suspension removes the high frequencies, and the sprung mass has no time to react to high frequencies due to its inertia. However, suspension cannot filter out low frequencies, and these may have a genuine effect that either increases or decreases the load. The typical track unevenness wavelength at Raisio's measurement site of a low maintenance level is approximately 3–10 m. At a measuring speed of 50 km/h, the wavelength range equals frequencies of under 5 Hz, and such frequencies can also be assumed to transfer mostly to the sprung mass. According to the acceleration measurements taken from the bearing housing, the acceleration of a wheelset produced by track unevenness is less than ±1 m/s^2 on average at a measuring speed of 50 km/h (Figure 4.26). At a slower measuring speed of 10 km/h, the dynamic loading effect is nearly non-existent.

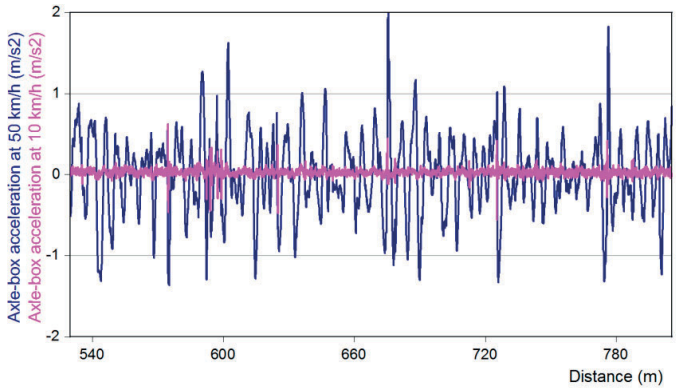

Figure 4.26. Vertical axle-box acceleration filtered with a 5-Hz low-pass filter at two different speeds, shown in relation to distance.

Because the measurement location in Raisio represents the track type of clearly the weakest condition, the dynamic effects are to be at their greatest there. The axle load's dynamic variation due to the unevenness of the track during the measurement performed at 50 km/h is at most ±20%, although typically no more than ±10%. The effect of load variation on the measured track deflection can be assumed to be no greater than this, because the increase in deflection is non-linear in relation to the increase in load.

5. Results and discussion

5.1. Monitoring deformations in road and railway structures

Sensors installed inside a structure or measuring methods that take measurements at a single point are effective when studying the behaviour of a narrow section of a structure. Sensors installed inside a structure often require that the structure be excavated, which significantly limits their application options. Acceleration sensors and MDD are among the few instruments that can be installed from the surface into the structure without disrupting the entire structure during the installation. The labour-intensive nature and the high cost of the instrumentations limit the number of sensors, and observations can only be made at a few points.

The notable benefit of monitoring is the accuracy and representability of the measurement results. When measuring frost heave, the sensor installed for this purpose will indicate the frost heave in relation to time very accurately. The challenge in utilising monitoring methods is their poor general applicability. An individual frost heave observation on an entire section of track will not contribute greatly to the frost management of that section, even if it does reveal the cause for the problem at a particular point. Monitoring methods require the support of a more comprehensive measuring method that can be used to expand the monitoring to cover an entire road or track section. Continuous measuring methods that are based on measuring the geometry or stiffness are examples of such methods.

Gaining comprehensive data requires the use of several measuring methods, because only a correctly selected measuring arrangement can provide valuable information about a structure's behaviour. Using acceleration sensors to measure recoverable settlement has proven to be a potentially suitable approach for small-scale studies, in which real vehicles can be used as the load. The method has been successfully applied on both roads and railways. The monitoring has allowed researchers to measure the effect of frost on road structure stiffness and has provided valuable information on the deflection variation that forms at bridge approaches within the railway network.

Deformation sensors measuring recoverable and permanent deformation in road structures have shown that the location of the loading is a key factor affecting the performance of a structure constructed with unbound materials. Deformations on a low-volume road depend heavily on the lateral distribution of the loading. Monitoring has shown that a structure expands due to shear deformations before a wheel pass, but also next to a wheel. The deformations of a single point depend on the loading history, because two consecutive loadings at a measuring point produce a notably smaller deformation than if vehicles alternate between passing directly over the measuring point and to one side of the point. This behaviour explains in part the rutting of a low-volume road. The phenomenon is amplified by a road's narrow cross-section and steep ditch walls, which result in poor horizontal support to the structure. Therefore, deformations are greater in magnitude on the side of a road than in the middle.

The recoverable and permanent deformation of a structure can be monitored with displacement sensors, as well as MDD, as shown by the frost monitoring stations. MDD is suitable for layered measuring, and the monitoring method that is based on a single displacement sensor can be used to measure the surface movements of a structure. Measuring recoverable settlement with displacement sensors is relatively cumbersome in comparison to the acceleration sensors. However, the best technique available for monitoring permanent deformation is based on displacement sensors. The observations made through monitoring include the following:

- The frost heave in Finnish railway structures is usually created at the borderline between the substructure and subsoil.
- The permanent deformations during spring thaw are considerably larger on railway tracks subjected to frost heave than on those built with non-frost-susceptible materials.
- A supporting layer will degrade and become compacted as a function of traffic volume, due to which the elevation line typically drops by 2–4 mm annually.
- The effect of tamping can be directly seen in millimetres as a function of time. The measuring system intended for frost monitoring is also suitable for monitoring the permanent deformations.
- A half of the recoverable displacement of the sleeper occurs in the ballast layer, the other half comes from all the layers below.
- Furthermore, the slow recovery occurring in some structures can be detected with a measuring technique that uses displacement sensors.

The settlement pipe is clearly a point-based monitoring method, but its ingenuity is in its ability to detect the vertical displacements of relatively many points simultaneously. A settlement pipe can be used to measure both settlement and frost heave. The method is best suited for monitoring done for safety reasons, because a single measuring device enables the monitoring of vertical displacements in embankments as long as 200 m. The long-term observation conducted with the prototype has also shown that the equipment still works many years after its instrumentation.

5.2. Continuous track stiffness measurement

The findings obtained with the monitoring methods confirm that investigating the load-bearing capacity comprehensively at a network level requires continuous measurements. The development of permanent deformations is regularly monitored by measuring the geometry of both roads and tracks, but the measuring methods only register relative unevenness. Often, the cause of an unevenness cannot be identified based on these measurements. Therefore, a continuously operating measuring device, the Stiffmaster, was developed to measure track stiffness. The device was needed to build, because the other devices developed elsewhere in Europe use the standard gauge of 1,435 mm, whereas Finland uses a wider gauge of 1,524 mm.

The device measures a track’s vertical geometry, both loaded and unloaded, during the same measurement run. The track deflection is determined as the difference of these two geometries. The deflection, in turn, can be used to calculate the track’s stiffness; however, in this study, the

term ‘deflection’ has been used instead of ‘stiffness’. The amount of deflection is easier to comprehend, as the unit is millimetre.

The calculated repeatability of the Stiffmaster’s deflection measurements will be approximately ±0.1 mm and the reproducibility ±0.2 mm, as long as the measurements are taken in the same direction. This means that the measurement results from two separate measuring sessions are 95% likely to differ from one another by less than ±0.2 mm. In addition, a systematic level difference has been detected between the measurements, with variation as significant as over 0.5 mm. Therefore, the method in its prototype phase is not yet absolutely accurate. The measuring errors are sufficiently small to study deflection variation, and the measuring method is best suited for assessing the need for tamping. In analyses based on the absolute level of deflection, special attention must be paid to the curves, sudden changes in measurement speed, and other secondary factors that may change the absolute level of a measured deflection during a measurement run. The reliability of the measurement results can be improved by repeating the measurements in the same direction or, if possible, also in the opposite direction. The repeated measuring will reveal a large error, but will not remove any systematic ones. Verifying the measurement method with another method is problematic, because no other measurement method that is as effective so far exists.

The results from measurements taken with a 14 t axle load have shown that track deflection varies only slightly on a track that is in good condition and of a high maintenance level. The highest deflection variations are formed across a distance of a few sleepers where the track deflection has significantly increased. These hanging sleepers are the result of impaired support, and they can be easily fixed by tamping. The actual reason for impaired support is a permanent deformation in the supporting layer, embankment or subsoil, which can develop due to a number of reasons. Deflection variation usually occurs at a track’s transition zones, such as turnouts, bridge approaches, level crossings and other notable areas of change in the structure.

A significant change in the deflection level can be detected when moving from one track line type to another. A concrete-sleeper track will typically have slightly less deflection than one with wooden sleepers. The rail weight and embankment thickness have a significant impact on the deflection level. On thin-structured tracks of a low maintenance level, the absolute deflection and deflection variation may be significantly higher compared with high maintenance level tracks that are in good condition. Fishplate joints are one of the main factors causing deflection variation. The condition of the support layer will also greatly affect the deflection variation. Therefore, the Stiffmaster measuring device is best suited for assessing a current support condition and the need for tamping. Deflection variation can be significantly reduced with tamping, at least temporarily. A well-supported track can resist the development of permanent deformation better than a track in poor condition, because the dynamic loading effect caused by deflection variation and geometry errors decreases.

In the literature, the main factor contributing to track deflection is thought to be the subsoil, but in the Finnish railway structures it does not play as significant a role. A change in the subsoil may be detected in the Stiffmaster’s measurement results, but a change in the subsoil will cause only little

change in the deflection. The measurement accuracy is also at its lowest when determining the absolute deflection. The minor effect that the subsoil has on the measuring results is partly due to the relatively light axle load (14 t) used in the measurements and partly because of the thick Finnish railway structures due to frost protection.

5.3. Development of unevenness on railway track

Continuous stiffness measurement has been used to study the effects of structural change areas to track deflection. For example, on a bridge with a supporting layer, the railway structure is slightly stiffer than on an embankment constructed directly on the ground. Measurements taken on dozens of bridges show that the deflection difference between a bridge and an embankment is usually very small. The difference cannot even always be detected, but typically deflection on a bridge is 0.3 mm less than on an embankment. Hanging sleepers are very common at bridge approaches and cause a 1–2-mm variation in the deflection. Deflection exceeding this is rare on a track that is in good condition.

The root cause of the development of hanging sleepers is the rate at which permanent deformations develop at the transition between two different structures. For example, monitoring has shown that permanent deformations are constantly developing due to the traffic load. Greater deflection will result in a faster accumulation of permanent deformations on an embankment in comparison to bridges, which are less susceptible to permanent deformations. This causes unevenness in the stiffness change area as a function of traffic volume. The deflection difference does not need to be great in order to create unevenness. Transition slabs and other similar transition structures can be used to spread out a deflection difference over a longer area, but they can never completely remove the effects of that difference.

The general notion that deflection variation in itself significantly increases the dynamic loading effect of a train is probably not true. For example, the deflection difference between a bridge and an embankment is relatively small compared with the normal variation in track geometry. However, because of traffic load, the structural difference will lead to unevenness, which as it becomes advanced will cause an added dynamic load. The dynamic loading effect is mainly created by unevenness and only indirectly by stiffness variation. The geometry can be maintained with regular tamping, even in a transition zone. Structural solutions affect how long a track will remain even at a bridge approach without maintenance. Only the hanging sleepers in a transition zone cause a sufficiently large deflection difference to result in significant dynamic loading effects on high-speed trains.

On a homogeneous track, the deflection variation caused by the structural layer’s material properties and a change in the subsoil are usually so small that the dynamic loading effects of track deflection are almost negligible. However, unevenness is being created due to traffic in a manner similar to the transition zones, only more slowly. The geometry must undergo occasional maintenance, which improves the support of sleepers and the geometry. The length of the maintenance intervals can be maximised by building a uniform structure where the deflection variation caused by structural differences is as small as possible.

Unevenness will inevitably develop in a railway structure due to traffic loading. A railway structure can be initially homogenised with tamping to remove the unevenness. If the supporting layer has degraded, cleaning or changing the supporting layer may be necessary. In some cases, even this is not enough, and the entire railway structure may need to be rehabilitated. Continuous stiffness measurement is one potential tool for assessing the extent of the necessary maintenance measures and area.

6. Conclusions and suggestions for further work

This study presents the measuring and monitoring methods for road and railway tracks that the author has developed and applied in practice to measure vertical displacements and analyse the performance of the structure. The research section of the study consists of a description of the development of the measuring methods and the main findings from the monitoring. These completely new measuring methods included the settlement pipe, frost monitoring stations and the Stiffmaster (all developed by the author). The study also presents several case examples, in which a previously known measuring method was used in a new way to acquire information that can be utilised in scientific analyses. The measurement results indicated several structural behaviour mechanisms that were previously poorly understood to truly exist. These include the effect of varying driving lines on road deformations, identifying the bottom of the substructure and subsoil as the area susceptible to frost heave in railway structures, the faster development of permanent deformations in railway structures during frost thawing, and several findings regarding factors and mechanisms that have an impact on track stiffness.

Monitoring deformations in road and railway structures

Accelerometers were found to be a very practical way of monitoring vertical deformations caused by a moving vehicle. The accuracy of commercial sensors is suitable for measuring both road surface and rail displacements. Accelerometers are not suitable for measuring the development of permanent deformations; instead, displacement sensor-based monitoring was successful in several applications. The settlement pipe is one of the most practical ways of monitoring moderately long road or railway track sections. Point-based monitoring methods are not sufficiently effective in analysing a large-scale road or track section. The measurement results from a few cross-sections can be expanded to cover the entire length of a track or road, for example, by measuring its stiffness with a continuous method.

Continuous track stiffness measurement

A new measurement device, Stiffmaster, was developed to measure track stiffness in a continuous manner. The accuracy of the measurement method could be slightly better for analysing the total track stiffness accurately. The accuracy is sufficient to study stiffness variation, and the measuring method is best suited to assess the need for tamping. The highest stiffness variations are formed across a distance of a few sleepers where the track stiffness has significantly decreased. These hanging sleepers are the result of impaired support, and, in most cases, they can be easily fixed by tamping. The actual reason for impaired support is a permanent deformation in the supporting layer and to a lesser extent in the embankment or subsoil, which can develop for a number of reasons. Stiffness variation usually occurs at a track's transition zones such as turnouts, bridge approaches, level crossings and other notable areas of change in the structure. The minor effect that the subsoil has on the measuring results is partly because of the relatively light axle load (14 t) used in the measurements and partly because of the thick Finnish railway structures due to frost protection.

Suggestions for further studies

On the basis of this study, the following are suggested for further studies:

- Continuous track stiffness measurement produces massive amounts of information that could be used in designing maintenance measures. Developing parameters for stiffness variation and absolute deflection are ongoing processes, and the aim is to develop these in the future. These parameters could be key indicators for assessing the extent of the necessary maintenance measures and area.
- An efficient way of using track stiffness measurements includes developing data analysis methods. Data mining could be one way of increasing an understanding about the relationship between the track stiffness and the load-bearing capacity of the railway track.
- Dimensioning the load-bearing capacity of an existing railway track could be partly based on the measured track stiffness. A deflection-based dimensioning has already been used in embankment width design, but the dimensioning could also cover the quality and thickness of embankment materials. Track stiffness measurement is one approach evaluating the quality of materials in places where the frequent development of unevenness occurs.
- Transition zones are the most problematic areas when it comes to the development of unevenness and track stiffness variation. New solutions to neutralize the effects between two different structures should be developed.
- Several developed measuring methods could be commercialised; these include the settlement pipe, frost monitoring stations and Stiffmaster.
- Improving the accuracy of absolute deflection measurement and increasing the axle load used in the measurements are the most important steps to commercialise Stiffmaster.

7. References

Aho, S., & Saarenketo, T. (2006). Design and repair of roads suffering spring thaw weakening. The ROADEX III Project, Northern Periphery.

Andersland, O. B., & Ladanyi, B. (2004). Frozen ground engineering. John Wiley & Sons.

Arraigada, M., Partl, M. N., Angelone, S. M., & Martìnez, F. (2009). Evaluation of accelerometers to determine pavement deflections under traffic loads. Materials and structures, 42(6), pp. 779-790.

ASTM D4694-09 (2009). Standard Test Method for Deflections with a Falling-Weight-Type Impulse Load Device. ASTM International.

ASTM E2583-07 (2011). Standard Test Method for Measuring Deflections with a Light Weight Deflectometer (LWD). ASTM International.

Augustin S., Gudehus G., Huber G. & Schünemann A. 2003. Numerical model and laboratory tests on settlement of ballast track. In System Dynamics and Long-term Behaviour of Railway Vehicles, Track and Subgrade, Berlin, pp. 317–336.

Baladi, G. Y. (1990). Resilient Modulus. Proceedings of the Workshop on Resilient Modulus Testing. Publication No. FHWA-TS-90-031. s. III/67-92.

Baltzer, S., Pratt, D., Weligamage, J., Adamsen, J., & Hildebrand, G. (2010). Continuous bearing capacity profile of 18,000 km Australian road network in 5 months. In Proc. 24th ARRB Conf.–Build. 50 Years Road Transp. pp. 1-11.

Banimahd, M., Woodward, P. K., Kennedy, J., & Medero, G. M. (2012). Behaviour of train–track interaction in stiffness transitions. Proceedings of the ICE-Transport, 165(3), pp. 205-214.

Berggren, E. (2005). Dynamic Track Stiffness Measurement–A New Tool for Condition Monitoring of Track Substructure, Licentiate Thesis, Report TRITA AVE 2005:14, Royal Institute of Technology (KTH), Stockholm 2005. 85 p.

Berggren, E. (2009). Railway Track Stiffness, Dynamic Measurements and Evaluation for Efficient Maintenance. PhD Thesis. Stockholm 2009. Royal Institute of Technology (KTH), Aeronautical and Vehicle Engineering, Division of Rail Vehicles. 123 p.

Berggren, E. G., Nissen, A., & Paulsson, B. S. (2014). Track deflection and stiffness measurements from a track recording car. Proceedings of the Institution of Mechanical Engineers, Part F: Journal of Rail and Rapid Transit, 0954409714529267.

Bilodeau, J. P., Doré, G., & Schwarz, C. (2011). Effect of seasonal frost conditions on the permanent strain behaviour of compacted unbound granular materials used as base course. International Journal of Pavement Engineering, 12(5), pp. 507-518.

Bowness, D., Lock, A. C., Powrie, W., Priest, J. A. & Richards, D. J. (2007). Monitoring the dynamic displacements of railway track. Proceedings of the Institution of Mechanical Engineers, Part F: Journal of Rail and Rapid Transit. Vol. 221. No. 1. pp. 13-22.

Bozozuk, M. (1969). A fluid settlement gauge: research note. Canadian Geotechnical Journal, 6(3), pp. 362-364.

Brough, M., Stirling, A., Ghataora, G. & Madelin, K. (2003). Evaluation of railway trackbed and formation: a case study. NDT & E International. Vol. 36. No. 3. pp. 145-156

Brown, S. F., Pappin, J.W. (1985). Modelling of Granular Materials in Pavements. Transportation Research Record 1022. Analysis and Testing of Granular Bases and Subbases. Washington D.C. pp. 45-51.

Brown, S. F., and Hyde, A. F. L. (1975). ‘‘Significance of cyclic confining stress in repeated-load triaxial testing of granular material.’’ Transp.Res. Rec. 537, Transportation Research Board, Washington, D.C., pp. 49–58.

Burmister, D. M. 1943. The Theory of Stresses and Displacements in Layered Systems and Applications to the Design of Airport Runways. Proceedings, Highway Research Board, Vol. 23, pp. 126-144.

Burrow, M. P. N., Chan, A. H. C. & Shein, A. (2007). Deflectometer-based analysis of ballasted railway tracks. Proceedings of the ICE-Geotechnical Engineering. Vol. 160. No. 3. pp. 169-177.

Cannon, D. F., EDEL, K. O., Grassie, S. L., & Sawley, K. (2003). Rail defects: an overview. Fatigue & Fracture of Engineering Materials & Structures, 26(10), pp. 865-886.

Chai, J. C., & Miura, N. (2002). Traffic-load-induced permanent deformation of road on soft subsoil. Journal of Geotechnical and Geoenvironmental Engineering, 128(11), pp. 907-916.

Craig, R. F. (1997). Soil Mechanics E&FN Spon. London, UK.

Dawson, A. (2009). Water in Road Structures. Movements, drainage and effects. Geotechnical, Geological and Earthquake Engineering, Vol. 5. Springer eBooks, Springer Netherlands, Dordrecht.

Dawson, A. & Kolisoja, P., (2004). Permanent deformation. Report on task 2.1. Available at: www.roadex.org. 47 p.

Doré, G., & Zubeck, H. K. (2009). Cold regions pavement engineering. New York, ASCE (American Society of Civil Engineering). 416 p.

Douglas, R. A. (1997). Heavy load, low tire pressure rutting of unbound granular pavements. Journal of transportation engineering, 123(5), pp. 357-363.

Dunnicliff, J. (1993). Geotechnical instrumentation for monitoring field performance. John Wiley & Sons.

Dynatest 2014. Available at: http://www.dynatest.com. Accessed 11.3.2014.

Ehrola, E. (1996). Liikenneväylien rakennesuunnittelun perusteet. Rakennustieto Oy. Helsinki. 358 p. + 7 app. (In Finnish)

Engstrand, A. (2011). Railway surveying-A case study of the GRP 5000. Master’s of Science Thesis in Geodesy no. 3123. Division of Geodesy and Geoinformatics, Royal Institute of Technology (KTH), Stockholm. 53 p.

Esveld, C. (2001). Modern railway track. Second Edition. MRT-Productions.

Esveld, C. (1980). Track Stiffness Measurements Using an Adapted Tamping Machine, Rail International.

Esveld, C. (1978). Comparison between Theoretical and Actual Transfer Functions of Track Maintenance Machines. Doctoral Thesis, Warsaw, May 1978.

Finlex (2013). Valtioneuvoston asetus ajoneuvojen käytöstä tiellä annetun asetuksen muuttamisesta 407/2013. Available at: www.finlex.fi. Accessed 15.1.2014.

Fredlund, D.G., & Xing, A. (1994). Equations for the soil-water characteristic curve. Can. Geotech. J, 31, pp. 521-532.

Fröhling, R., D. (1997). Deterioration of railway track due to dynamic vehicle loading and spatially varying track stiffness. Eng.D Thesis. University of Pretoria, Faculty of Engineering. 149 p.

Gandahl, R. (1957) Determination of the depth of soil freezing with a new frost meter. Statens Väginstitut Stockholm Rapport 30, Stockholm (1957), pp. 3–15 (in Swedish)

Gani, A., & Salami, M. J. E. (2002). A LabVIEW based data acquisition system for vibration monitoring and analysis. In Research and Development, 2002. SCOReD 2002. Student Conference on (pp. 62-65). IEEE.

Gräbe, P. J., & Clayton, C. R. (2009). Effects of principal stress rotation on permanent deformation in rail track foundations. Journal of Geotechnical and Geoenvironmental Engineering, 135(4), pp. 555-565.

Haakana, V., Kalliainen, A., Kolisoja, P. (2015). Raskaista ajoneuvoista tierumpuihin kohdistuvat rasitukset. Liikennevirasto tutkimuksia ja selvityksiä 18/2015. Liikennevirasto, Helsinki.

Hayhoe, H. N., & Balchin, D. (1986). Electrical determination for soil frost. Can. Agric. Eng, 28(2), pp. 77-80.

Hetényi, M. (1971). Beams on elastic foundation: theory with applications in the fields of civil and mechanical engineering. University of Michigan.

Holm G., Bengtsson P-E., Carlsten P., Johansson L. O. & Larsson R. (2002) "State of the art" Upgrading of existing railway lines for increased axle loads and speed. Diagnosis and improvement methods. Swedish Geotechnical Institute, SGI. Linköping. Varia 520. 102 p.

Holtz, R. D., & Kovacs, W. D. (1981). An introduction to geotechnical engineering. Prentice-Hall, Incorporated, USA.

Hosseingholian, M., Froumentin, M. & Robinet, A. (2011). Dynamic Track Modulus from Measurement of Track Acceleration by Portancemetre. Proceedings of 9th World Congress on Railway Research (WCRR), Lille, France, 22-26 May 2011. 12 p

Huang, Y. H, (2004). Pavement analysis and design. Pearson Prentice Hall, Upper Saddle River, New Jersey. 775 p.

INNOTRACK–project. (2006). Methods of track stiffness measurements. Available at: http://www.innotrack.net/IMG/pdf/d2111-f3-methods_of_track_stiffness_measurements.pdf. Accessed 8.6.2015.

Jaakkola, A., Hyyppä, J., Hyyppä, H., & Kukko, A. (2008). Retrieval algorithms for road surface modelling using laser-based mobile mapping. Sensors, 8(9), pp. 5238-5249.

Jacob, B., & Feypell-de La Beaumelle, V. (2010). Improving truck safety: Potential of weigh-in-motion technology. IATSS research, 34(1), pp. 9-15.

Jacob, B., & O'Brien, E. J. (2005). Weigh-in-motion: Recent developments in Europe. International Society for Weigh-In-Motion.

Kalliainen A., Luomala H., Jäniskangas T., Nurmikolu A., Kolisoja P. (2011). Radan eristys- ja välikerrosten tiiviys- ja kantavuustutkimus. Liikennevirasto tutkimuksia ja selvityksiä 10/2011. (In Finnish).

Kalliainen, A., Kolisoja, P., & Nurmikolu, A. (2010, January). Modeling of the effect of embankment dimensions on the mechanical behavior of railway track. In 2010 Joint Rail Conference (pp. 389-398). American Society of Mechanical Engineers.

Kalliainen, A. & Kolisoja, P. (2011). Modeling of the effect of embankment dimensions on the mechanical behavior of railway track-Model scale test embankments. Proceedings of 9th International Congress on Railway Research, WCRR 2011, May 22-26, Lille, France.

Kane, W. F., Holzhausen, G. R., & Constable, E. (2004). Coastal Bluff Monitoring/Alert System for Railways. In Geotechnical Engineering for Transportation Projects, pp. 2067-2074.

Kim, D., Kim, S. & Lee, J. (2006). Easy Detection and Dynamic Behavior of the Unsupported Sleepers in High Speed Ballasted Track. 7th World Congress on Railway Research, Montreal, Canada, 4-8 June 2006, 8 p.

King, G., & Bilham, R. (1976). A Geophysical wire strainmeter. Bulletin of the Seismological Society of America, 66(6), pp. 2039-2047.

Kinzie, P. A. (1973). Thermocouple temperature measurement. New York: Wiley.

Kolisoja, P. (1997). Resilient Deformation Characteristics of Granular Materials. Doctorial Thesis. Tampere University of Technology, Publications 233. Tampere. 188 p. 13 app.

Kolisoja, P., & Makela, E. (2001). Instrumentation and mechanical modeling of a full-scale railway embankment. In Proceedings of the international conference on soil and geotechnical engineering, Vol. 3, pp. 2111-2116, Balkema Publishers.

Koopmans, R. W. R., & Miller, R. D. (1966). Soil freezing and soil water characteristic curves. Soil Science Society of America Journal, 30(6), pp. 680-685.

Kropáč, O., & Múčka, P. (2005). Be careful when using the International Roughness Index as an indicator of road unevenness. Journal of sound and vibration, 287(4), pp. 989-1003.

Kujala, K. (1991). Factors affecting frost susceptibility and heaving pressure in soils. PhD thesis. ACTA Universitatis Ouluensis Series C58. 99 p., 5 app.

Köhler, J., (1999) Track Loading Vehicle–Description, Internal report: Banverket BMA 98/22k, Borlänge.

Laaksonen, A. (2011). Structural Behaviour of Long Concrete Integral Bridges. Doctoral Thesis. Tampere University of Technology. Publication 978.

Ladanyi, B., & Shen, M. (1989, March). Mechanics of freezing and thawing in soils. In Proc., International Symposium on Frost in Geotechnical Engineering, Saariselka, Finland, Vol. 94, pp. 73-104.

Lahti, O. (2008). Junan pyörävikojen havainnointi raiteeseen asennetulla mittalaitteella. Ratahallintokeskuksen julkaisuja A 12/2008. 90 p. 2 app.

Lekarp, F., Isacsson, U., & Dawson, A. (2000). State of the art. I: Resilient response of unbound aggregates. Journal of transportation engineering, 126(1), pp. 66-75.

Lekarp, F., Isacsson, U., & Dawson, A. (2000). State of the art. II: Permanent strain response of unbound aggregates. Journal of Transportation Engineering, 126(1), pp. 76-83.

Lemke, J. (2006). In-place inclinometer using low-G accelerometer network. In ASCE Conf. Proc., Vol. 187, pp. 65-70.

Li, D. Selig, E. T. (1998). Method for railroad track foundation design. Part 1: development. Journal of Geotechnical and Geoenvironmental Engineering, 124(4), pp. 316-322.

Li, D., Thompson, R., Marquez, P. & Kalay, S. (2002). Development and Implementation of a Continuous Vertical Track Support Testing Technique. TRB 2003 Annual Meeting. 20 p.

Luomala, H. & Lehtonen, V. (2011). Monitoring Techniques of Low Stability Railway Embankments. Proceedings of International Heavy Haul Association Conference, IHHA 2011, June 19-22, 2011, Galgary, Canada.

Luomala, H. & Nurmikolu, A. (2012). Railway track stiffness measurements on the bridge transition zones. Proceedings of the 2nd International Conference on Transportation Geotechnics, Sapporo, Japan, September 10-12, 2012.

Luomala, H. (2010). Ratapenkereiden monitorointi. Liikenneviraston tutkimuksia ja selvityksiä 22/2010. 85 p. 2 app. (in Finnish)

Luomala, H., Peltokangas, O., Rantala, T., Nurmikolu, A. (2015). Radan kokonaisjäykkyyden mittaaminen ja modifiointi. Liikenneviraston tutkimuksia ja selvityksiä 19/2015. 108 p. (in Finnish)

Luomala, H., & Kolisoja, P. (2008). Effects of seasonal frost on pavement stiffness in Finland according to a pavement monitoring system. In Transportation Research Board 87th Annual Meeting (No. 08-2091).

Luomala, H., Peltokangas, O., Nurmikolu, A. (2014). Stiffmaster-A continuous track stiffness measurement device. GEORAIL 2014: 2nd International symposium-Railway geotechnical engineering, 6-7 November 2014, France, pp. 109-118.

Luomala, H., Rantala, T., Kolisoja, P., & Mäkelä, E. (2017). Assessement of track quality using continuous track stiffness measurements. Georail 2017, 3rd International Symposium Railway Geotechnical Engineering: 23-24 November 2017, Marne La Vallee, France, pp. 281-290. IFSTTAR.

McCarthy, D. F., (1977). Essentials of soil mechanics and foundations (p. 505). Reston Publishing Company.

McKenna, J.M., (1974). Monitoring the M5 motorway embankments on soft ground in Somerset, pp. 262-274.

Mansikkamäki, J. (2015). Effective Stress Finite Element Stability Analysis of an Old Railway Embankment on Soft Clay. Doctoral Thesis. Tampere University of Technology. Publication 1287.

Mill, T., Ellmann, A., Aavik, A., Horemuz, M., & Sillamaee, S. (2014). Determining Ranges and Spatial Distribution of Road Frost Heave by Terrestrial Laser Scanning. Baltic Journal of Road and Bridge Engineering, 9(3).

Metsovuori, L. (2013). Sulamispainuminen radan epätasaisuuden aiheuttajana. Master's thesis. Tampere University of Technology. 93 p. (in Finnish)

Mäkelä, E. & Kolisoja, P. (2002). Ratarumpututkimus, mallinnus. Ratahallintokeskuksen julkaisuja A10/2002. Finnish Rail Administration.

Nickitopoulou, A., Protopsalti, K., & Stiros, S. (2006). Monitoring dynamic and quasi-static deformations of large flexible engineering structures with GPS: accuracy, limitations and promises. Engineering Structures, 28(10), pp. 1471-1482.

Norman, C., Farritor, S., Arnold, R., Elias, S.E.G. Fateh, M. & Sibaie, M. E. (2004). Design of a System to Measure Track Modulus from a Moving Railcar. Proceedings from Railway Engineering, London 2004. 25 p.

Nurmikolu, A. (2005). Degradation and frost susceptibility of crushed rock aggregates used in structural layers of railway track. Doctoral Thesis, Tampere University of Technology.

Nurmikolu, A., & Kolisoja, P. (2005). Extruded polystyrene (XPS) foam frost insulation boards in railway structures. In Proceedings of the 16th International Conference on Soil Mechanics and Geotechnical Engineering, Osaka, Japan, September 12-16, 2005.

Nurmikolu, A. & Kolisoja, P. 2011. Mechanism & effects of railway ballast degradation. EURAILmag, 2011, Issue 24. Blue Line & Bro, Paris, France, pp. 128-134.

Nurmikolu A. ja Kolisoja P. (2010). Sepelinpuhdistuksen vaikutukset raidesepelin ominaisuuksiin. Liikenneviraston tutkimuksia ja selvityksiä 11/2010. 64 p., 3 app. (in Finnish)

Nurmikolu, A., & Kolisoja, P. (2008). The effect of fines content and quality on frost heave susceptibility of crushed rock aggregates used in railway track structure. In Proceedings of the 9th International Conference on Permafrost, Fairbanks, USA, June 29-3 July 2008.

Nurmikolu, A., Salmenperä, P., Mäkitupa, S. & Lane, K. (2013). Statistical analysis of wheel impact load data and impact load limits in Finnish railways. Proceedings of the 10th International Heavy Haul Conference, New Delhi, India, February 4-6, 2013, pp. 669-675.

Peltokangas, O., Luomala, H., Nurmikolu, A. (2013). Radan kokonaisjäykkyyden mittaaminen ja modifiointi. Liikenneviraston tutkimuksia ja selvityksiä 6/2013. 190 p. 4 app. (in Finnish)

Profillidis V. A. 2000. Railway Engineering, 2. ed. Aldershot: Ashgate, cop. 291 p.
Pylkkänen, K., Nurmikolu A. (2015). Routa ja routiminen ratarakenteessa. Liikenneviraston tutkimuksia ja selvityksiä 22/2015. 210 p., 10 app. (in Finnish)

Pylkkänen, K., Luomala, H., Guthrie, W. S., & Nurmikolu, A. (2014). Real-Time In Situ Monitoring of Frost Depth, Seasonal Frost Heave, and Moisture in Railway Track Structures. Cold Regions Engineering 2012: pp. 446-455.

Pylkkänen, K., Luomala, H., Guthrie, W.S. & Nurmikolu, A. 2012. Real-time in-situ monitoring of frost depth, seasonal frost heave, and moisture in railway track structures. Proceedings of 15th International Conference on Cold Regions Engineering, Quebec, Canada, August 19-22, 2012

Pylkkänen, K. & Nurmikolu, A. (2011). Frost Susceptibility of Railway Track subballast Materials. Proceedings of International Heavy Haul Association Conference, IHHA 2011, June 19-22, 2011, Galgary, Canada.

Radd, F. J., & Oertle, D. H. (1973, July). Experimental pressure studies of frost heave mechanism and the growth-fusion behavior of ice. In North Am. Contrib. Sect. Int. Permafrost Conf. Washington, DC, pp. 377-383.

Rasmussen, S., Krarup, J. A. & Hildebrand, G. (2002). Non-contact Deflection Measurement at High Speed. 6th International Conference on the Bearing Capacity of Roads, Railways and Airfields, 24-26th June, 2002 Lisbon, Portugal. 8 p.

Ratatekniset määräykset ja ohjeet (Ramo) osa 13. Radan tarkastus. (2004). Ratahallintokeskus, Helsinki. 51 p. 27 app. (in Finnish)

Ratatekniset ohjeet (Rato) osa 3. Radan rakenne. (2008). Ratahallintokeskus, Helsinki. 50 p. 37 app. (in Finnish)

Ratatekniset ohjeet (Rato) osa 21, Liikkuva kalusto. (2012) Liikenneviraston ohjeita 21/2012, Helsinki. 37 p. 24 app. (in Finnish)

Remennikov, A. M., & Kaewunruen, S. (2008). A review of loading conditions for railway track structures due to train and track vertical interaction. Structural control and Health monitoring, 15(2), pp. 207-234.

Rickard, W., & Brown, J. (1972). The performance of a frost-tube for the determination of soil freezing and thawing depths. Soil science, 113(2), pp. 149-154.

RIVAS (2013). Railway Induced Vibration Abatement Solutions. Collaborative project. Overview of Methods for Measurement of Track Irregularities, Important for Ground-Borne Vibration, Deliverable D2.5, Submission date: 07/02/2013.

Roberts, F. L, Kandhal, P. S, Brown, E. R, Lee, D-Y, Kennedy, T. W (1996). Hot mix asphalt materials, mixture design and construction. Second edition. National Asphalt Pavement Association Research and Education Foundation, 1996, 603 p.

Ryhänen, A., Ylönen, S., Luomala, H., Kolisoja, P., Mäkelä, H., & Halkola, H. (2007). Continuous ground movement measurements. Proceedings of the 14th European Conference on Soil Mechanics and Geotechnical Engineering, Madrid, Spain, 24-27 September 2007.

Saarenketo, T., & Scullion, T. (2000). Road evaluation with ground penetrating radar. Journal of applied geophysics, 43(2), pp. 119-138.

Saarenketo, T., Matintupa, A., & Varin, P. (2012, January). The Use of Ground Penetrating Radar, Thermal Camera and Laser Scanner Technology in Asphalt Crack Detection and Diagnostics. In 7th RILEM International Conference on Cracking in Pavements (pp. 137-145). Springer Netherlands.

Saarenketo, T., Matintupa, A., Varin, P., Kolisoja, P., Herronen, T. & Hiekkalahti, A. (2012). Symmary of Pajala mine road impack analysis–Roadex implementation. Summary report.

Samppala, P. (2011). Rautateille asennettujen pyörävoimailmaisimien mittausdata ja pyörävoiman raja-arvot. Diplomityö. Tampereen teknillinen yliopisto. (in Finnish)

Sayers, M. W. (1995). On the calculation of international roughness index from longitudinal road profile. Transportation Research Record, (1501), pp. 1-12.

Seed, H. B., Chan, C. K., & Lee, C. E. (1962). Resilience characteristics of subgrade soils and their relation to fatigue failures in asphalt pavements. In International Conference on the Structural Design of Asphalt Pavements. Supplement. pp. 77-113.

Selig, E. T. & Li, D. (1994). Track modulus: Its meaning and factors influencing it. Transportation Research Record. No. 1470, Railroad Research Issues. pp. 47-54.

Selig, E.T. & Waters, J.M. (1994). Track geotechnology and substructure management. London, Thomas Telford Publications. 407 p.

SFS-EN 13848-2. (2006). Railway applications. Track. Track geometry quality. Part 2: Measuring systems. Track recording vehicles. European committee for standardization.

SFS-EN 15528 + A1 (2013). Railway applications. Line categories for managing the interface between load limits of vehicles and infrastructure. European committee for standardization.

SFS-EN 1997-1:en (2005). Eurocode 7: Geotechnical design. Part 1: General rules.

Silvast, M., Nurmikolu, A., Viljanen, B., Mäkelä, E. (2014). Condition-based track maintenance and rehabilitation design using combined data analysis. Proceedings of International Symposium Georail 2014, pp. 649-656.

Silvast, M., Nurmikolu, A., Wiljanen, B. & Levomäki, M. 2012. Identifying frost-susceptible areas on Finnish railways using GPR technique. Proc. IMechE, Part F: J. Rail and Rapid Transit, 27 June 2012.

Simonsen, E., & Isacsson, U. (1999). Thaw weakening of pavement structures in cold regions. Cold regions science and technology, 29(2), pp. 135-151.

Simonsen, E., Janoo, V.C., & Isacsson, U. (2002). ”Resilient Properties of Unbound Road Materials during Seasonal Frost Conditions.” Journal of Cold Regions Engineering, 16(1), pp. 28-50.

Sivilevičius, H., & Petkevičius, K. (2002). Regularities of defect development in the asphalt concrete road pavements. Journal of Civil Engineering and Management, 8(3), pp. 206-213.

Sharma, J. S., Hefny, A. M., Zhao, J., & Chan, C. W. (2001). Effect of large excavation on deformation of adjacent MRT tunnels. Tunnelling and Underground Space Technology, 16(2), pp. 93-98.

Sharpe, P. (2014). The "RTST"–A new machine for detailed measurement of trackbed stiffness characteristics. Proceedings of International Symposium Georail 2014, pp. 149-158.

Skempton, A. W. (1951). Selected Papers on Soil Mechanics, The bearing capacity of clays. Published in association of Geotechnique by Thomas Telford Ltd. London.

Stratman, B., Liu, Y., & Mahadevan, S. (2007). Structural health monitoring of railroad wheels using wheel impact load detectors. Journal of Failure Analysis and Prevention, 7(3), pp. 218-225.

Sun, L. (2001). Developing spectrum-based models for international roughness index and present serviceability index. Journal of transportation engineering, 127(6), pp. 463-470.

Sun, Y., Cheng, Q., Xue, X., Fu, L., Chai, J., Meng, F., Schulze Lammers, p., Jones, S. B. (2012). Determining in-situ soil freeze–thaw cycle dynamics using an access tube-based dielectric sensor. Geoderma, 189, pp. 321-327.

Sustained Performance of Railway Tracks (SUPERTRACK). (2005). Final report by CEDEX, Instrumentation, monitoring and physical modeling of highspeed line. 34 p.

The Aasho Road Test, Washington, D.C. (1962). Highway Research Board, Special Report 61 A-G.

Tholen, O., Sharma, J., & Terrel, R. L. (1985). Comparison of falling weight deflectometer with other deflection testing devices. Transportation research record, 1007, pp. 20-26.

Uzan, J. (1985). Characterization of Granular material. Transportation Research Record 1022, pp. 52-59.

Vuorimies N., Luomala H., Munro R., Kolisoja P. (2012). Stynie Wood Demonstration Project, Mosstodloch, Scotland. The ROADEX "Implementing Accessibility" Project. 45 p.

Wangqing, W., Geming, Z., Kaiming, L. & Lin, L. (1997). Development of inspection car for measuring railway track elasticity. Proceedings from 6th International Heavy Haul Conference, Cape Town 1997.

Weinmann, T. L., Lewis, A. E., & Tayabji, S. D. (2004). Pavement sensors used at accelerated pavement test facilities. In Proceedings of the second international conference on accelerated pavement testing.

Wu, J., Fedder, G. K., Carley, L. R. (2004). A low-noise low-offset capacitive sensing amplifier for a 50-μg/√ Hz monolithic CMOS MEMS accelerometer. Solid-State Circuits, IEEE Journal of, 39(5), pp. 722-730.

Zarembski, A. M., McConnell, D. P. & Lovelace, W. S. (1980). New Car for Measurement and Evaluation of Gage-Widening Resistance of Track. Proceedings of American Railway Engineering Association (AREA). Bulletin 678. Vol. 81. pp. 402-429.

Zeiner, A. 2007. Reporter 56, The Global Magazine of Leica Geosystems. Leica Geosystems AG, Heerbrugg, Switzerland 2007. 24 p

Zeiner, A. 2007. Reporter 57, The Global Magazine of Leica Geosystems. Leica Geosystems AG, Heerbrugg, Switzerland 2007. 24 p.

Zimmerman, H. (1941). Die Berechnung des Eisenbahnoberbaues (Railway permanent way design). Ernst & Sohn, Berlin.